



Technische Universität München

TUM School of Engineering and Design

Design and analysis of the very high temperature gas-cooled reactor-driven nuclear hydrogen production system based on sulfur-iodine thermochemical cycle and gas-steam combined cycle

Qi Wang

Vollständiger Abdruck der von der TUM School of Engineering and Design der Technischen Universität München zur Erlangung eines

Doktors der Ingenieurwissenschaften (Dr.-Ing.)

genehmigten Dissertation.

Vorsitz: Prof. Dr.-Ing. Hartmut Spliethoff
Prüfer*innen der Dissertation: Prof. Rafael Macián-Juan, Ph.D.
Assoc. Prof. Jun Sun, Ph.D.

Die Dissertation wurde am 17.03.2023 bei der Technischen Universität München eingereicht und durch die School of Engineering and Design am 11.07.2023 angenommen.

Acknowledgement

I have lived in China for more than 20 years, where I completed my undergraduate and master studies. During the long years of studying, I have dreamed countless times that one day I can study abroad and have the opportunity to see how different the outside world is. Finally, this wish came true in the late autumn of 2020. I came to Germany as a scholarship student and started my overseas life.

Undoubtedly, the first person I would like to thank is my supervisor, Prof. Dr. Rafael Macián-Juan, who accepted me as his Ph.D. student three years ago and gave me such a precious opportunity to carry out my doctoral research at the Technische Universität München (TUM), one of the top universities in the world. Prof. Macián is an amiable supervisor. During the few years with him, I deeply felt his approachability and kindness towards the students. When I encountered some scientific problems, Prof. Macián always gave me warm encouragement and tried his best to provide me with all kinds of help. It can be said that without the long-standing support and help of Prof. Macián, I would not have been able to complete my doctoral research so smoothly. I cannot express in words how grateful I am to Prof. Macián.

Secondly, I would like to express my heartfelt thanks to Dr.-Ing. Chunyu Liu, who helped me a lot throughout my doctoral study and gave me too many important suggestions. From the formulation of my doctoral project, to the application and registration of doctoral candidate, and to the installation and use of computer software, Chunyu's help has been everywhere. And I will never forget that Chunyu accompanied me to see a doctor when I was sick and helped me tide over the difficulties. For me, Chunyu is not only an amazing colleague, but also an older brother.

This work would not have been possible without the help and contribution of many. A big thank you to Dr. Run Luo, who accepted my invitation to be my mentor three years ago and has always encouraged me to bravely face and overcome any obstacles in my doctoral research. I am also very grateful to my colleague Tianqi Li. Thanks to him for sharing with me some of his life experiences in Germany and giving me a lot of advice and help. Besides, I would like to express my deep gratitude to all my colleagues at the Chair of Nuclear Technology of TUM. It was an honor to meet and work with all of you.

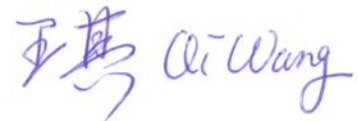
A special acknowledgement goes to Prof. Dr. Weimin Ma at the Royal Institute of Technology (KTH) of Sweden, not only for the visiting research opportunity he provided, but also for his strong support and warm welcome during the research period. I thank my friend Di Fang and appreciate to meet many research staff and nice people during the research stay at KTH: Yan Xiang, Yucheng Deng, Wanhong

Wang, Lu Zhao, Liang Chen, Disen Liang, etc. Thank you all for making it a very enjoyable time at the end of my doctoral research.

Also, I would like to thank Assoc. Prof. Dr. Jun Sun from Tsinghua University for accepting to review this thesis and giving many important suggestions. I thank Prof. Dr.-Ing. Hartmut Spliethoff for his willingness to spend his precious time as the chairman of my doctoral defense committee.

I have to say that my heart has always been in China, where I have my old friends and family. I would like to send my deepest gratitude and love to my parents who always supported me in all my decisions and gave me unconditional love. Their love and support are the source of strength for me to overcome many difficulties in life. My life has become extraordinarily happy because of their company.

Finally, I would like to thank the China Scholarship Council (CSC) for funding this work (Grant No. 202006280024). Without the financial support from the CSC, I could not realize my dream of studying abroad.

Handwritten signature of Qi Wang in blue ink.

25.07.2023, TUM Garching

Abstract

Some pressing issues including the increasing energy demand, dwindling fossil fuel reserves, severe environmental pollution, and notable climate change force people to vigorously develop clean energy resources such as renewable energy and nuclear energy. Due to the high stability and low cost, nuclear energy is considered to be the most promising carbon-free energy to replace fossil energy on a large scale in the future. Hydrogen, as a clean energy carrier, can link multiple sectors such as energy, industry, agriculture, and transportation to form a hydrogen economy. The realization of large-scale hydrogen production is a prerequisite for the development of hydrogen economy. In this context, nuclear hydrogen production has attracted the attention of more and more countries in recent years, because this technology can not only achieve large-scale carbon-free hydrogen production, but also improve the operational flexibility and economic competitiveness of existing nuclear power plants. Among various hydrogen production methods, the Sulfur-Iodine (S-I) thermochemical cycle is one of the most promising water-splitting hydrogen production processes, which can be coupled with Very High Temperature gas-cooled Reactors (VHTRs) for large-scale nuclear hydrogen production. However, due to the complex system configuration, there are very few studies on the nuclear hydrogen production system based on the coupled VHTR and S-I thermochemical cycle, especially when the Gas-Steam Combined Cycle (GSCC) is further integrated into the system as a power cycle.

To fill the above research gap and enrich the existing research on nuclear hydrogen production technology, two promising VHTR-driven nuclear hydrogen production systems using S-I thermochemical cycle and GSCC were designed and analyzed in this thesis. First, a S-I thermochemical hydrogen production process was developed and analyzed using Aspen Plus simulation software, and a feasible internal heat exchange network was further designed to improve process efficiency. Then, the operating characteristics of the conventional coupled VHTR and S-I thermochemical cycle nuclear hydrogen production system with GSCC as the power cycle were analyzed based on the first and second laws of thermodynamics. In addition, a novel system layout was also proposed to improve the thermodynamic performance of the conventional system. After that, a comprehensive system layout improvement and integrated design were carried out, and two complete system design schemes (namely independent operating system and coupled operating system) were proposed. Finally, an economic evaluation model was developed based on the six-tenths-factor rule and some existing equipment investment cost equations, and the cost distribution of the system and the effects of some key parameters on the unit hydrogen production cost of the system were analyzed to clarify the economic characteristics and cost-influencing mechanism of the VHTR-driven nuclear hydrogen production system using S-I thermochemical cycle and GSCC.

The investigation results of the S-I thermochemical hydrogen production process show that more than 90% of the energy consumption of the S-I cycle is caused by the concentration and decomposition process of H_2SO_4 and HI solutions, and the energy consumption of the Bunsen section is very small. The thermal efficiency of the S-I cycle is estimated to be in the range of 15%-42%, which is greatly affected by the internal heat recovery situation. The thermodynamic analysis results of the system show that when more energy is used to produce hydrogen, the overall thermodynamic efficiencies of the system will decrease significantly. Thus, it is concluded that the S-I cycle-based nuclear hydrogen production efficiencies are lower than the GSCC-based nuclear power generation efficiencies. In addition, it is found that the maximum exergy loss of the system occurs in the VHTR, with an exergy efficiency of about 70.7%, while the exergy efficiency of the S-I cycle is very low, only about 50.8%. The system integration design and economic analysis results show that under the same operating conditions, the coupled operating system can always obtain greater net electrical power output, higher system efficiency and lower unit hydrogen production cost than the independent operating system. The unit hydrogen production cost of the VHTR-driven nuclear hydrogen production system using S-I thermochemical cycle and GSCC is estimated to lay between 1.5 \$/kg and 12 \$/kg, which is affected by many factors. It is found that increasing the reactor thermal power, cost capacity factor, system lifetime and electricity price or decreasing the mass flow rate ratio and interest rate all help to reduce the unit hydrogen production cost of the system.

In summary, the proposed system design ideas and the obtained analysis results not only provide some important data references for future engineering applications, but also lay a theoretical foundation for understanding the thermo-economic characteristics of the VHTR-driven nuclear hydrogen production system based on S-I thermochemical cycle and GSCC.

Zusammenfassung

Einige drängende Probleme wie der steigende Energiebedarf, die schwindende Reserven an fossilen Brennstoffen, die starke Umweltverschmutzung und der bemerkenswerte Klimawandel zwingen die Menschen zur energischen Entwicklung sauberer Energiequellen wie erneuerbare Energien und Kernenergie. Die Kernenergie gilt aufgrund ihrer hohen Stabilität und niedrigen Kosten als die vielversprechendste kohlenstofffreie Energie, um fossile Energien in Zukunft in großem Umfang zu ersetzen. Wasserstoff als sauberer Energieträger kann mehrere Sektoren wie Energie, Industrie, Landwirtschaft und Verkehr miteinander verbinden und eine Wasserstoffwirtschaft bilden. Die Realisierung einer großtechnischen Wasserstoffproduktion ist eine Voraussetzung für die Entwicklung der Wasserstoffwirtschaft. In diesem Zusammenhang hat die nukleare Wasserstoffzeugung in den letzten Jahren die Aufmerksamkeit von immer mehr Ländern auf sich gezogen, da diese Technologie nicht nur eine groß angelegte kohlenstofffreie Wasserstoffzeugung ermöglichen kann, sondern auch die betriebliche Flexibilität und die wirtschaftliche Wettbewerbsfähigkeit der bestehenden Kernkraftwerke verbessert. Unter den verschiedenen Verfahren zur Wasserstoffherzeugung ist der thermochemische Schwefel-Jod-Kreislauf (S-I) eines der vielversprechendsten wasserspaltenden Wasserstoffherzeugungsverfahren, das mit gasgekühlten Hochtemperaturreaktoren (VHTRs) für die großtechnische nukleare Wasserstoffherzeugung gekoppelt werden kann. Aufgrund der komplexen Systemkonfiguration gibt es jedoch nur sehr wenige Studien über das gekoppelte VHTR- und S-I-thermochemische Kreislaufsystem zur nuklearen Wasserstoffherzeugung, insbesondere wenn der Gas-und-Dampf-Kombikreislauf (GSCC) als Stromkreislauf weiter in das System integriert wird.

Um die oben genannte Forschungslücke zu schließen und die bestehende Forschung zur nuklearen Wasserstoffherzeugungstechnologie zu bereichern, wurden in dieser Arbeit zwei vielversprechende VHTR-betriebene nukleare Wasserstoffherzeugungssysteme mit S-I-thermochemischem Kreislauf und GSCC entworfen und analysiert. Zunächst wurde ein thermochemisches S-I-Wasserstoffherzeugungsverfahren entwickelt und mit der Aspen Plus-Simulationssoftware analysiert, und ein praktikables internes Wärmeaustauschnetz wurde weiter entworfen, um die Prozesseffizienz zu verbessern. Dann wurden die Betriebseigenschaften des konventionellen gekoppelten VHTR- und S-I-thermochemischen Kreislauf-Kernwasserstoffherzeugungssystems mit GSCC als Stromkreislauf basierend auf dem ersten und zweiten Hauptsatz der Thermodynamik analysiert. Darüber hinaus wurde ein neuartiges Systemlayout vorgeschlagen, um die thermodynamische Leistung des konventionellen Systems zu verbessern. Danach wurden eine umfassende Verbesserung des Systemlayouts und

ein integriertes Design durchgeführt und zwei vollständige Systemdesignschemata (nämlich ein unabhängiges Betriebssystem und ein gekoppeltes Betriebssystem) gebildet. Schließlich wurde ein wirtschaftliches Bewertungsmodell basierend auf der Sechs-Zehntel-Faktoren-Regel und einigen bestehenden Gleichungen für die Investitionskosten der Ausrüstung entwickelt, und die Kostenverteilung des Systems und die Auswirkungen einiger Schlüsselparameter auf die Wasserstofferzeugungskosten pro Einheit des Systems wurden analysiert, um die wirtschaftlichen Eigenschaften und den kostenbeeinflussenden Mechanismus des VHTR-getriebenen nuklearen Wasserstofferzeugungssystems unter Verwendung des S-I-thermochemischen Kreislaufs und GSCC zu klären.

Die Untersuchungsergebnisse des S-I-thermochemischen Wasserstofferzeugungsverfahrens zeigen, dass mehr als 90% des Energieverbrauchs des S-I-Kreislaufs durch den Konzentrations- und Zersetzungsverfahren von H_2SO_4 - und HI-Lösungen verursacht wird und der Energieverbrauch der Bunsen-Sektion sehr gering ist. Der thermische Wirkungsgrad des S-I-Kreislaufs wird auf 15 % bis 42 % geschätzt, was stark von der internen Wärmerückgewinnung beeinflusst wird. Die Ergebnisse der thermodynamischen Analyse des Systems zeigen, dass die thermodynamischen Gesamtwirkungsgrade des Systems erheblich abnehmen, wenn mehr Reaktorwärme zur Wasserstofferzeugung verwendet wird. Daher wird der Schluss gezogen, dass die auf dem S-I-Kreislauf basierenden Wirkungsgrade der nuklearen Wasserstofferzeugung niedriger sind als die auf dem GSCC basierenden Wirkungsgrade der nuklearen Stromerzeugung. Außerdem wird festgestellt, dass der maximale Exergieverlust des Systems im VHTR mit einer Exergieeffizienz von etwa 70,7 % auftritt, während die Exergieeffizienz des S-I-Kreislaufs mit nur etwa 50,8 % sehr niedrig ist. Das Systemintegrationsdesign und die Ergebnisse der wirtschaftlichen Analyse zeigen, dass das gekoppelte Betriebssystem unter den gleichen Betriebsbedingungen stets eine höhere elektrische Nettoleistung, einen höheren Systemwirkungsgrad und niedrigere Wasserstofferzeugungskosten pro Einheit als das unabhängige Betriebssystem erzielen kann. Die Einheitskosten der Wasserstoffproduktion des VHTR-betriebenen nuklearen Wasserstoffproduktionssystems mit S-I-thermochemischen Kreislauf und GSCC werden auf 1,5 \$/kg bis 12 \$/kg geschätzt, was von vielen Faktoren beeinflusst wird. Es hat sich herausgestellt, dass eine Erhöhung der thermischen Reaktorleistung, des Kostenkapazitätsfaktors, der Systemlebensdauer und des Strompreises oder eine Verringerung des Massendurchflussratenverhältnisses und des Zinssatzes alle dazu beitragen, die Einheitskosten für die Wasserstofferzeugung des Systems zu verringern.

Zusammenfassend liefern die vorgeschlagene Systemdesignidee und die erhaltenen Analyseergebnisse nicht nur einige wichtige Datenreferenzen für zukünftige technische Anwendungen, sondern auch eine Grundlage für das Verständnis der thermoökonomischen Eigenschaften des VHTR-getriebenen nuklearen Wasserstofferzeugungssystems unter Verwendung des S-I-thermochemischen Kreislaufs und GSCC.

Contents

Acknowledgement	i
Abstract	iii
Zusammenfassung	v
List of Figures	xi
List of Tables	xv
Abbreviations	xvii
Nomenclature	xix
1 Introduction	1
1.1 Research background	1
1.1.1 Nuclear energy and Generation IV reactors.....	1
1.1.2 Hydrogen and hydrogen economy	4
1.1.3 Nuclear hydrogen production.....	5
1.2 Research status	8
1.2.1 Global interest in nuclear hydrogen production	8
1.2.2 Thermochemical water-splitting cycles	10
1.2.3 The coupled VHTR and S-I cycle nuclear hydrogen production system	13
1.3 Research gaps, objectives and main work.....	15
1.3.1 Research gaps.....	15
1.3.2 The objectives and main work of this thesis.....	17
2 Design and analysis of the S-I thermochemical hydrogen production system	19
2.1 Design and modeling of the S-I system.....	19
2.1.1 Design of the S-I system	19
2.1.2 Modeling of the S-I system	24
2.2 Process simulation and performance analysis of the S-I system.....	26

2.2.1	Process simulation of the S-I system	26
2.2.2	Performance analysis of the S-I system.....	30
2.3	Design and analysis of the internal heat exchange network.....	36
2.3.1	Design of the internal heat exchange network.....	36
2.3.2	Analysis of the internal heat exchange network.....	41
2.4	Summary of this chapter	46
3	Design and analysis of the GSCC power conversion system	47
3.1	Description and modeling of the conventional GSCC power conversion system	47
3.1.1	System description.....	47
3.1.2	Thermodynamic modeling	49
3.2	System simulation and performance analysis.....	53
3.2.1	System simulation	53
3.2.2	Performance analysis.....	57
3.3	Design and analysis of a novel GSCC power conversion system.....	62
3.3.1	System design	62
3.3.2	System simulation and performance analysis.....	63
3.4	Summary of this chapter	68
4	System layout improvement and integrated design	71
4.1	System layout improvement.....	71
4.1.1	Overall system	71
4.1.2	S-I hydrogen production system.....	72
4.1.3	GSCC power conversion system.....	74
4.2	System integrated design	74
4.2.1	Independent operating system.....	74
4.2.2	Coupled operating system	77
4.3	System simulation and performance analysis.....	80
4.3.1	System simulation	80
4.3.2	Performance analysis.....	85
4.4	Summary of this chapter	88
5	System economic evaluation	91
5.1	Cost composition of a thermochemical hydrogen production plant.....	91
5.1.1	The total capital investment	91
5.1.2	The total product cost	93

5.2	Economic modeling of the nuclear hydrogen production system.....	96
5.2.1	Economic modeling of the S-I hydrogen production plant.....	96
5.2.2	Economic modeling of the nuclear power system.....	101
5.2.3	Unit hydrogen production cost and results comparison	104
5.3	Cost distribution and parametric studies	105
5.3.1	Cost distribution	106
5.3.2	Parametric studies.....	110
5.4	Summary of this chapter	116
6	Conclusion and outlook	117
6.1	Conclusion.....	117
6.2	Outlook.....	119
	Bibliography	121
	Publications	133

List of Figures

1-1	Schematic of six advanced Generation IV nuclear reactor systems (Reproduced from Ref. [3]): (a) Very High Temperature gas-cooled Reactor (VHTR), (b) Sodium-cooled Fast Reactor (SFR), (c) Molten Salt Reactor (MSR), (d) Gas-cooled Fast Reactor (GFR), (e) Lead cooled Fast Reactor (LFR), and (f) Super-Critical Water-cooled Reactor (SCWR)..	2
1-2	Schematic of the relationship between hydrogen and various industries and energy sectors [9].....	4
1-3	Schematic of potential pathways of nuclear hydrogen production.....	6
1-4	Schematic of possible integrations of different nuclear reactors with various hydrogen production processes based on operating temperature ranges (Modified from Ref. [13])	6
1-5	Schematic of the VHTR and S-I cycle-based nuclear hydrogen production system	14
2-1	Schematic of the S-I thermochemical cycle coupled with a VHTR or HTGR (Modified from Ref. [94]).....	20
2-2	Schematic of the S-I thermochemical hydrogen production system developed in Aspen Plus	21
2-3	Schematic representation of three main options for the HI concentration and decomposition section (Reproduced from Ref. [97]).....	22
2-4	Schematic representation of the working principle of an EED cell	25
2-5	Energy consumption distribution of the S-I system: (a) Each section and (b) Each component.....	31
2-6	Effect of reflux ratio on the heat consumption of (a) H ₂ SO ₄ DST-Reboiler and (b) HIDST-Reboiler.....	33
2-7	Effect of heat recovery coefficient on the thermal efficiency of the S-I system	34
2-8	Flow chart of the complete design process of the S-I system	38
2-9	Schematic of the designed S-I hydrogen production system with an internal heat exchange network	39
2-10	Heat exchange process of IHE1.....	42
2-11	Heat exchange processes of (A) IHE2, (B) IHE3, (C) IHE4, and (D) IHE5.....	43
2-12	Heat exchange processes of (A) IHE6, (B) IHE7, (C) IHE8, and (D) IHE9.....	44
3-1	Schematic of the conventional VHTR and S-I cycle-based nuclear hydrogen production	

	system with GSCC as the power conversion unit (Modified from Ref. [87]).....	48
3-2	Schematic of the improved VHTR and S-I cycle-based nuclear hydrogen production system with GSCC as the power conversion unit	48
3-3	Flowchart of the model solving procedure	56
3-4	Thermodynamic performance of the system under different mass flow rate ratios and different IHX's primary side helium outlet temperatures: (a) Hydrogen production rate, (b) Net electrical power output, (c) Thermal efficiency, and (d) Exergy efficiency.....	57
3-5	Schematic diagram of the calculation of the thermal efficiency of nuclear hydrogen production.....	59
3-6	Exergy analysis results of the system under different IHX's primary side helium outlet temperatures ($x = 0.5$): (a) $T_{out,ps,IHX} = 400^{\circ}\text{C}$, (b) $T_{out,ps,IHX} = 500^{\circ}\text{C}$, (c) $T_{out,ps,IHX} = 600^{\circ}\text{C}$, and (d) $T_{out,ps,IHX} = 700^{\circ}\text{C}$	61
3-7	Three promising system layouts for the VHTR and S-I cycle-based nuclear hydrogen production system [127]: (a) The series connection layout, (b) The parallel connection layout, and (c) The mixed connection layout	62
3-8	Schematic diagram of a novel GSCC power conversion system with two SGs.....	63
3-9	Exergy analysis results of the two systems under the benchmark conditions: (a) The conventional system and (b) The proposed new system	67
3-10	Effects of the mass flow rate ratio on system performance: (a) Hydrogen production rate, (b) Net electrical power output, (c) Thermal efficiency, and (d) Exergy efficiency.....	67
3-11	Effects of the IHX's primary side helium outlet temperature on system performance: (a) Hydrogen production rate, (b) Net electrical power output, (c) Thermal efficiency, and (d) Exergy efficiency	68
4-1	Three main nuclear reactor connection concepts for nuclear hydrogen production systems based on VHTR and S-I cycle: (a) direct PGS plus indirect S-I cycle, (b) indirect PGS and S-I cycle, and (c) indirect PGS plus double indirect S-I cycle	72
4-2	Schematic of the improved S-I hydrogen production system developed in Aspen Plus. .	73
4-3	Schematic diagram of an independent operating system based on VHTR, S-I cycle and combined cycle.....	75
4-4	Schematic temperature-heat duty (1 mol H ₂ /s) diagram of the heat exchange process of the helium heat carrier flowing through R201, E202 and R301	76
4-5	Schematic diagram of a coupled operating system based on VHTR, S-I cycle and combined cycle.....	78
4-6	Schematic temperature-entropy diagram of the heat exchange process in SG.....	79
4-7	Performance parameters of the two operating systems under different mass flow rate ratios: (a) Hydrogen production rate, (b) Net electrical power output, (c) Thermal efficiency, and (d) Exergy efficiency	87
5-1	Schematic diagram of the cost structure of a typical chemical plant (Reproduced from Ref. [130])	95

5-2	Economic cost distribution of the independent operating system under the benchmark conditions: (a) Annual cost distribution, (b) Equipment investment cost distribution of the overall system, (c) Equipment investment cost distribution of the nuclear power system, and (d) Equipment investment cost distribution of the S-I plant.....	107
5-3	Economic cost distribution of the coupled operating system under the benchmark conditions: (a) Annual cost distribution, (b) Equipment investment cost distribution of the overall system, (c) Equipment investment cost distribution of the nuclear power system, and (d) Equipment investment cost distribution of the S-I plant.....	108
5-4	Effects of the reactor thermal power on (a) Daily hydrogen production and (b) Unit hydrogen production cost.....	111
5-5	Effects of the mass flow rate ratio on (a) Daily hydrogen production and (b) Unit hydrogen production cost.....	112
5-6	Effects of the cost capacity factor on (a) Equipment investment cost of the S-I plant and (b) Unit hydrogen production cost.....	113
5-7	Effects of the interest rate on (a) Capital Recovery Factor and (b) Unit hydrogen production cost	114
5-8	Effects of the system lifetime on (a) Capital Recovery Factor and (b) Unit hydrogen production cost	114
5-9	Effects of the electricity price on (a) Annual electricity income and (b) Unit hydrogen production cost	115

List of Tables

1-1	Summary of some existing design parameters of the Generation IV reactors (Modified from Ref. [6]).....	3
1-2	Performance comparison of different nuclear hydrogen production methods (Modified from Ref. [6]).....	7
1-3	Some nuclear hydrogen production R&D activities around the world	8
2-1	Component information of the S-I system developed in Aspen Plus	23
2-2	Main operating parameters of the S-I system with a hydrogen production rate of 1 mol/s	27
2-3	Material flow data of the simulated S-I hydrogen production system.....	29
2-4	Model validation of the H ₂ SO ₄ distillation column (H2SO4DST)	30
2-5	Model validation of the HI distillation column (HIDST)	30
2-6	Energy consumption statistic of the S-I system.....	31
2-7	Summary of the thermal efficiency estimation results of the S-I system.....	34
2-8	Heat transfer constraints in the design process.....	37
2-9	Material flow data of the designed S-I hydrogen production system with an internal heat exchange network	40
2-10	Detailed operating data of the designed internal heat exchange network	42
2-11	Several different analysis results of the S-I system's energy consumption.....	46
3-1	Exergy loss equation and exergy efficiency equation of each component in the system	52
3-2	Main fuel parameters of the HTR-10.....	53
3-3	Key operating parameters of the system	54
3-4	Model validation of the GSCC nuclear power system.....	56
3-5	Performance data of the two systems under the benchmark conditions	64
3-6	State-point parameters of the conventional system (see Figure 3-2) under the benchmark conditions	64
3-7	State-point parameters of the proposed new system (see Figure 3-8) under the benchmark conditions.....	65

4-1	Turbine operating and extraction parameters for two different systems.....	81
4-2	Material flow data of the improved S-I system under a hydrogen production rate of 1 mol/s.....	81
4-3	State-point parameters of the independent operating system when the mass flow rate ratio is equal to 0.5	83
4-4	State-point parameters of the coupled operating system when the mass flow rate ratio is equal to 0.5	84
4-5	Performance parameters of the two operating systems when the mass flow rate ratio is equal to 0.5	88
5-1	Five different estimation methods and their accuracy [130].....	93
5-2	Description of the manufacturing costs and general expenses [130]	94
5-3	The S-I plant's fixed capital investment breakdown	98
5-4	The S-I plant's total product cost breakdown (calculated at annual cost).....	100
5-5	Equipment investment cost equations of the nuclear power system [137,141,142].....	102
5-6	CEPCI indexes from 1985 to 2020	103
5-7	Comparison of results between this work and Ref. [89]	105
5-8	Some important parametric variables and their base values.....	105
5-9	Cost data of the two operating systems under the benchmark conditions	106
5-10	Equipment investment cost data of the nuclear power system under the benchmark conditions.....	109
5-11	Equipment investment cost data of the S-I hydrogen production plant under the benchmark conditions (hydrogen production rate of 202.86 mol/s).....	109

Abbreviations

AC	Auxiliary Cooler
ALWR	Advanced Light Water Reactor
BWR	Boiling Water Reactor
Ca-Br	Calcium-Bromine
CANDU	CANada Deuterium-Uranium
CEA	Commissariat à l'Énergie Atomique
CEPCI	Chemical Engineering Plant Cost Index
CFP	Condensate Feed Pump
Co-Cl	Cobalt-Chlorine
CRF	Capital Recovery Factor
Cu-Cl	Copper-Chlorine
EED	Electro-ElectroDialysis
ELECNRTL	ELECTrolytic Non-Random Two-Liquid
Fe-Cl	Iron-Chlorine
FWP	Feed Water Pump
G	Generator
GC	Gas Compressor
GFR	Gas-cooled Fast Reactor
GIF	Generation IV International Forum
GSCC	Gas-Steam Combined Cycle
GT	Gas Turbine
GTHTTR300C	Gas Turbine High Temperature Reactor 300-Cogeneration
HHV	High Heating Value
HP	High Pressure
HPE	High Pressure Electrolysis
HTGR	High Temperature Gas-cooled Reactor
HTR-PM	High Temperature gas-cooled Reactor-Pebble bed Module
HTSE	High Temperature Steam Electrolysis
HTTR	High Temperature Test Reactor
HyS	Hybrid Sulfur
IHX	Intermediate Heat eXchanger

INET	Institute of Nuclear and New Energy Technology
IP	Intermediate Pressure
JAEA	Japan Atomic Energy Agency
KAERI	Korea Atomic Energy Research Institute
LCA	Life Cycle Analysis or Life Cycle Assessment
LF	Load Factor
LFR	Lead-cooled Fast Reactor
LMTD	Logarithmic Mean Temperature Difference
LP	Low Pressure
LWR	Light Water Reactor
Mg-Cl	Magnesium-Chlorine
MOX	Mixed OXide fuel
MSFR	Molten Salt Fast Reactor
MSR	Molten Salt Reactor
NGTCC	Nuclear Gas Turbine Combined Cycle
NRTL-RK	Non-Random Two-Liquid-Redlich-Kwong
OFC	Organic Flash Cycle
ORC	Organic Rankine Cycle
PBMR	Pebble Bed Modular Reactor
PEME	Polymer Electrolyte Membrane Electrolysis
PGS	Power Generation System
PWR	Pressurized Water Reactor
R&D	Research and Development
S-I or SI	Sulfur-Iodine
SCBC	Supercritical CO ₂ Brayton Cycle
SCWR	Super-Critical Water-cooled Reactor
SFR	Sodium-cooled Fast Reactor
SG	Steam Generator
SMR	Steam Methane Reforming
SNL	Sandia National Laboratory
SOE	Solid Oxide Electrolysis
SRC	Steam Rankine Cycle
ST	Steam Turbine
TFC	Trilateral Flash Cycle
V-Cl	Vanadium-Chlorine
VHTR	Very High Temperature gas-cooled Reactor

Nomenclature

Symbols

A	area	m^2
b	fission exergy	$\text{MeV}\cdot\text{nucleon}^{-1}$
c	unit cost	$\text{\$}\cdot\text{unit}^{-1}$
C	cost	$\text{\$}$
e	fission energy	$\text{MeV}\cdot\text{nucleon}^{-1}$
E	electricity	kJ
\dot{E}	electrical power	kW
ex	specific exergy	$\text{kJ}\cdot\text{kg}^{-1}$
$\dot{E}x$	exergy flow rate	kW
F	Faraday constant	$96,485 \text{ C/mol}$
g	gravitational acceleration	$9.8 \text{ m}\cdot\text{s}^{-2}$
h	specific enthalpy	$\text{kJ}\cdot\text{kg}^{-1}$
H	head	m
i_r	interest rate	—
I	current	A
IN	income	$\text{\$}$
K	overall heat transfer coefficient	$\text{kW}\cdot\text{m}^{-2}\cdot\text{K}^{-1}$
l	lifetime	year
\dot{m}	mass flow rate	$\text{kg}\cdot\text{s}^{-1}$
M	mass	kg
\dot{n}	molar flow rate	$\text{mol}\cdot\text{s}^{-1}$
N	annual operating hours	hour
p	pressure	kPa
q	dryness	—
Q	heat	kJ
\dot{Q}	heat flow rate	kW
s	specific entropy	$\text{kJ}\cdot\text{kg}^{-1}\cdot\text{K}^{-1}$
t_+	proton transport number	—
T	temperature	K

U	voltage	V
\dot{V}	volumetric flow rate	$\text{m}^3 \cdot \text{s}^{-1}$
\dot{W}	mechanical power	kW
x	mass flow rate ratio	—

Greek symbols

α	amplification factor	—
β	electro-osmosis coefficient	—
γ	maintenance factor	—
ε	exergy loss coefficient	—
η	efficiency	—
θ	heat recovery coefficient	—
σ	cost capacity factor	—
φ	fractional fission	%
χ	mole fraction	%
Δ	difference	—

Superscripts & Subscripts

0	ambient conditions	fis	fission	ph	physical
an	anode	fix	fixed	pp	pinch point
ann	annual	gen	generated	pro	product
ca	cathode	he	heat exchanger	ps	primary side
cap	capital	hf	hot fluid	rec	recoverable
cf	cold fluid	in	inlet	Ref	reference
ch	chemical	is	isentropic	sta	stack
con	consumption	m	mechanical	ter	terminal
CON	condenser	M	Motor	th	thermal
cp	circulating pump	max	maximum	tot	total
cv	control volume	mem	membrane		
cw	cooling water	min	minimum		
E	electricity	mn	mean		
eq	equilibrium	NPS	nuclear power system		
equ	equipment	out	outlet		
ex	exergy	O&M	operating and maintenance		

Chapter 1

Introduction

1.1 Research background

1.1.1 Nuclear energy and Generation IV reactors

Nowadays, research on the development and utilization of clean energy sources, including nuclear energy and renewable energy, has attracted more and more attention from scholars all over the world due to the increasing energy demand, decreasing fossil fuel reserves, serious environmental problems, and noticeable climate change. Since most renewable energy sources, such as solar energy and wind energy, are intermittent and highly dependent on weather conditions and geographic location [1], nuclear energy is considered to be the most promising carbon-free energy source to replace fossil energy on a large scale in the future [2].

As we all know, nuclear energy comes from two kinds of nuclear reactions, namely nuclear fission and nuclear fusion. The most common way to use nuclear energy peacefully is to generate electricity through the fission reactor technology, which has been widely investigated over the past several decades. Currently, there are approximately 440 commercial nuclear reactors in operation worldwide, generating about 11.5% of the world's total electricity [3]. In addition, there are more than 55 and 110 nuclear reactors under construction and planned, respectively. It is expected that the nuclear reactor capacity will double in 2030 [4]. Together, nuclear energy is now the largest scale energy source that does not emit CO₂ and any air pollutants, and can continue to be a major source of sustainable energy in the long term [4].

Most existing nuclear reactors are the third and earlier generations of nuclear reactors, mainly Light Water Reactors (LWRs, such as Pressurized Water Reactors (PWRs) and Boiling Water Reactors (BWRs)) with core outlet temperatures around 280-330°C. Due to the low reactor outlet temperature, the thermal efficiency of currently operating nuclear power plants is comparatively low, only about 30-35% [3]. In other words, about two-thirds of the nuclear heat is lost during the conversion process of heat to electricity, and is eventually dissipated into the environment. To improve system efficiency and use nuclear fuel more efficiently, six advanced nuclear reactors, better known as Generation IV reactors, have been proposed and are being actively developed for applications in the near future (2030+) [5]. Figure 1-1 shows a schematic diagram of the six advanced Generation IV nuclear reactor systems, and Table 1-1 summarizes some existing design parameters of the Generation IV reactors.

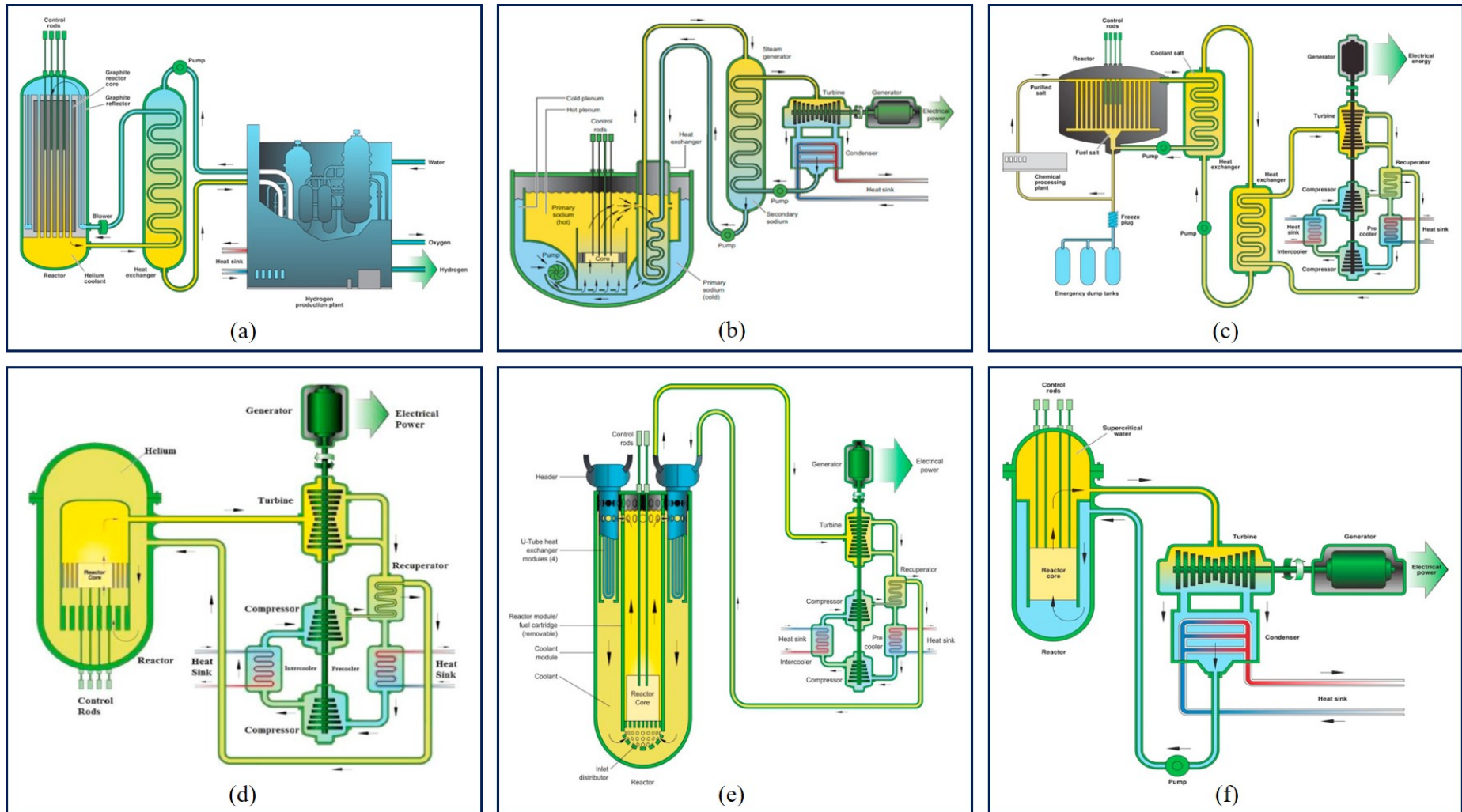


Figure 1-1. Schematic of six advanced Generation IV nuclear reactor systems (Reproduced from Ref. [3]): (a) Very High Temperature gas-cooled Reactor (VHTR), (b) Sodium-cooled Fast Reactor (SFR), (c) Molten Salt Reactor (MSR), (d) Gas-cooled Fast Reactor (GFR), (e) Lead-cooled Fast Reactor (LFR), and (f) Super-Critical Water-cooled Reactor (SCWR).

Table 1-1. Summary of some existing design parameters of the Generation IV reactors (Modified from Ref. [6]).

Parameters	VHTR	SFR	MSR	GFR	LFR	SCWR
Size (MWe)	250-300	50-150, 600-1500	1000 (fast) or 1000-1500 (thermal)	1200	20-180, 300-1200	300-700, 1000-1500
Fuel	UO ₂ prism or pebbles	U-238 and MOX	UF in salt (fast) or UO ₂ particles (thermal)	U-238 (with some U-235 or Pu-239)	U-238 (with some U-235 or Pu-239)	UO ₂
Fuel cycle	Open	Closed	Closed (fast) or Open (thermal)	Closed	Closed	Closed (fast) or Open (thermal)
Pressure ^a	High	Low	Low	High	Low	Very high
Core outlet temperature (°C)	900-1000	500-550	700-800 (fast) or 750-1000 (thermal)	850	480-570 (or 550-800 ^b)	510-625
Coolant	Helium	Sodium	Fluoride salts	Helium	Lead or Lead-bismuth eutectic	Water
Neutron spectrum	Thermal	Fast	Fast or Thermal	Fast	Fast	Fast or Thermal
Use	Electricity generation and hydrogen production	Electricity generation	Electricity generation and hydrogen production	Electricity generation and hydrogen production	Electricity generation and hydrogen production	Electricity generation and hydrogen production

^a High = 7-15 MPa.

^b Outlet coolant temperature range for advanced LFRs.

It can be seen from Table 1-1 that all these six advanced reactors can achieve a higher core outlet temperature than the traditional LWR, and among which the VHTR has the highest core outlet temperature of 900-1000°C. The significant increase in the reactor outlet temperature not only improves the thermal efficiency of nuclear power plants, but also creates the possibility of nuclear reactors for direct heat applications, such as hydrogen production [4].

1.1.2 Hydrogen and hydrogen economy

As the first chemical element of the Periodic Table of Elements, hydrogen is the lightest element and also is the most abundant element in the universe [7]. Although hydrogen is the most common chemical element on Earth, it is not found free in nature, but mainly exists in molecular compounds such as organic matters and water, because it can easily form covalent compounds with most non-metallic elements [6]. Hydrogen is an important clean energy carrier and has the highest energy content per unit mass among all fuels [8]. As a secondary energy source, hydrogen has many advantages, such as high heating value, environmental friendliness, renewability, and abundant element reserves, which conversely make it a very important chemical feedstock used widely in many sectors such as agricultural (fertilizer production), petrochemical, metallurgical, transportation, aerospace, synthetic fuels, and other industries. Figure 1-2 shows a schematic diagram of the relationship between hydrogen and various industries and energy sectors. It can be seen that hydrogen is a key link between various industries and energy sectors and plays an important role in integrating these sectors [10].

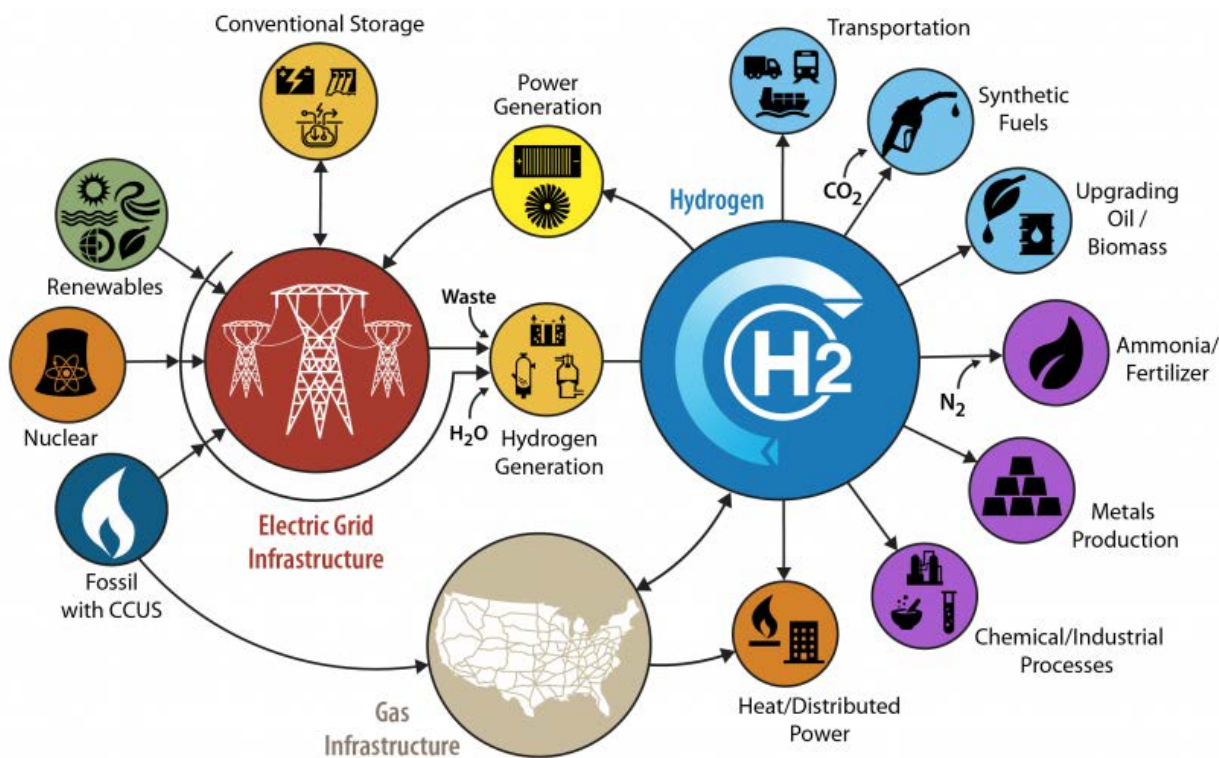


Figure 1-2. Schematic of the relationship between hydrogen and various industries and energy sectors [9].

At present, about 70 million tons of hydrogen are produced and consumed globally each year [7], and more than two-thirds of hydrogen is used to produce ammonia and refine petroleum [11]. As the world's population grows steadily, the demand for hydrogen will increase substantially in the near future. According to a report issued by Hydrogen Council in 2017, about 18% of the global energy demand will be supplied by hydrogen in 2050 [12]. As a result, hydrogen is today enjoying an unprecedented development momentum [13], and the development of hydrogen economy has become a common goal of many countries.

The so-called hydrogen economy (or hydrogen energy economy) refers to the economic infrastructure with hydrogen as the energy carrier, including the three functional links of hydrogen production, storage and transportation, and use, which run through all aspects of the economy [6]. Under the hydrogen economy, a large amount of hydrogen is produced and stored as a clean energy carrier to replace fossil fuels (e.g. coal, petroleum, and natural gas) used in today's fossil energy economy. However, more than 95% of the hydrogen currently produced is extracted from hydrocarbons through chemical reforming (in more detail, 18% from oil, 30% from coal, and 48% from natural gas [14]), and only about 4% of hydrogen is produced from water through electrolysis [15]. The current hydrogen production industry not only consumes a large amount of non-renewable fossil fuels, but also leads to massive CO₂ emissions [16]. To build a sustainable hydrogen economy, hydrogen should be produced using non-CO₂ emitting energy sources, such as renewable energy and nuclear energy. Given the intermittent nature of renewable energy, it is currently not economically feasible to produce hydrogen on a large scale [6]. Therefore, hydrogen production from nuclear energy will become a key technology for the development of hydrogen economy, and is attracting more and more attention from countries in the world.

1.1.3 Nuclear hydrogen production

Nuclear hydrogen production is to couple one or more nuclear reactors with a hydrogen production plant using an advanced hydrogen production process to achieve large-scale hydrogen production [17]. Generally, there are five main hydrogen production processes that can be coupled with nuclear reactors for large-scale hydrogen production: low-temperature electrolysis, high-temperature electrolysis, pure thermochemical water-splitting cycle, hybrid thermochemical water-splitting cycle, and chemical reforming [18]. Figure 1-3 shows a schematic diagram of potential pathways of nuclear hydrogen production, and Figure 1-4 presents a schematic diagram of possible integrations of different types of nuclear reactors with various hydrogen production processes based on operating temperature ranges. It can be seen that the VHTR with the highest reactor outlet temperature can be integrated with some high-temperature hydrogen production processes including High Temperature Steam Electrolysis (HTSE), Steam Methane Reforming (SMR), and Sulfur-Iodine (S-I or SI) thermochemical water-splitting cycle, while the traditional LWR with low reactor outlet temperatures can only be coupled with low-temperature electrolysis processes such as alkaline electrolysis and Polymer Electrolyte Membrane Electrolysis (PEME).

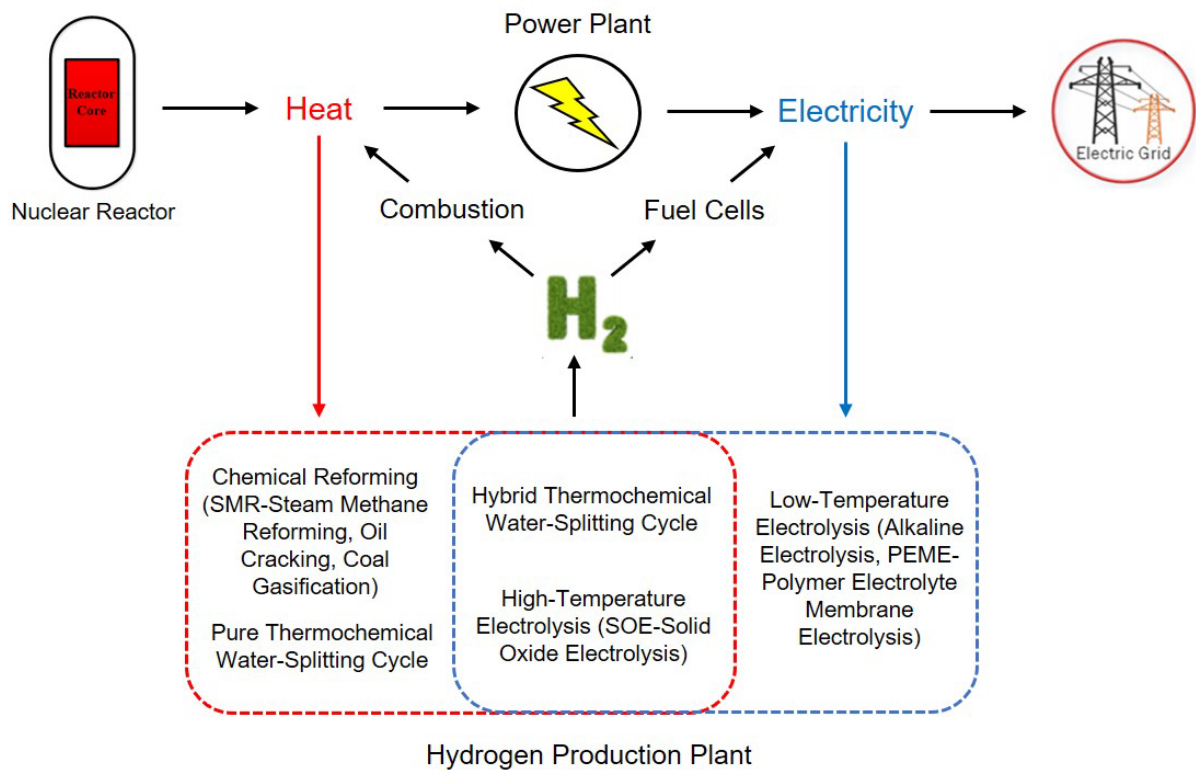


Figure 1-3. Schematic of potential pathways of nuclear hydrogen production.

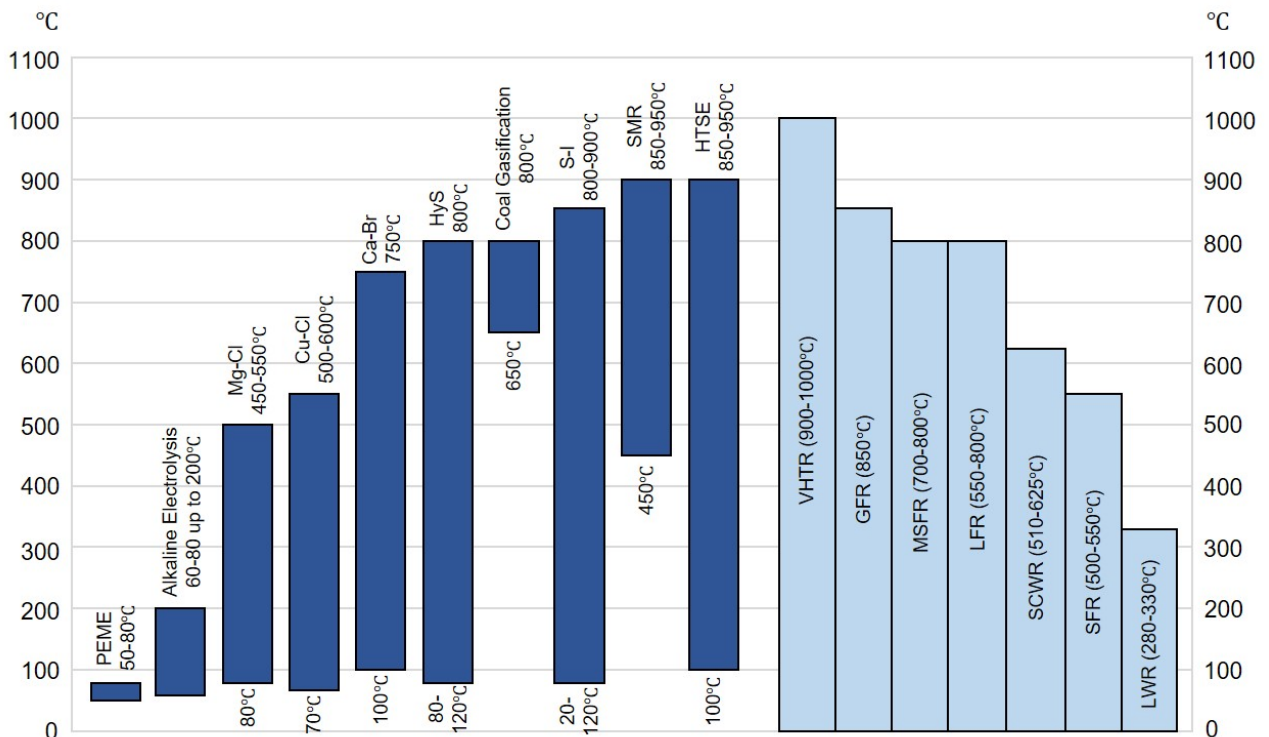


Figure 1-4. Schematic of possible integrations of different types of nuclear reactors with various hydrogen production processes based on operating temperature ranges (Modified from Ref. [13]).

Table 1-2 gives a performance comparison of different nuclear hydrogen production methods. It can be seen that both HTSE and thermochemical water-splitting processes can achieve a higher overall hydrogen production efficiency than low-temperature electrolysis, because part of the nuclear heat is directly used for the hydrogen production process without undergoing the conversion stage of heat to electricity. However, due to the challenges of high temperature and/or corrosive operating environments, these two technologies have not yet been commercialized, requiring further Research and Development (R&D). In addition, although the SMR-based nuclear hydrogen production method is highly efficient and technologically mature, the consumption of natural gas and the consequent CO₂ emissions make it not a green and sustainable large-scale hydrogen production route. Anyway, by integrating nuclear reactors with advanced water-splitting hydrogen production processes (such as electrolysis or thermochemical cycles), nuclear energy will become a very promising energy source for large-scale carbon-free hydrogen production.

Table 1-2. Performance comparison of different nuclear hydrogen production methods (Modified from Ref. [6]).

Performance	Low-temperature electrolysis	HTSE	SMR	Thermochemical water-splitting cycles
Process efficiency of H ₂ production	75-80%	85-90%	70-80%	>30% ^c
Overall efficiency (coupled to LWR)	25-27% ^a	28-30% ^a	Not feasible	Not feasible
Overall efficiency (coupled to HTGR)	<40%	40-60% ^b	>70%	30-60% ^c
Advantages	Proved technology; No CO ₂ emissions; No fossil fuels consumed	No CO ₂ emissions; No fossil fuels consumed	Proved technology; High efficiency	No CO ₂ emissions; No fossil fuels consumed
Disadvantages	Low efficiency	Immature technology	Emitting CO ₂ ; Consuming natural gas	Immature technology

^a Based on an electricity generation efficiency of 33% for today's LWRs.

^b Depending on electrolysis temperature.

^c Depending on cycle type and process flow (or design).

In addition to enabling large-scale carbon-free hydrogen production, nuclear hydrogen production can also help nuclear power plants improve their load-following capability and cost competitiveness [19]. As shown in Figures 1-2 and 1-3, hydrogen can be produced as an energy storage medium during off-peak electricity consumption periods or converted into electricity through fuel cells or turbine power generation technologies during peak electricity consumption periods, thereby helping nuclear power plants match the electricity production curve with the demand curve [20]. Additionally, with the advent of hydrogen economy, hydrogen will develop its own market where it can be converted into electricity and then sold to electricity grid, or sold as a commodity to hydrogen-consuming industries such as transportation, chemical plants, etc. [20]. Accordingly, by using excess nuclear heat or cheap off-peak electricity to produce hydrogen, the economics of nuclear power plants can be improved. In short, conducting an in-depth study on nuclear hydrogen production technology is of great academic significance for building a sustainable hydrogen economy and ensuring a safe and clean energy future.

1.2 Research status

1.2.1 Global interest in nuclear hydrogen production

Given that nuclear hydrogen production is a very promising technology to achieve large-scale hydrogen production and plays a key role in developing hydrogen economy and ensuring energy security, many countries and regions, including Argentina, Canada, China, European Union, France, India, Japan, Russia, South Africa, South Korea, the United Kingdom, and the United States, are currently conducting research on nuclear hydrogen production technology as part of their national hydrogen energy development strategies. Table 1-3 summarizes some nuclear hydrogen production R&D activities around the world.

Table 1-3. Some nuclear hydrogen production R&D activities around the world.

Country	R&D activities
Argentina	R&D activities are mainly focused on two hydrogen production processes: (1) Coal gasification and (2) Metallic chloride-based thermochemical cycles [6]; Theoretical and experimental studies on the performance of several metallic chloride thermochemical cycles have been performed to figure out the mechanisms and kinetics of these cycles and to improve the energy efficiency and hydrogen yield of these cycles as a step for the future scaling up of the experimental facility [6,21].
Canada	R&D activities are mainly focused on integrating Canadian Generation IV SCWRs (e.g., the advanced CANDU (CANada Deuterium-Uranium) reactor) with Copper-Chlorine (Cu-Cl) thermochemical cycles [6,22]; The main sub-processes of the Cu-Cl thermochemical cycle have been experimentally investigated and verified [23], and an integrated

	laboratory-scale Cu–Cl facility (with a hydrogen production capacity of 100 g/day) is under examination [24].
China	R&D activities are mainly focused on integrating High Temperature Gas-cooled Reactors (HTGRs) with two hydrogen production processes: (1) HTSE and (2) S-I thermochemical cycle [25]; The world's first commercial pebble-bed modular high temperature gas-cooled reactor (i.e., the HTR-PM) was been successfully commissioned in 2021, and the 600MWe multi-modular high temperature reactor (i.e., the HTR-PM600) is now under development [26]; A HTSE system (10-cell stack) with a hydrogen production capacity of 105 NL/h has been running stably for 62 hours, and the design of 30-cell stack is in progress [23]; A laboratory-scale S-I facility with a hydrogen production rate of 60 NL/h was successfully operated for 60 hours in 2014 [27], and a pilot-scale S-I facility made by industrial structural materials was been experimentally tested in 2021 [28].
European Union	During 2005-2010, the nuclear hydrogen project - Reactor for Process Heat, Hydrogen, and Electricity Generation Integrated Project was carried out, which aimed to study advanced gas-cooled reactor technologies required for industrial reference designs; R&D activities on hydrogen production technologies have focused on CO ₂ -neutral or CO ₂ -free processes such as biomass conversion, thermochemical cycles (e.g., the S-I cycle and the Westinghouse cycle or Hybrid Sulfur (HyS) cycle), and fossil fuels reforming with CO ₂ sequestration [6].
France	France is involved in different European programs on HTGR and hydrogen production [6]; In early 2000s, R&D activities on nuclear hydrogen production were mainly focused on HTSE and high-temperature thermochemical cycles (e.g., the S-I cycle and the Westinghouse cycle), and current interest focuses on water electrolysis combined with small and large modular reactors to obtain low-carbon hydrogen for industrial applications [29].
India	R&D activities on hydrogen production technologies have focused on water electrolysis [30], steam electrolysis [31], intermediate-temperature thermochemical cycles (e.g., the Cu-Cl cycle [32]), and high-temperature thermochemical cycles (e.g., the S-I cycle [33]); The development of advanced high-temperature molten salt or liquid metal cooled reactors to support high-temperature nuclear hydrogen production and other industrial applications is also underway [34].
Japan	R&D activities are mainly focused on integrating the VHTR with the S-I thermochemical cycle; The 30MWth High Temperature Test Reactor (HTTR) developed by the Japan Atomic Energy Agency (JAEA) achieved the first criticality in 1998 [6,21], and in recent years, a series of studies on the first-of-a-kind nuclear hydrogen production test plant (i.e., the HTTR-GT/H ₂ test plant using the HTTR, helium Gas Turbine (GT), and the S-I thermochemical cycle) have been carried out to accelerate the development of the commercial Gas Turbine High Temperature Reactor 300-Cogeneration (GTHTR300C) system [35,36].
Russia	In the short term, R&D activities are mainly focused on SMR with heat supply from HTGRs [6,37]; In the long term, more attention will be

	paid to water-splitting nuclear hydrogen production methods, such as HTSE, thermochemical cycles, thermo-electrochemical cycles, and various combined methods for producing hydrogen from water [37].
South Africa	R&D activities are mainly focused on two nuclear hydrogen production pathways: (1) SMR with heat supply from HTGRs and (2) HTSE and thermochemical cycles (e.g., the Westinghouse cycle) integrated with the Pebble Bed Modular Reactor (PBMR) [6].
South Korea	R&D activities are mainly focused on integrating the VHTR with the S-I thermochemical cycle [38]; The Korea Atomic Energy Research Institute (KAERI) has developed a national plan to demonstrate large-scale production of hydrogen using a VHTR by the early 2020s [39]; South Korea has built a bench-scale S-I test facility with a hydrogen production capacity of 50 NL/h [40].
United Kingdom	As part of its recently announced national hydrogen strategy, the possibility of developing and deploying nuclear hydrogen production in SMR and advanced nuclear reactors is under review [29].
United States	R&D activities are mainly focused on: (1) Electrolysis combined with existing water-cooled reactors (e.g., PWRs) and small modular reactors based on Generation IV design concepts [29] and (2) The integration of HTGRs (or VHTRs) and high-temperature hydrogen production processes such as HTSE, S-I thermochemical cycle, and HyS cycle [6,41]; Plans to produce nuclear hydrogen at three power plant sites in the near term (within 2025) and distribute it to on-site users and co-located steel production industrial facilities [29,42].

It can be seen from Table 1-3 that many nuclear hydrogen production R&D activities currently conducted are related to various thermochemical water-splitting cycles (e.g., the S-I cycle, the HyS cycle, and the Cu-Cl cycle), which indicates that the thermochemical water-splitting cycle-based nuclear hydrogen production technology is attracting global attention as a recognized large-scale clean hydrogen production method.

1.2.2 Thermochemical water-splitting cycles

Thermochemical water-splitting cycles are based on water decomposition process where the water molecule is dissociated into hydrogen and oxygen through a set of chemical reactions using intermediate substances which are recycled during the process [18,43]. Thermochemical water-splitting cycles are divided into two types: pure thermochemical cycles and hybrid thermochemical cycles. The key difference between pure thermochemical cycles and hybrid thermochemical cycles is that the former requires only the support of thermal energy whereas the latter requires the support of thermal energy and another form of energy such as electrical or photonic energy [10]. In theory, water can be directly decomposed into hydrogen and oxygen by one-step pyrolysis, which is the simplest thermochemical process. However, the one-step pyrolysis of water takes place at temperatures higher than 4000°C [44], and the issues including undesirable thermodynamics and a lack of high-temperature

resistant materials make this process practically infeasible. Therefore, the more common thermochemical water-splitting cycle is considered a set of chemical reactions in which water is decomposed at temperatures below 2000°C and usually in two or multi steps [45].

R&D activities on thermochemical water-splitting cycles were initiated by Funk and Reinstrom [46] in the 1960s, and by the end of the 1960s, more than 19 publications had been published on thermochemical water-splitting cycles suitable for nuclear hydrogen production [47]. In 1969, the first conference on hydrogen production based on thermochemical water-splitting cycles was held in Ispra, Italy, and 24 cycles (the so-called Mark cycles) were identified to be studied during 1970 to 1983 [48]. Since then, many theoretical and experimental studies have been carried out and various thermochemical water-splitting cycles have been proposed. Although more than 200 kinds of thermochemical water-splitting cycles have been proposed for hydrogen production up to now, very few of them are identified to have the ability of producing hydrogen on a large scale [10]. Among these cycles, the S-I cycle, the HyS cycle, and the Cu-Cl cycle are three most famous and well-studied thermochemical water-splitting cycles, which are very promising to be integrated with a Generation IV nuclear reactor for large-scale carbon-free hydrogen production in the near future.

The S-I (or I-S) cycle proposed by General Atomics in the mid-1970s [44] is the most developed thermochemical water-splitting cycle [49], which shows great potential in nuclear hydrogen production when integrated with the HTGR or VHTR. R&D activities on the S-I cycle have been carried out by many celebrated research institutions, such as the JAEA in Japan [50], the Institute of Nuclear and New Energy Technology (INET) of Tsinghua University in China [51], General Atomics, Sandia National Laboratory (SNL) in the United States [52], Commissariat à l'Énergie Atomique (CEA) in France [53], and the KAERI in South Korea [54]. JAEA has been studying the S-I cycle since the mid-1980s, and in 1997, a laboratory-scale S-I system made of glass equipment was built, producing hydrogen continuously for 48 hours at a rate of 1 NL/h [55]. During 1999-2005, JAEA had completed the research on the design, construction, and operation of a bench-scale experimental S-I facility for hydrogen production at a rate of 50 NL/h [18]. In 2004, a bench-scale S-I facility with a hydrogen production rate of 31 NL/h was continuously operated for one week [56], which first confirmed the controllability and feasibility of the closed S-I process. In 2020, a S-I test facility made of industrial structural materials was successfully operated for 150 hours at a rate of 30 NL/h [57], which is considered a milestone of the S-I cycle in practical industrial applications [28]. INET initiated research on the S-I cycle since 2005, and many fundamental studies on the three main chemical reactions in the S-I cycle (namely the Bunsen reaction, the H₂SO₄ decomposition reaction, and the HI decomposition reaction) had been carried out during 2005-2007 [18]. At the end of 2008, a proof-of-concept closed-loop S-I test facility with a hydrogen production capacity of 10 NL/h (the so-called IS-10) was designed and built [58], which was continuously operated for seven hours in 2009 [59]. In 2014, an integrated laboratory-scale S-I facility with a hydrogen production capacity of 100 NL/h (the so-called IS-100) was designed and built at INET, and more than 60 hours of continuous hydrogen production at a rate of 60 NL/h was successfully performed in this facility [27,51]. At present, INET is focused on developing a pilot-scale S-I facility made of engineering materials. In addition to the

above-mentioned R&D activities, an integrated laboratory-scale S-I facility made of engineering materials was jointly developed by General Atomics, SNL, and CEA [52], and a bench-scale S-I test facility with a hydrogen production capacity of 50 NL/h was designed and built at KAERI [40,54].

The HyS cycle, also known as the Westinghouse cycle or ISPRA Mark 11 cycle, is the most well-known hybrid thermo-electrochemical water-splitting cycle, which was originally developed by Westinghouse electric corporation in the 1970s for large-scale hydrogen production [60]. The HyS cycle is also the first demonstrated hybrid thermochemical water-splitting cycle with only two reactions which are the thermal decomposition of H_2SO_4 (i.e., $\text{H}_2\text{SO}_4 \rightarrow \text{SO}_2 + \text{H}_2\text{O} + 0.5\text{O}_2$) and the electrochemical oxidation of SO_2 with H_2O (i.e., $\text{SO}_2 + 2\text{H}_2\text{O} \rightarrow \text{H}_2\text{SO}_4 + \text{H}_2$), respectively [10,61]. Compared to the S-I cycle, the HyS cycle has a simpler process flow, which requires about 180 kJ of thermal energy and 55-80 kJ of electrical energy to produce one mole of hydrogen [13]. The early studies of the HyS cycle were conducted at Westinghouse in the 1970s and 1980s [62-64], and during the same period, the European Joint Research Centre and the German Nuclear Research Centre [65,66] also carried out research on this cycle [13]. In recent years, Savannah River National Laboratory has conducted extensive research on flowsheet simulation and component development of the HyS cycle [67-69]. Although many issues have been addressed through various R&D activities, the HyS cycle still faces some challenges, including SO_2 depolarization, SO_2 transport through the membrane, catalyst activity and degradation, and high-corrosion resistant materials [13].

The Cu-Cl cycle is another very famous hybrid thermo-electrochemical water-splitting cycle, which was first proposed by Dokyia et al. [70] in 1976. After that, the U.S. Institute of Gas Technology conducted further research on the hydrolysis of cupric chloride [71], and in 1992, Sim et al. [72] proposed some thermochemical cycles composed of copper compounds with three-step reactions. By the beginning of the 21st century, there was a growing interest in the Cu-Cl cycle, mainly through the collaboration of Atomic Energy of Canada Limited, the University of Ontario Institute of Technology in Canada, Argonne National Laboratory, and other partner institutes within the framework of the Generation IV International Forum (GIF) [47]. Different from the S-I cycle and the HyS cycle, the Cu-Cl cycle has several different cycle configurations depending on the number and type of chemical reactions in the cycle, such as the three-step Cu-Cl cycle, the four-step Cu-Cl cycle, and the five-step Cu-Cl cycle [17]. In addition, the thermal energy temperature requirement of the Cu-Cl cycle is generally less than 550°C (according to Ref. [73], the maximum required thermal energy temperature by the Cu-Cl cycle is about 530°C), which is significantly lower than that of the S-I cycle and the HyS cycle. Therefore, in terms of coupling with various Generation IV nuclear reactor types, the Cu-Cl cycle has more possibilities than the S-I cycle and the HyS cycle. For example, the Cu-Cl cycle has been proposed to be integrated with a Generation IV SCWR [20,73] and LFR [74] for large-scale nuclear hydrogen production. Up to now, many experimental and simulation studies on the main sub-reactions of the Cu-Cl cycle have been conducted, and an integrated laboratory-scale Cu-Cl facility (with a hydrogen production capacity of 100 g/day) is under examination [24]. Besides this, all kinds of analysis methods, including energy & exergy analysis [75,76], exergoeconomic & exergoenvironmental analysis [77], specific exergy costing analysis [78], and life cycle

assessment [79,80], have been used to analyze and assess the performance of various Cu-Cl cycles. Despite recent progress in the demonstration of an integrated laboratory-scale Cu-Cl facility, further development of a pilot-scale plant is required before this cycle can take a solid step towards commercialization [13].

Besides the above three cycles, there are some other promising thermochemical water-splitting cycles under R&D, such as the Calcium-Bromine (Ca-Br) cycle (i.e., the UT-3 cycle, developed by the University of Tokyo of Japan), the Magnesium-Chlorine (Mg-Cl) cycle, the Iron-Chlorine (Fe-Cl) cycle, the Cobalt-Chlorine (Co-Cl) cycle, the Vanadium-Chlorine (V-Cl) cycle, and the ZnO/Zn cycle. However, research on these cycles is progressing slowly, and some cycles still face many uncertainties and challenges regarding the chemical kinetics, thermodynamics, and side reactions [13].

1.2.3 The coupled VHTR and S-I cycle nuclear hydrogen production system

As mentioned above, the S-I cycle is the most well-known and developed thermochemical water-splitting cycle, which has been successfully verified for continuous hydrogen production in a laboratory-scale test facility made of industrial structural materials and is moving towards the pilot-scale plant demonstration. Since the maximum required thermal energy temperature by the S-I cycle is around 800-900°C, the VHTR with a reactor outlet temperature of 950°C (or even higher [81]) is considered the most suitable reactor type for hydrogen production integrated with the S-I cycle. Nowadays, with the commissioning and completion of advanced HTGRs (e.g., the HTR-PM), R&D activities on the VHTR and S-I cycle-based nuclear hydrogen production system are being actively carried out around the world.

Generally, a nuclear hydrogen production system is composed of four main parts: nuclear reactor, Intermediate Heat eXchanger (IHX), hydrogen production plant, and power conversion system [82]. Figure 1-5 shows a schematic diagram of the VHTR and S-I cycle-based nuclear hydrogen production system. Depending on the S-I process configuration, thermodynamic cycle type, and overall system layout, some different designs have been proposed for nuclear hydrogen production systems based on the VHTR and S-I cycle. For instance, Qu et al. [18] designed two different VHTR and S-I cycle-based nuclear hydrogen production systems in which the Steam Rankine Cycle (SRC) was adopted as the power conversion system. To achieve the cascade utilization of high-grade thermal energy, the S-I hydrogen production plant and the SRC power conversion system were placed in series. Their thermodynamic analysis results showed that when the hydrogen production load was equal to 100 mol/s, the proposed two systems could achieve thermal efficiencies of 43.6% and 39.2%, respectively. In addition, they investigated the effects of the hydrogen-electricity ratio on the exergy efficiency of the overall system, and found that the system exergy efficiency decreased with the increase of the hydrogen-electricity ratio [83]. Similarly, Ni et al. [84] proposed and investigated a novel VHTR and S-I cycle-based hydrogen-electricity-heat polygeneration system with a supercritical reheated SRC as the power conversion system. It was reported that by connecting the S-I hydrogen production plant and the SRC power conversion system in series, the proposed polygeneration system could simultaneously produce 183.57 mol/s of hydrogen, 48.78 MW of electricity, and 26.92 MW of heat. Besides this, the series

layout was also adopted by the JAEA's HTTR-GT/H₂ test plant [35] and GTHTTR300C system [85], however, the power conversion system is no longer the SRC but the helium Brayton cycle.

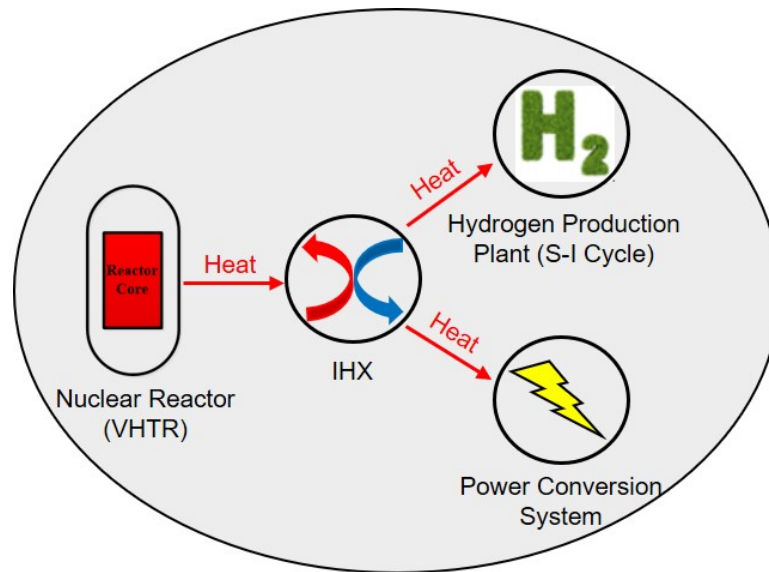


Figure 1-5. Schematic of the VHTR and S-I cycle-based nuclear hydrogen production system.

In addition to the series layout, the hydrogen production plant and the power conversion system can also be arranged in parallel or mixed. For example, González Rodríguez et al. [86] proposed a VHTR and S-I cycle-based nuclear hydrogen production system where the helium Brayton cycle was used as the power conversion system deployed in parallel with the S-I hydrogen production plant. The calculation results showed that the helium Brayton cycle could achieve a power generation efficiency of 53.27% and the S-I plant could achieve a hydrogen production efficiency of 22.56%. Jaszczur et al. [87] proposed and analyzed a VHTR and S-I (or Cu-Cl) cycle-based nuclear hydrogen production system which uses the Gas-Steam Combined Cycle (GSCC, namely topping gas Brayton cycle plus bottoming SRC) as the power conversion unit. It was calculated that by adopting the parallel layout, the proposed system could achieve a thermal efficiency of approximately 50%. Jędrzejewski et al. [88] proposed and investigated two novel HTGR and S-I cycle-based nuclear hydrogen production systems which use the combined helium Brayton cycle and Organic Rankine Cycle (ORC) as the power conversion system. In order to realize the cascade utilization of the high-grade thermal energy of the reactor, the power conversion units and hydrogen production units in these two systems were alternately placed in a mixed layout. The investigation results showed that the two hydrogen and electricity cogeneration systems could achieve thermal efficiencies of 36.0% and 37.5%, respectively.

In addition to system design and thermodynamic analysis, economic analysis is also an important and essential work, because entrepreneurs and investors are more concerned about the hydrogen production cost of the system. However, the nuclear hydrogen production system usually has very complex system configurations (especially the thermochemical hydrogen production part), which brings great

difficulties to economic analysis. On the other hand, due to the immaturity of the technology, the actual data available are very limited. Moreover, some factors, such as the size of system capacity, price fluctuations, governmental policies and regulations, etc., also have great impact on the final economic analysis results. Heretofore, several studies have been conducted on the economic analysis of the VHTR and S-I cycle-based nuclear hydrogen production system. For instance, Brown et al. [89] performed a comprehensive economic assessment of a modular helium reactor and S-I cycle-based nuclear hydrogen production system. To obtain the system capital cost as accurate as possible, they calculated the sizes of major chemical plant components while determining the corresponding structures and materials. In addition, they also considered various operating costs such as operating labor, supervisory and clerical labor, maintenance and repairs, operating supplies, laboratory charges, taxes, and administrative costs. The economic analysis results showed that the system could achieve a hydrogen production cost of \$1.42-2.01/kg, which was highly dependent on the capital cost of the system. Botterud et al. [90] of Argonne National Laboratory roughly estimated the levelized cost of hydrogen production for three different nuclear hydrogen production systems: HPE-ALWR (i.e., High Pressure Electrolysis-Advanced Light Water Reactor), HTSE-HTGR, and SI-HTGR. The estimation results showed that the SI-HTGR system was more economic with a hydrogen production cost of \$2.26/kg versus the HTSE-HTGR system at \$2.51/kg and the HPE-ALWR system at \$2.91/kg. Cerri et al. [91] performed a conceptual design and economic analysis of a S-I thermochemical hydrogen production plant matched to a 600 MWth VHTR system. The economic analysis results showed that the plant could achieve a hydrogen production cost of \$4-6.4/kg, which was strongly affected by the adopted technologies. In addition, Lee et al. [92] also conducted a cost assessment study on the S-I chemical plant coupled with a VHTR, and the estimation results showed that the hydrogen production cost was about \$5.36/kg. Recently, two review articles on thermochemical water-splitting hydrogen production have been published, in which the hydrogen production cost of the nuclear-powered S-I process was reported to be in the range of \$2.46-5.65/kg [13,93].

1.3 Research gaps, objectives and main work

1.3.1 Research gaps

From the above literature review, it can be seen that nuclear hydrogen production is a very important technology for the development of hydrogen economy and the construction of safe, clean and sustainable energy future. The VHTR, as a typical Generation IV reactor, has the highest core outlet temperature, and is recommended as the most suitable reactor type for hydrogen production. The S-I cycle that has been widely studied during the past several decades, is considered the most promising thermochemical water-splitting cycle integrated with a VHTR for large-scale clean hydrogen production. So far, some studies on the design and thermodynamic analysis of nuclear hydrogen production systems based on VHTR and S-I cycle have been

carried out. In addition, several studies were conducted to evaluate the economic performance of the system. Although these studies have promoted the development of the VHTR and S-I cycle-based nuclear hydrogen production system to a certain extent, the thermo-economic characteristics and performance-influencing mechanisms of the system are still not fully elucidated. A more in-depth and comprehensive research is urgently needed to fill the following research gaps:

- (1) The existing research on the design and optimization of the S-I hydrogen production process is very limited. As we all know, the S-I thermochemical cycle is composed of three sub-chemical reactions, and each sub-chemical reaction contains some process components, which ultimately leads to a complex process configuration. Although many experimental and numerical studies have been performed on the S-I thermochemical cycle, most studies are focused on the mechanism analysis of the three sub-chemical reactions, and only few studies are related to the design and analysis of the entire hydrogen production process. In addition, the existing research on the process optimization of the S-I hydrogen production system is also insufficient, especially the research on the design and analysis of the internal heat exchange network.
- (2) The thermodynamic characteristics of the VHTR and S-I cycle-based nuclear hydrogen production system with GSCC as the power cycle are still unclear. As mentioned in Section 1.2.3, most of the existing system designs employed the SRC or helium Brayton cycle as the power conversion unit of the VHTR and S-I cycle-based nuclear hydrogen production system, and only one study (i.e., Ref. [87]) proposed to use the GSCC as the power cycle of the system. In view of the great potential of the GSCC to achieve high power generation efficiency, it is necessary to carry out an in-depth study to comprehensively understand the thermodynamic characteristics of the nuclear hydrogen production system with GSCC as the power cycle.
- (3) The existing research lacks the integrated design of the system. As mentioned earlier, the VHTR and S-I cycle-based nuclear hydrogen production system usually has a very complex system configuration. In order to reduce the difficulty in modeling the entire nuclear hydrogen production system, most of the previous studies divided the whole nuclear hydrogen production system into several sub-modules for individual modeling and analysis (that is, the whole system was studied by means of sub-module analysis). However, the sub-module analysis method cannot reflect the coupling effect between different sub-modules, so the actual system characteristics cannot be fully demonstrated and the obtained simulation results may not be used to guide actual engineering. In this case, it is necessary to carry out the system integrated design to further calibrate the simulation results obtained by the sub-module analysis.
- (4) The existing research on the economic performance of the VHTR and S-I cycle-based nuclear hydrogen production system is still insufficient. As mentioned in Section 1.2.3, few studies have been performed on the economic analysis of the VHTR and S-I cycle-based nuclear hydrogen production system, mainly due to the complex system configuration and the lack of available actual data. Additionally, due to various impact factors, the economic estimation results in

these studies are also significantly different. To the best of the author's knowledge, there is little research on the cost-influencing mechanism of the nuclear hydrogen production system. Therefore, it is necessary to conduct an in-depth study to figure out the economic characteristics of the VHTR and S-I cycle-based nuclear hydrogen production system.

1.3.2 The objectives and main work of this thesis

The objectives of this thesis are to fill the above-mentioned research gaps and enrich the existing research on the design, thermodynamic analysis and economic assessment of the VHTR and S-I cycle-based nuclear hydrogen production system. To achieve these objectives, this thesis has carried out the following work:

- (1) A complete S-I thermochemical hydrogen production system was designed and modeled using the commercial chemical process simulation software Aspen Plus, and the energy consumption and efficiency of the system were further analyzed and discussed according to the obtained simulation results. In addition, based on the energy cascade utilization principle, an internal heat exchange network was initially designed to improve the performance of the S-I hydrogen production system. This work is implemented in Chapter 2, which aims to fill the first research gap mentioned in the previous section.
- (2) The conventional VHTR and S-I cycle-based nuclear hydrogen production system with GSCC as the power conversion unit was modeled and analyzed, based on the first and second laws of thermodynamics. In addition, the effects of several key operating parameters on the performance of the system were investigated, and a new system layout was proposed to further improve the thermodynamic performance of the conventional system. This work is implemented in Chapter 3, which aims to fill the second research gap mentioned in the previous section.
- (3) According to the preliminary investigation results obtained in Chapter 2 and Chapter 3, the system layout improvement and integration design were further carried out, and two complete system design schemes were finally formulated. In addition, the thermodynamic efficiencies of the system under the two different design schemes were also calculated and analyzed. This work is implemented in Chapter 4, which aims to fill the third research gap mentioned in the previous section.
- (4) A complete economic model of the VHTR and S-I cycle-based nuclear hydrogen production system was developed, based on some existing equipment investment cost equations and the six-tenths-factor rule (a scaling method). The cost distribution of the system was analyzed, and the unit hydrogen production cost of the system under different operating conditions was calculated. Moreover, the relationship between several key parameter variables and the cost of hydrogen production was also investigated. This work is implemented in Chapter 5, which aims to fill the last research gap mentioned in the previous section.
- (5) Based on the obtained results, some important conclusions were summarized in Chapter 6. In addition, some interesting research directions were also pointed out in this chapter, as the end of the thesis.

Chapter 2

Design and analysis of the S-I thermochemical hydrogen production system

In this chapter, a complete S-I thermochemical hydrogen production system was first designed and modeled using the commercial chemical process simulation software Aspen Plus. Then, the process simulation and performance analysis of the S-I system were performed. Lastly, according to the energy cascade utilization principle, an internal heat exchange network was manually designed to reduce system energy consumption and improve system efficiency. This chapter aims to enrich the existing research on the S-I thermochemical hydrogen production process and promote future applications of the S-I cycle.

2.1 Design and modeling of the S-I system

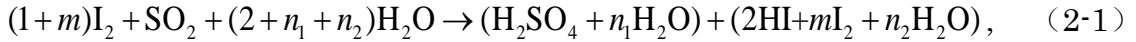
2.1.1 Design of the S-I system

Figure 2-1 presents a schematic diagram of the S-I thermochemical cycle coupled with a VHTR or HTGR. It can be seen that the S-I thermochemical cycle is equivalent to splitting water into hydrogen and oxygen through three intermediate reactions: the Bunsen reaction, the H_2SO_4 decomposition reaction, and the HI decomposition reaction.

The Bunsen reaction is an exothermic reaction that occurs in the temperature range of 20-120°C. The H_2SO_4 decomposition reaction is an endothermic reaction that is accomplished in two stages: (1) gaseous H_2SO_4 is first decomposed into H_2O and SO_3 at 400-500°C; (2) the resulting SO_3 is then catalytically decomposed into SO_2 and O_2 at 800-900°C. The HI decomposition reaction is also an endothermic reaction in which gaseous or liquid HI is decomposed into I_2 and H_2 at 300-500°C. Based on these cycle characteristics and existing process designs, a complete S-I thermochemical hydrogen production system was developed, as shown in Figure 2-2. It is seen that the designed S-I system consists of three sections which are respectively the Bunsen section, the H_2SO_4 concentration and decomposition section, and the HI concentration and decomposition section.

In the Bunsen section, the feed water from ambient conditions (Stream 1) is pressurized and heated before being sent to the BUNSEN reactor where it reacts

with the recycled materials including SO₂ and I₂, and generates two immiscible acid solutions (i.e., H₂SO₄ and HI) according to the following chemical equation [95]:



where m , n_1 and n_2 are three variable coefficients, which are determined according to the process operation requirements. It should be noted that in order to obtain two immiscible acid solutions, the reactants H₂O and I₂ in the above chemical equation should be in excess.

After completing the Bunsen reaction, the resulting immiscible H₂SO₄ and HI solutions (Stream 8) are separated by L-L-SEP (a liquid-liquid separator) on the basis of density differences. Then, the heavy phase (Stream 9, namely the HI_x phase consisting of H₂O, HI, I₂, and a little amount of H₂SO₄) and the light phase (Stream 10, namely the H₂SO₄ phase consisting of H₂O, H₂SO₄, and a little amount of HI and I₂) are respectively purified in HIPUR (the HI purification tower) and H₂SO₄PUR (the H₂SO₄ purification tower) through the reverse Bunsen reaction, and the impurities (Streams 6 and 7) are sent back to the BUNSEN reactor for recycling.

In the H₂SO₄ concentration and decomposition section, the purified H₂SO₄ phase (Stream 16) is first concentrated in H₂SO₄DST (the H₂SO₄ distillation column) to increase the concentration of H₂SO₄. Then, the top gaseous distillates (Stream 17) are returned to the BUNSEN reactor via BLOWER, while the bottom high-concentration H₂SO₄ solution (Stream 19) is further heated to the H₂SO₄ decomposition temperature via HEATER2. As mentioned earlier, the H₂SO₄ decomposition process is accomplished in two steps: (1) gaseous H₂SO₄ is first decomposed into H₂O and SO₃ in H₂SO₄DEC (the H₂SO₄ decomposition reactor); (2) the generated SO₃ is then decomposed into SO₂ and O₂ in SO₃DEC (the SO₃ decomposition reactor). Lastly, the undecomposed SO₃ reacts with H₂O in SO₃ABS (the SO₃ absorber) and turns into H₂SO₄ that is incorporated into H₂SO₄DST for recycling, as depicted in Figure 2-2.

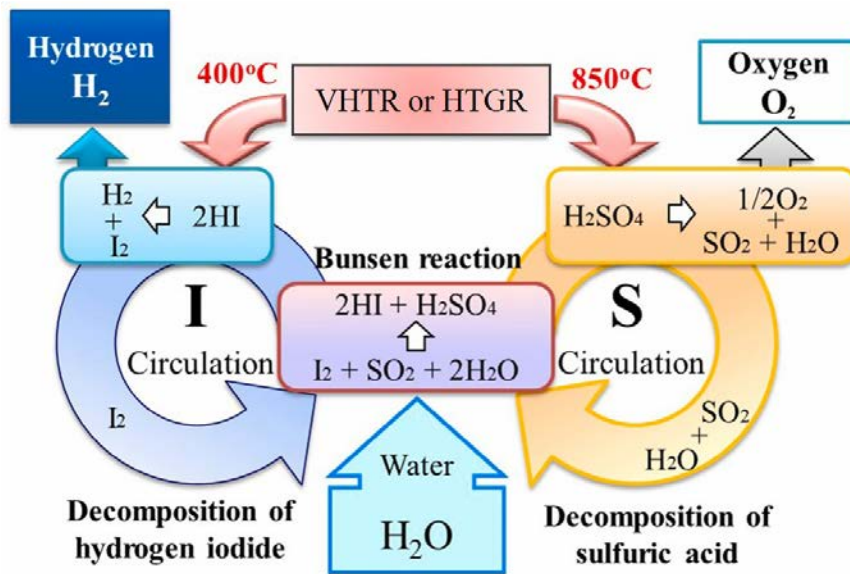


Figure 2-1. Schematic of the S-I thermochemical cycle coupled with a VHTR or HTGR (Modified from Ref. [94]).

The HIx phase obtained from the Bunsen section (Stream 14) is essentially a ternary pseudo-azeotropic mixture, which means that the traditional distillation method is unavailable to extract high-purity HI from the HIx phase [96]. Therefore, the primary task of the HI concentration and decomposition section is to produce high-purity HI vapor or solution. Up to now, three promising methods, including extractive distillation, Electro-ElectroDialysis (EED) and distillation, and reactive distillation, have been proposed for the HI concentration and decomposition section [97,98], as shown in Figure 2-3. The extractive distillation method proposed by General Atomics employs phosphoric acid (H_3PO_4) as the extractant to induce the separation of I_2 , allowing the simple distillation of HI [97]. The distilled HI is then decomposed into I_2 and H_2 , and finally hydrogen is separated from the HI/ I_2 / H_2 mixture using a membrane. The EED and distillation method favored by JAEA and INET uses an EED cell to remove some water from the HIx mixture and increase the HI concentration to a hyper-azeotropic state, thereby enabling the simple distillation of HI. The subsequent decomposition and separation steps are the same as in the extractive distillation process, as shown in Figure 2-3. The reactive distillation method proposed by RWTH Aachen in the 1980s [99] combines HI distillation and HI decomposition processes in a single distillation column at high pressure and temperature. Iodine is dissolved in the lower liquid phase of the column, while a mixture of hydrogen and water is obtained at the top of the column [97]. Given that the EED and distillation method has been successfully applied to several bench-scale closed-loop S-I test facilities (e.g., the test facilities built at JAEA and INET), in this study, it is used to obtain high-purity HI for hydrogen production, as shown in Figure 2-2.

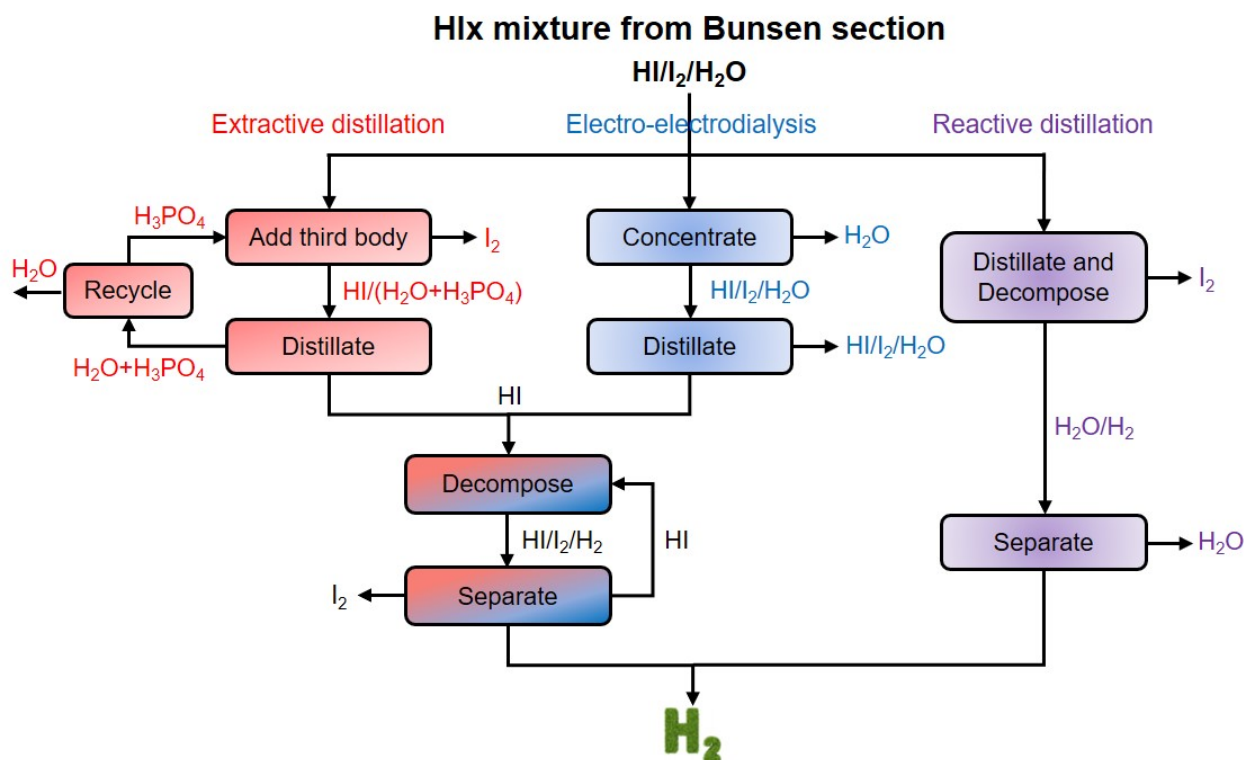


Figure 2-3. Schematic representation of three main options for the HI concentration and decomposition section (Reproduced from Ref. [97]).

It is seen that an EED cell is first used to produce the hyper-azeotropic HI solution (Stream 28), which is then fed to a traditional distillation column (HIDST) to obtain high-purity HI (Stream 33). After that, the resulting high-purity HI (Stream 33) is heated to the corresponding HI decomposition temperature via HEATER4, and hydrogen is produced in HIDEC (the HI decomposition reactor). Finally, the product H₂ (Stream 37) is separated by H2-SEP (a membrane separator) and the other materials (Stream 36) are returned to HIDST for recycling. It should be noted that, in order to reduce the energy consumption of the HI section and the HI concentration returned to the Bunsen section, the bottom HI solution of HIDST (Stream 30) is incorporated into the EED cell instead of being directly sent back to the BUNSEN reactor [96], as shown in Figure 2-2. Table 2-1 summarizes the detailed component information of the S-I system developed in Aspen Plus.

Table 2-1. Component information of the S-I system developed in Aspen Plus.

Component	Type	Function
PUMP1	Pump	Pumping water to the Bunsen reactor
HEATER1	Heat exchanger	Heating feed water for the Bunsen reactor
BUNSEN	Chemical reactor	Generating H ₂ SO ₄ and HI solutions
L-L-SEP	Separator	Separating H ₂ SO ₄ and HI solutions
HIPUR	Chemical reactor	Removing H ₂ SO ₄ from HI solution
H2SO4PUR	Chemical reactor	Removing HI from H ₂ SO ₄ solution
SEP1	Separator	Recycling impurities to the Bunsen reactor
SEP2	Separator	Recycling impurities to the Bunsen reactor
COOLER1	Heat exchanger	Cooling the generated O ₂
H2SO4DST	Distillation column	Concentrating H ₂ SO ₄ solution
BLOWER	Blower	Conveying steam, O ₂ and SO ₂
COOLER2	Heat exchanger	Cooling steam, O ₂ and SO ₂
HEATER2	Heat exchanger	Heating the concentrated H ₂ SO ₄ solution
H2SO4DEC	Chemical reactor	Decomposing H ₂ SO ₄ into H ₂ O and SO ₃
HEATER3	Heat exchanger	Heating products of the H ₂ SO ₄ decomposer
SO3DEC	Chemical reactor	Decomposing SO ₃ into SO ₂ and O ₂
COOLER3	Heat exchanger	Cooling products of the SO ₃ decomposer
SO3ABS	Chemical reactor	Converting SO ₃ and H ₂ O into H ₂ SO ₄
EED	Electrodialysis cell	Increasing HI concentration
PUMP2	Pump	Pumping HI solution to HIDST
HIDST	Distillation column	Generating high-purity HI
COOLER4	Heat exchanger	Cooling the bottom HI solution of HIDST
HEATER4	Heat exchanger	Heating high-purity HI
HIDEC	Chemical reactor	Decomposing HI into H ₂ and I ₂
H2-SEP	Separator	Separating H ₂ from products of HIDEC

COOLER5 Heat exchanger Cooling the generated H₂

2.1.2 Modeling of the S-I system

As mentioned earlier, in this work, the S-I thermochemical hydrogen production system was designed and modeled using Aspen Plus, a commercial chemical process simulation software developed by Aspen Technology, Inc. (AspenTech) in 1981. As a chemical process simulator with the best tools for handling non-ideal chemical systems, Aspen Plus includes the capability of modeling electrolytes through several different modeling techniques including the ELECNRTL model (ELECTrolytic Non-Random Two-Liquid model, namely an electrolytic version of the non-random two-liquid model, which is thought to be able to simulate the S-I process) [89]. In addition, Aspen Plus has the user-defined function and the ability to regress model parameters from some experimental data to generate new thermodynamic models for specific chemical systems. In view of the powerful functions and good user interaction of Aspen Plus, it was chosen as the process simulator for this work.

Since the thermodynamic models of most system components, such as chemical reactor, distillation column, separator, heat exchanger, and pump, have already been embedded in Aspen Plus, the only mission left for us is to construct the mathematical model of the EED cell (the electrolyzer model is not available with Aspen Plus). In this work, the user-defined module of Aspen Plus®, USER2, is employed to simulate the EED unit (see Figure 2-2), and its mathematical model is created and executed by developing an external EXCEL program. Figure 2-4 schematically shows the working principle of an EED cell. It is seen that the EED cell is divided into two independent compartments (i.e., anode and cathode) via a membrane, and in the two compartments, a pair of opposite electrochemical reactions occurs. In more detail, the iodine ions are oxidized into iodine molecules at the anode, while the iodine molecules are reduced into iodine ions at the cathode. During this process, some hydrogen ions (H⁺) pass through the membrane from anode to cathode in the form of hydronium ions (H₃O⁺), and conversely, some iodide ions penetrate through the membrane from cathode to anode. Finally, the solution with a high HI concentration (namely the hyper-azeotropic HI solution) is obtained at the cathode outlet, and the diluted solution with a low HI concentration is obtained at the anode outlet. In general, the net effect of the EED cell is to transfer HI from anode to cathode, thereby increasing the HI concentration at the cathode outlet and obtaining the hyper-azeotropic HI solution. Note that the diluted HI solution obtained at the anode outlet will be sent back to the BUNSEN reactor for recycling (see Figure 2-2).

Based on the mass conservation law and Faraday's second law, the electrode inlet and outlet equations of the total molar flow rate and each composition's molar flow rate can be respectively expressed by:

$$\begin{cases} \dot{n}_{\text{out}}^{\text{ca}} = \dot{n}_{\text{in}}^{\text{ca}} + \frac{(2t_+ - 1 + 2\beta t_+)}{2F} I \\ \dot{n}_{\text{out}}^{\text{an}} = \dot{n}_{\text{in}}^{\text{an}} - \frac{(2t_+ - 1 + 2\beta t_+)}{2F} I \end{cases}, \quad (2-2)$$

$$\left\{ \begin{array}{l} \dot{n}_{\text{out,HI}}^{\text{ca}} = \dot{n}_{\text{in,HI}}^{\text{ca}} + \frac{t_+ I}{F} \\ \dot{n}_{\text{out,HI}}^{\text{an}} = \dot{n}_{\text{in,HI}}^{\text{an}} - \frac{t_+ I}{F} \\ \dot{n}_{\text{out,I}_2}^{\text{ca}} = \dot{n}_{\text{in,I}_2}^{\text{ca}} - \frac{I}{2F} \\ \dot{n}_{\text{out,I}_2}^{\text{an}} = \dot{n}_{\text{in,I}_2}^{\text{an}} + \frac{I}{2F} \\ \dot{n}_{\text{out,H}_2\text{O}}^{\text{ca}} = \dot{n}_{\text{in,H}_2\text{O}}^{\text{ca}} + \frac{\beta t_+ I}{F} \\ \dot{n}_{\text{out,H}_2\text{O}}^{\text{an}} = \dot{n}_{\text{in,H}_2\text{O}}^{\text{an}} - \frac{\beta t_+ I}{F} \end{array} \right. , \quad (2-3)$$

where superscripts ca and an denote cathode and anode, respectively; subscripts in and out represent inlet and outlet, respectively; symbols \dot{n} , t_+ , β , F , and I are molar flow rate, proton transport number, electro-osmosis coefficient, Faraday constant (96,485 C/mol), and current, respectively.

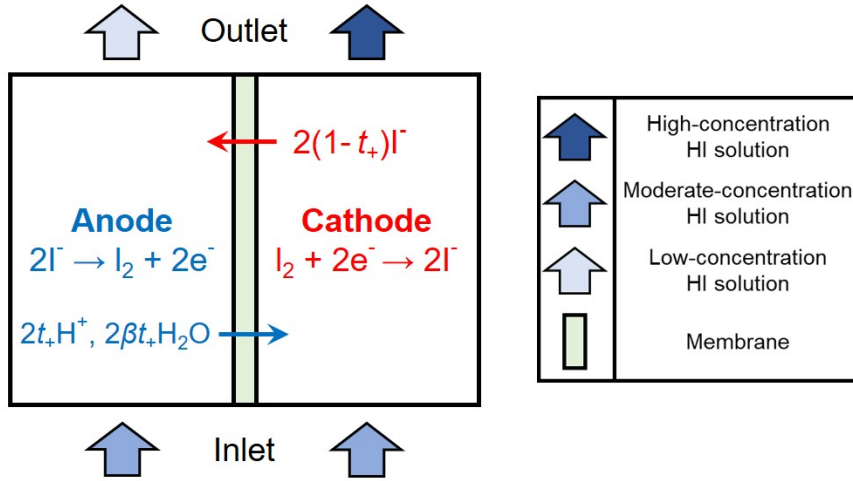


Figure 2-4. Schematic representation of the working principle of an EED cell.

The electrical power consumption of the EED cell, $\dot{E}_{\text{con,EED}}$, can be calculated by:

$$\dot{E}_{\text{con,EED}} = U \cdot I = (U_{\text{eq}} + U_{\text{mem}}) \cdot I, \quad (2-4)$$

where terms U_{eq} and U_{mem} represent the equilibrium potential difference between two electrodes and the membrane potential drop, respectively. According to Refs. [96,100], the equilibrium potential difference, U_{eq} , can be calculated by:

$$U_{\text{eq}} = -4.7 \times 10^{-6} \cdot T \cdot \exp\left(\frac{1.6 \times 10^3}{T}\right) \cdot \ln \left[\left(\frac{\chi_{\text{mn,HI}}^{\text{an}}}{\chi_{\text{mn,HI}}^{\text{ca}}} \right)^2 \left(\frac{\chi_{\text{mn,I}_2}^{\text{an}}}{\chi_{\text{mn,I}_2}^{\text{ca}}} \right)^{\frac{1}{2}} \right], \quad (2-5)$$

where the term $\chi_{\text{mn},i}$ is the mean mole fraction of composition i at the inlet and outlet of the electrode.

According to Ref. [96], the membrane potential drop, U_{mem} , can be calculated by:

$$U_{\text{mem}} = \left[-10.91 \times (\chi_{\text{mn,HI}}^{\text{ca}} + \chi_{\text{mn,HI}}^{\text{an}}) + 76.74 \times (\chi_{\text{mn,I}_2}^{\text{ca}} + \chi_{\text{mn,I}_2}^{\text{an}}) \right] \times (T - 273.15)^{-1.059}. \quad (2-6)$$

Thus, the thermal efficiency of the S-I hydrogen production system, $\eta_{\text{th,S-I}}$, can be calculated by:

$$\eta_{\text{th,S-I}} = \frac{\text{HHV}_{\text{H}_2}}{Q_{\text{con,S-I}} + \frac{E_{\text{con,S-I}}}{\eta_{\text{E}}}}, \quad (2-7)$$

where $Q_{\text{con,S-I}}$ and $E_{\text{con,S-I}}$ respectively represent the heat consumption and electricity consumption of the S-I system to produce 1 mol of hydrogen; the term η_{E} denotes the electricity generation efficiency. Since most of the existing studies used the High Heating Value of hydrogen (HHV_{H_2} , set as 285.83 kJ/mol [18]) to estimate the thermal efficiency of the S-I cycle, this value is also adopted in this work for the convenience of conducting the comparison of efficiency estimation results.

2.2 Process simulation and performance analysis of the S-I system

2.2.1 Process simulation of the S-I system

Taking the hydrogen production rate of 1 mol/s as a simulation case, the main operating parameters of the S-I system are summarized in Table 2-2. In the actual operation process, the initial feed conditions of the Bunsen reaction (or the molar ratio of I_2 and H_2O in the Bunsen reaction, namely the coefficients m and n in Eq. (2-1)) should be determined carefully because it affects not only the phase compositions of the Bunsen products, but also the material flow and energy consumption of the entire S-I system. In this work, to verify the reliability of simulation results, the phase compositions of the Bunsen products are directly specified by referring to the experimental study of Guo et al. [101]. In more detail, the $\text{H}_2\text{O}/\text{H}_2\text{SO}_4/\text{HI}/\text{I}_2/\text{O}_2$ mixture (Stream 8) with the molar flow rate of about 34.023/1.659/5.864/7.045/0.5 (i.e., the molar ratio of about 0.680/0.033/0.117/0.141/0.010 [101]) is assumed to be obtained at the BUNSEN reactor outlet. Further, when this mixture is fed to the liquid-liquid separator (L-L-SEP), the $\text{H}_2\text{O}/\text{H}_2\text{SO}_4/\text{HI}/\text{I}_2$ mixture (Stream 10) with the molar flow rate of about 4.318/1.091/0.182/0.068 can be obtained at the H_2SO_4 phase outlet (i.e., the light phase outlet) of L-L-SEP according to the simulation data of Ref. [101]. Besides, in order to simplify the modeling process, the assumption of a 100% conversion rate for purification processes is adopted in this work based on Ref. [95].

As mentioned earlier, the H_2SO_4 decomposition process is accomplished by two independent sub-reactions which are respectively occurring in the H_2SO_4 decomposition reactor (H2SO4DEC) and the SO_3 decomposition reactor (SO3DEC). In this work, it is assumed that the gaseous H_2SO_4 is decomposed into SO_3 and H_2O at 773.15 K (500°C) with a 100% conversion rate, and SO_3 is catalytically decomposed into SO_2 and O_2 at 1123.15 K (850°C) with 78% conversion rate (In Ref. [101], the

gaseous H_2SO_4 is considered to be directly decomposed into SO_2 , O_2 and H_2O at 1123 K with 78% conversion rate). In addition, it should be noted that the H_2 membrane separator is used in this study to improve the conversion rate of HI decomposition. According to Refs. [102-104], the HI conversion rate can reach 44% to 50% when the membrane separation technology is applied. However, considering the current technology uncertainty and potential operating risks, this value is conservatively set to 40% [105]. Lastly, it should be emphasized that in Figure 2-2, all the chemical reactors, such as BUNSEN, HIPUR, $\text{H}_2\text{SO}_4\text{PUR}$, $\text{H}_2\text{SO}_4\text{DEC}$, etc., are the type of Stoichiometric Reactor, and all the separation components, such as L-L-SEP, SEP1, SEP2, H2-SEP, etc., are ordinary component separators.

Table 2-2. Main operating parameters of the S-I system with a hydrogen production rate of 1 mol/s.

Sections	Components	Main operating parameters
Bunsen section	BUNSEN	SO_2 conversion rate: 100% [101]; $T = 353$ K [101]; $p = 0.5$ MPa Molar flow rate of the Bunsen products (mol/s): $\text{H}_2\text{O}/\text{H}_2\text{SO}_4/\text{HI}/\text{I}_2/\text{O}_2 = 34.023/1.659/5.864/7.045/0.5$ (Molar ratio: 0.680/0.033/0.117/0.141/0.010 [101])
	L-L-SEP	Molar flow rate of the H_2SO_4 phase (mol/s): $\text{H}_2\text{O}/\text{H}_2\text{SO}_4/\text{HI}/\text{I}_2 = 4.318/1.091/0.182/0.068$ (Derived from the data reported in Ref. [101])
	HIPUR	H_2SO_4 conversion rate: 100% [95]; $T = 353$ K; $p = 0.5$ MPa
	$\text{H}_2\text{SO}_4\text{PUR}$	HI conversion rate: 100% [95]; $T = 353$ K; $p = 0.5$ MPa
H_2SO_4 concentration and decomposition section	$\text{H}_2\text{SO}_4\text{DST}$	Number of stages: 5 [101]; reflux ratio ^a : 1 [101]; distillate rate: 6.056 mol/s; feed location: stage 3 [101]; $p = 1$ atm [101]
	$\text{H}_2\text{SO}_4\text{DEC}$	H_2SO_4 conversion rate: 100%; $T = 773.15$ K; $p = 1$ atm
	SO_3DEC	SO_3 conversion rate: 78%; $T = 1123.15$ K; $p = 1$ atm (Based on Ref. [101])
HI concentration and decomposition section	SO_3ABS	SO_3 absorption rate: 100% [95]; $T = 473.15$ K [95]; $p = 1$ atm [95]
	EED	Molar fraction of the cathode outlet stream: $\text{HI}:\text{I}_2:\text{H}_2\text{O} = 0.182:0.05:0.768$ (HI molality: 13.17 mol/kg· H_2O [102]); proton transport number: $t_+ = 1$ [102]; electro-osmosis coefficient: $\beta = 1$ [102]; $T = 353$ K; $p = 0.5$ MPa
	HIDST	Number of stages: 7 [103]; reflux ratio ^a : 3; distillate rate: 5 mol/s; feed location: stage 4; $p = 1.17$ MPa [103,104]
	HIDEC	HI conversion rate: 40% [105]; $T = 723$ K [103,104]; $p = 1.17$ MPa [103,104]

^a The reflux ratio is defined as the molar ratio of the reflux rate to the distillate rate.

After specifying the operating parameters of the system, the next step is to determine the physical property methods used for process simulation. The S-I thermochemical cycle is a typical non-ideal and polar system [95], and in this system, two acid solutions (i.e., the H_2SO_4 and HI solutions) are both easy to be dissociated into ionic compounds via several electrochemical reactions. Therefore, it is essential to integrate some electrochemical reactions into the thermodynamic model of the S-I cycle [106]. As the most versatile electrolyte property method, the ELECNRTL physical property method of Aspen Plus not only can handle very low and very high concentrations but also can handle aqueous and mixed solvent systems. Therefore, this physical property method is adopted to simulate the Bunsen section and the H_2SO_4 concentration and decomposition section [103]. Since the ternary HI-I₂-H₂O mixture (i.e., the HI_x phase) has a complex phase behavior, it is very difficult to accurately predict the thermodynamic properties of the HI-I₂-H₂O system. Up to now, several physical property methods including NRTL-RK (Non-Random Two-Liquid-Redlich-Kwong), SR-Polar (Schwartzentruber-Renon-Polar), ELECNRTL, and so on, have been used to simulate the HI-I₂-H₂O system. However, it should be pointed out that each of these physical property methods has its own applicable parameter range, and none of the available physical property models can accurately predict the thermodynamic properties of this complex three-phase mixture under the full parameter range. The development of a complete physical property model requires a large amount of experimental data, and this work exceeds the research scope of the thesis. However, given that the operating conditions of the HI concentration/distillation process and the HI decomposition process are significantly different, in this work, the NRTL-RK and SR-Polar physical property methods are respectively used to simulate these two processes [103]. The main equations, application ranges, and limitations of these physical property methods have been summarized in detail in Ref. [107].

After determining the physical property methods, the software simulation begins, and no errors are reported in the Results Summary when software calculations are completed. Table 2-3 summarizes the detailed material flow data of the simulated S-I system. It should be noted that the slight error between the input molar flow rate of the Bunsen products (see Table 2-2) and the simulated molar flow rate of the Bunsen products (Stream 8 of Table 2-3) is caused by software iterative calculation and can be ignored. As shown in Table 2-2, the material flow of the Bunsen section in this work is determined based on the study of Guo et al. [101]. In this case, the model validation work left for us is to verify the reliability of the simulation results of the H_2SO_4 section and the HI section. Furtherly, since the conversion rates of the chemical decomposition reactions in the H_2SO_4 section and HI section have already been directly specified according to the existing published literature (see Table 2-2), the model validation of the acid decomposition processes is no longer required. At this time, only the simulation results of the acid concentration/distillation processes need to be verified.

Tables 2-4 and 2-5 respectively present the model validation results of the H_2SO_4 distillation process and the HI distillation process. As shown in the two tables, the simulation results obtained are in good agreement with the results reported in Refs. [101] and [102], and all relative errors are controlled within 3%. Thus, the simulation model used in this work is able to obtain some reliable analysis results.

Table 2-3. Material flow data of the simulated S-I hydrogen production system.

No.	T (K)	P (MPa)	Molar flow rate (mol/s)							
			H ₂ O	H ₂ SO ₄	HI	I ₂	SO ₂	SO ₃	O ₂	H ₂
1	298.15	0.101	1	0	0	0	0	0	0	0
2	298.17	0.5	1	0	0	0	0	0	0	0
3	353	0.5	1	0	0	0	0	0	0	0
4	353	0.5	30.841	0	2.546	8.545	0	0	0	0
5	353	0.5	4.556	0	0	0	1	0	0.5	0
6	353	0.5	0	0	0	0	0.565	0	0	0
7	353	0.5	0.944	0	0	0.159	0.091	0	0	0
8	353	0.5	34.028	1.656	5.859	7.048	0	0	0.5	0
9	353	0.5	29.71	0.565	5.677	6.98	0	0	0	0
10	353	0.5	4.318	1.091	0.182	0.068	0	0	0	0
11	353	0.5	0	0	0	0	0	0	0.5	0
12	313	0.5	0	0	0	0	0	0	0.5	0
13	353	0.5	30.841	0	4.546	7.545	0.565	0	0	0
14	353	0.5	30.841	0	4.546	7.545	0	0	0	0
15	353	0.5	4.5	1	0	0.159	0.091	0	0	0
16	353	0.5	3.556	1	0	0	0	0	0	0
17	365.54	0.101	4.556	0	0	0	1	0	0.5	0
18	546.71	0.5	4.556	0	0	0	1	0	0.5	0
19	417.21	0.101	0.439	1.282	0	0	0	0	0	0
20	773.15	0.101	0.439	1.282	0	0	0	0	0	0
21	773.15	0.101	1.721	0	0	0	0	1.282	0	0
22	1123.15	0.101	1.721	0	0	0	0	1.282	0	0
23	1123.15	0.101	1.721	0	0	0	1	0.282	0.5	0
24	473.15	0.101	1.721	0	0	0	1	0.282	0.5	0
25	473.15	0.101	1.439	0.282	0	0	1	0	0.5	0
26	354.23	0.5	33.513	0	5.229	7.21	0	0	0	0
27	353.13	0.5	43.408	0	8.237	4.335	0	0	0	0
28	353	0.5	46.08	0	10.92	3	0	0	0	0
29	353.18	1.17	46.08	0	10.92	3	0	0	0	0
30	422.17	1.17	46.08	0	8.92	4	0	0	0	0
31	396.32	0.5	46.08	0	8.92	4	0	0	0	0
32	353	0.5	46.08	0	8.92	4	0	0	0	0
33	315.10	1.17	0	0	5	0	0	0	0	0
34	723	1.17	0	0	5	0	0	0	0	0

35	723	1.17	0	0	3	1	0	0	0	1
36	723	1.17	0	0	3	1	0	0	0	0
37	723	1.17	0	0	0	0	0	0	0	1
38	723.63	0.101	0	0	0	0	0	0	0	1
39	313	0.101	0	0	0	0	0	0	0	1

Table 2-4. Model validation of the H₂SO₄ distillation column (H2SO4DST).

Parameters (Unit)	Ref. [101]	Present study	Relative errors (%)
H ₂ SO ₄ mass fraction of the feed H ₂ SO ₄ solution ^a (-)	0.585	0.583	0.34
Distillate ratio of H ₂ O ^b (-)	0.90	0.91	1.11
H ₂ SO ₄ mass fraction of the bottom product (-)	0.93 ^c	0.94	1.08

^a Only H₂O and H₂SO₄ are counted, excluding O₂ and SO₂.

^b The ratio of the distillate rate of H₂O to the feed rate of H₂O.

^c The experimental value is reported to be 0.92 to 0.94 [101].

Table 2-5. Model validation of the HI distillation column (HIDST).

Parameters (Unit)	Ref. [102]	Present study	Relative errors (%)
HI molality of the feed stream, Stream 29 (mol/kg·H ₂ O)	13.17	13.17	0
HI mole fraction of the top distillate (-)	0.98	1	2.04
HI molality of the bottom product (mol/kg·H ₂ O)	10.5	10.75	2.38

2.2.2 Performance analysis of the S-I system

According to the above simulation results, the energy consumption distribution of the S-I system can be obtained, as shown in Figure 2-5 (The detailed energy consumption data are summarized in Table 2-6). It can be seen from Figure 2-5(a) that approximately 94% of the energy consumption of the S-I system is caused by the H₂SO₄ section and the HI section, and the energy consumption of the Bunsen section is relatively small, accounting for only 6% of the system total energy consumption. From Figure 2-5(b), it can be seen that about half of the system energy consumption is used in the reboilers of the two distillation columns to concentrate H₂SO₄ and HI solutions, and nearly 13% of the system energy consumption is used by the EED cell to produce the hyper-azeotropic HI solution (The electricity consumption of the EED

cell has been converted into the equivalent heat consumption by assuming an electricity generation efficiency of 45% [95]). As a result, it can be inferred that more than 60% of the system energy consumption is used to produce high-concentration H_2SO_4 and high-purity HI. However, it should be pointed out that the above results are only applicable to the current simulation case, and the corresponding results may vary for different S-I process flowsheets, different operating parameters, and different system assumptions. In short, the results shown in Figure 2-5 indicate that the H_2SO_4 section and the HI section are the two energy-intensive parts of the S-I process, and it will be very important to optimize the process flow and parameters of these two sections to reduce the energy consumption of the system.

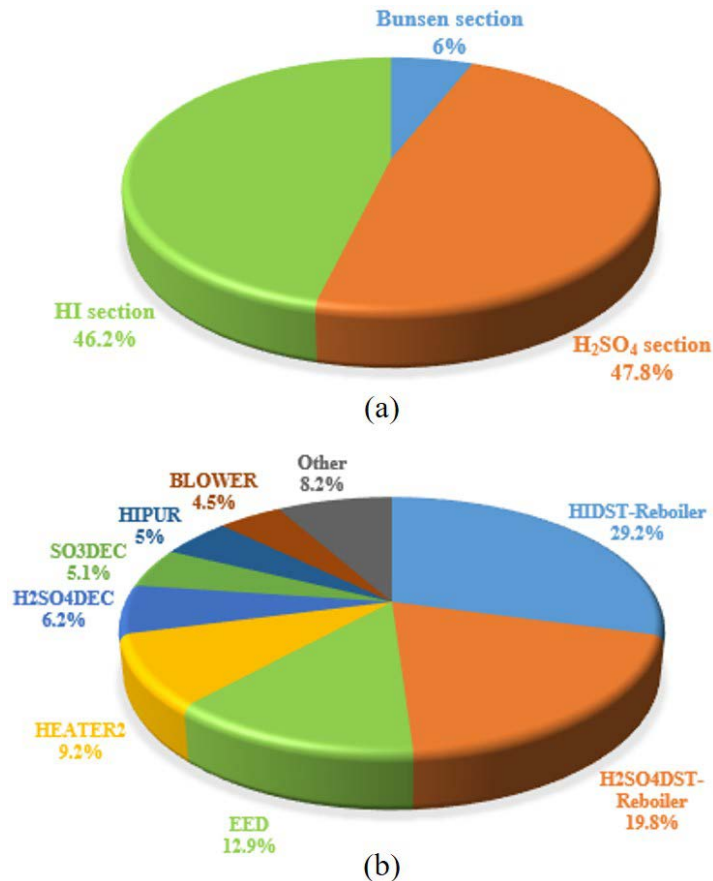


Figure 2-5. Energy consumption distribution of the S-I system: (a) Each section and (b) Each component.

Table 2-6. Energy consumption statistic of the S-I system ^a.

Sections	Components	Heat consumption ^b (kJ/mol · H ₂)	Electricity consumption (kJ/mol · H ₂)
Bunsen section	PUMP1	—	0.01
	HEATER1	4.13	—
	BUNSEN	-232.85	—
	HIPUR	95.49	—

	H2SO4PUR	15.37	—
	COOLER1	-0.60	—
	Total	114.99	0.01
H ₂ SO ₄ concentration and decomposition section	H2SO4DST- Reboiler	378.53	—
	H2SO4DST- Condenser	-249.62	—
	BLOWER	—	39.22
	COOLER2	-240.94	—
	HEATER2	175.37	—
	H2SO4DEC	119.20	—
	HEATER3	58.14	—
	SO3DEC	96.99	—
	COOLER3	-101.16	—
	SO3ABS	-47.56	—
	Total	828.23	39.22
HI concentration and decomposition section	EED	—	110.93
	PUMP2	—	1.24
	HIDST-Reboiler	559.03	—
	HIDST- Condenser	-252.57	—
	COOLER4	-373.80	—
	HEATER4	64.52	—
	HIDEC	12.56	—
	COOLER5	-11.99	—
	Total	636.11	112.17
The whole S-I system		1579.33	151.4

^a The energy consumption of all separators and mixers is not considered.

^b The minus sign represents the exothermic process.

Since a large part of the total heat consumption of the S-I system is caused by the reboilers of the two distillation columns (see Figure 2-5(b)), the operating parameters of the two distillation processes should be determined carefully. As we all know, the heat consumption of the reboiler is affected by many operating parameters, such as the number of stages, reflux ratio, feed location (or feed stage), feed composition, distillation pressure, etc., and among these parameters, the reflux ratio is the most direct parameter that greatly affects the heat consumption of the reboiler (or the heat release of the condenser). Figure 2-6 shows the effect of reflux ratio on the heat consumption of the reboilers of the two distillation columns (i.e., H₂SO₄DST-Reboiler and HIDST-Reboiler). It can be seen that for both distillation columns, the heat duty of the reboiler increases almost linearly with the increase of the reflux ratio, which means that there is a minimum reflux ratio that can achieve the least energy

consumption of the reboiler. For the current operating conditions, the minimum reflux ratios for H₂SO₄DST-Reboiler and HIDST-Reboiler are found to be 0.1 and 1.0, respectively.

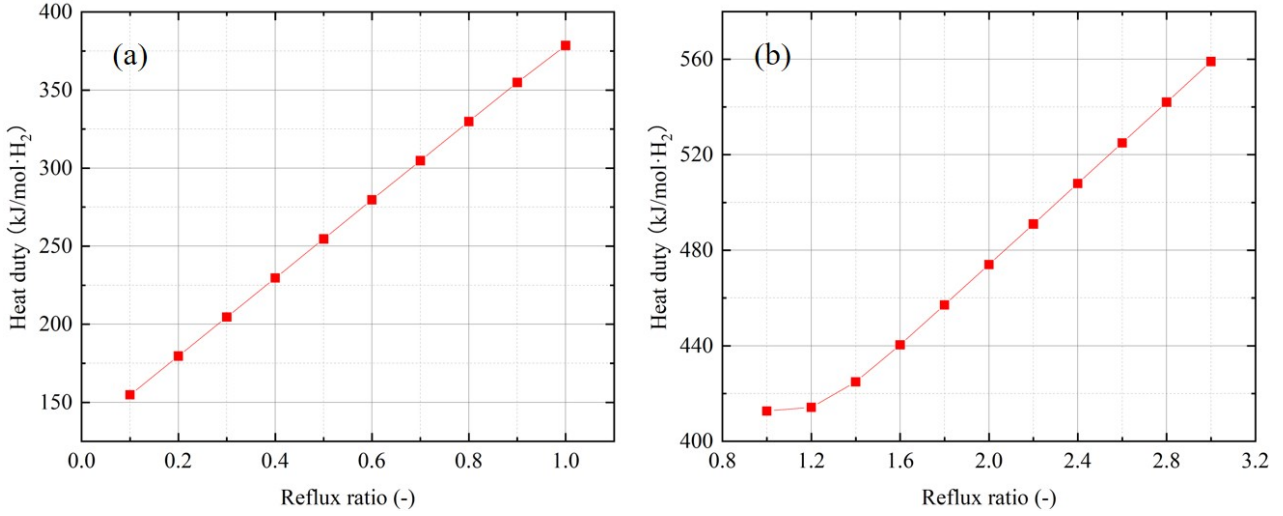


Figure 2-6. Effect of reflux ratio on the heat consumption of (a) H₂SO₄DST-Reboiler and (b) HIDST-Reboiler.

In addition to optimizing the operating parameters of the distillation process, it is also very important to use an efficient internal heat exchange network to reduce the energy consumption of the S-I system (or improve the efficiency of the S-I system), because some exothermic hot flows can be used to heat the endothermic cold flow. According to Ref. [95], only the heat released by the heat exchanger is considered recoverable, while the heat released by the chemical reactor such as the Bunsen reactor (BUNSEN) and the SO₃ absorber (SO₃ABS) is considered to be discharged directly to the environment without recovery. Accordingly, the thermal efficiency of the S-I system shown in Eq. (2-7) can be redefined as:

$$\eta_{\text{th,S-I}} = \frac{\text{HHV}_{\text{H}_2}}{Q_{\text{con,S-I}} - \theta \cdot Q_{\text{rec,tot}} + \frac{E_{\text{con,S-I}}}{\eta_{\text{E}}}}, \quad (2-8)$$

where $Q_{\text{rec,tot}}$ represents the total recoverable heat per 1 mol of hydrogen produced and θ is the heat recovery coefficient between 0 and 1. Assuming an electricity generation efficiency of 45% [95], the effect of heat recovery coefficient on the thermal efficiency of the S-I system is shown in Figure 2-7.

It can be seen from Figure 2-7 that the heat recovery coefficient has a great impact on the thermal efficiency of the S-I system, and the system thermal efficiency is significantly improved with the increase of the heat recovery coefficient. When all the heat released is discharged to the environment without recovery, a lowest thermal efficiency is calculated to be only about 15%. On the contrary, an ideal highest thermal efficiency of about 42% would be achieved by the current S-I system if all the recyclable heat were recovered. It should be noted that in reality, this highest thermal efficiency cannot be achieved because there is always a part of low-

temperature heat inevitably wasted. Assuming a feasible heat recovery coefficient of 0.5-0.9, the thermal efficiency of the proposed S-I system is estimated to be around 22%-35.4%.

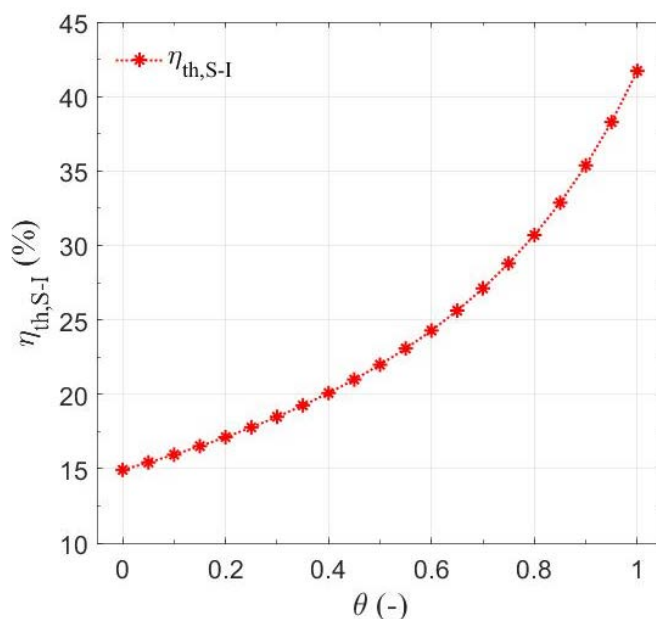


Figure 2-7. Effect of heat recovery coefficient on the thermal efficiency of the S-I system.

As mentioned earlier, the current calculation results are only applicable to the current simulation case. For different S-I systems or different operating conditions, the thermal efficiency calculated may be different. Table 2-7 summarizes some previous efficiency estimation results of the S-I system. It should be emphasized that all the results listed in Table 2-7 are obtained based on theoretical calculation or software simulation. It can be seen that the thermal efficiency estimation results in different studies are significantly different, and in general, the efficiency estimation value is in the range of 19.2%-56.8% (our estimation results of 22%-35.4% are covered by this range). Besides, it can also be seen that the process flowsheet of the conventional Bunsen reaction accompanied by concentration, distillation, and decomposition of H_2SO_4 and HI is adopted in most studies, and the main difference among these studies lies in the HI concentration and distillation method used (mainly the reactive distillation method and the EED and distillation method). It is worth noting that several new processes including the electrochemical Bunsen reaction and the HI electrolysis reaction are also used in some studies, such as Refs. [95,114,115], and in terms of thermal efficiency of the system, the S-I system proposed in this work can compete with the systems proposed in Refs. [86,105,111,112,115].

Table 2-7. Summary of the thermal efficiency estimation results of the S-I system.

References	Main process characteristics	Efficiency range (%)	Efficiency estimate (%)

Goldstein et al. [108]	Conventional Bunsen reaction; Multi-effect distillation for concentrating H_2SO_4 ; Reactive distillation for concentrating HI	≤ 51	33-36
Kasahara et al. [109]	Conventional Bunsen reaction; Multi-effect evaporation for concentrating H_2SO_4 ; EED and distillation for concentrating HI	≤ 57	34
Kasahara et al. [102]	Conventional Bunsen reaction; Depressurized flash evaporation for concentrating H_2SO_4 ; EED and distillation for concentrating HI	—	50.2
Kasahara et al. [104]	Conventional Bunsen reaction; Multi-effect evaporation for concentrating H_2SO_4 ; EED and distillation for concentrating HI	—	56.8
Lee et al. [110]	Optimized Bunsen reaction for producing over-azeotropic HI solution; Flash evaporation for concentrating H_2SO_4 ; Flash evaporation for concentrating HI	—	47-48
Liberatore et al. [111]	Conventional Bunsen reaction; Multi-stage flash evaporation for concentrating H_2SO_4 ; Reactive distillation for concentrating HI	—	21-34
González Rodríguez et al. [86,112]	Conventional Bunsen reaction; Multi-stage distillation for concentrating H_2SO_4 ; Reactive distillation for concentrating HI	—	22.56
Shin et al. [113]	Conventional Bunsen reaction; Multi-stage distillation for concentrating H_2SO_4 ; EED and distillation for concentrating HI	—	39.4
Ying et al. [114]	Electrochemical Bunsen reaction for producing over-azeotropic HI solution; Flash evaporation for concentrating H_2SO_4 ; Flash evaporation for concentrating HI	≤ 50	42
Ying et al. [95]	Conventional Bunsen reaction; Multi-stage distillation for concentrating H_2SO_4 ; HI electrolysis for H_2 production	25-42	33.3
Ying et al. [115]	Conventional Bunsen reaction; Multi-stage distillation for	15.3-31	19.2

	concentrating H ₂ SO ₄ ; HI electrolysis for H ₂ production		
Wang et al. [105]	Conventional Bunsen reaction; Multi-stage distillation for concentrating H ₂ SO ₄ ; EED and distillation for concentrating HI	17.7-43.3	23.7
Ni et al. [116]	Conventional Bunsen reaction; Multi-stage distillation for concentrating H ₂ SO ₄ ; EED and distillation for concentrating HI	≤ 51.9	30-37.1
This work	Conventional Bunsen reaction; Multi-stage distillation for concentrating H ₂ SO ₄ ; EED and distillation for concentrating HI	15-42	22-35.4

2.3 Design and analysis of the internal heat exchange network

2.3.1 Design of the internal heat exchange network

As mentioned in the previous section, the application of an efficient internal heat exchange network is a very important way to improve the efficiency of the S-I system. However, research on the design of the internal heat exchange network has been seldomly carried out so far. In particular, Ying et al. [95] proposed an improved S-I thermochemical hydrogen production system integrated with the HI electrolysis reaction. The simulation results proved that the improved S-I system could achieve a theoretical thermal efficiency of 25%-42%, which was depended on the performance of the internal heat exchange network used. By conducting a simple heat transfer analysis, a preliminary internal heat exchange network was designed by them, and a feasible thermal efficiency of 33.3% was ultimately reached. Besides this, they proposed another novel S-I system assembled with the HI-I₂-H₂O electrolysis reaction [115]. Using the same method, an internal heat exchange network was initially designed and a feasible thermal efficiency of 19.2% was achieved. Juárez-Martínez et al. [117] designed an internal heat exchange network for optimizing the energy use of the S-I process, based on the minimum heat transfer temperature difference method. The simulation results indicated that the average energy efficiency of the S-I system was improved by about 10% via using the internal heat exchange network. Recently, Ni et al. [116] also designed an internal heat exchange network for reducing the net energy consumption of the S-I hydrogen production system, based on the pinch (point) technology. The simulation results showed that when the internal heat exchange network was used and the pinch point temperature difference was set to 5°C-20°C, the heat consumptions of the H₂SO₄ section and the HI section were reduced by 23.9%-25.0% and 20.8%-50.8%, respectively.

It can be seen that most of the previous studies designed the internal heat exchange

network according to a simple heat transfer analysis or a minimum heat transfer temperature difference. Considering that the S-I cycle has a very large operating temperature range (as shown in Figure 1-4, the operating temperature range of the S-I cycle can vary from 20°C to 900°C), it is very necessary to apply different heat transfer constraints to different temperature zones during the design process of the internal heat exchange network. However, to the best of the author's knowledge, research on this subject has not been conducted until now. In addition, during the design process of the internal heat exchange network, most of the previous studies only considered the terminal heat transfer condition of the heat exchanger while the internal heat transfer process of the heat exchanger was not analyzed. Since most of the streams in the S-I system are multi-component mixtures and some of them will undergo phase change during the heating or cooling process, their temperature evolution profiles are likely to be some curved lines or broken lines. At this time, the complete heat transfer process inside the heat exchanger should be analyzed in detail to avoid the unreasonable intersection of temperature curves of the cold and hot fluids. In this case, the pinch point temperature difference constraint should be included in the design stage.

According to the above analysis, in this work, three sets of different heat transfer constraints corresponding to different temperature zones are simultaneously taken into account in the design process of the internal heat exchange network, as shown in Table 2-8. Clearly, the higher the operating temperature of the heat exchanger, the stricter the heat transfer temperature difference constraint (see Table 2-8). Figure 2-8 schematically shows the whole design process of the S-I system with an internal heat exchange network. It is seen that after completing the design of the S-I system without the internal heat exchange network, the next step is to collect and organize the heat exchange data (e.g., the inlet and outlet temperatures, heat duties, etc.) of all heat exchangers in the system by using Aspen Energy Analyzer (a computational software for pinch point analysis and heat exchange network design and optimization). Then, a heat exchange grid diagram can be drawn manually, based on the energy cascade utilization principle (that is, the hot stream with the highest exothermic temperature will be first used to heat the cold stream with the highest endothermic temperature). According to the grid diagram drawn, an initial internal heat exchange network can be designed, and then, the system simulation calculation can be restarted when the operating parameters of all heat exchangers newly added are entered into the software. If there is no error reported in the Results Summary and all the heat transfer constraints shown in Table 2-8 are satisfied, the software simulation and the entire system design will be both completed. Otherwise, the layout or parameter settings of the designed internal heat exchange network will be modified until the above conditions are met.

Table 2-8. Heat transfer constraints in the design process.

Temperature zones (°C)	Minimum terminal temperature difference (°C)	Minimum pinch point temperature difference (°C)
≥ 500	30	15
200-500	20	10
≤ 200	10	5

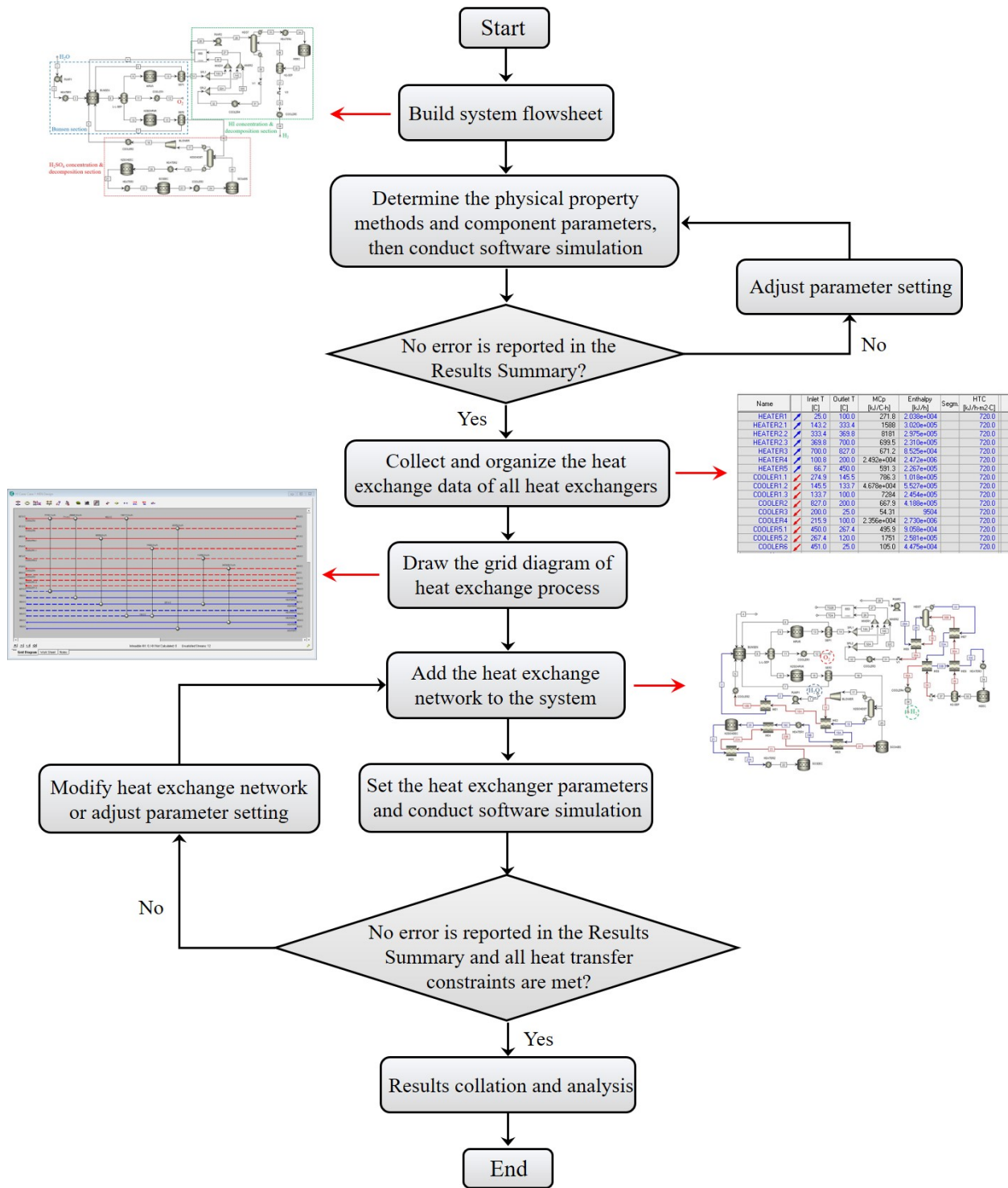


Figure 2-8. Flow chart of the complete design process of the S-I system.

According to the above design method, a S-I system with an internal heat exchange network is eventually developed, as shown in Figure 2-9. Table 2-9 summarizes the detailed material flow data of this system.

Table 2-9. Material flow data of the designed S-I hydrogen production system with an internal heat exchange network.

No.	T (K)	P (MPa)	Molar flow rate (mol/s)							
			H ₂ O	H ₂ SO ₄	HI	I ₂	SO ₂	SO ₃	O ₂	H ₂
1	298.15	0.101	1	0	0	0	0	0	0	0
2	298.17	0.5	1	0	0	0	0	0	0	0
3	353	0.5	1	0	0	0	0	0	0	0
4	353	0.5	30.841	0	2.546	8.545	0	0	0	0
5	353	0.5	4.556	0	0	0	1	0	0.5	0
6	353	0.5	0	0	0	0	0.565	0	0	0
7	353	0.5	0.944	0	0	0.159	0.091	0	0	0
8	353	0.5	34.028	1.656	5.859	7.048	0	0	0.5	0
9	353	0.5	29.71	0.565	5.677	6.98	0	0	0	0
10	353	0.5	4.318	1.091	0.182	0.068	0	0	0	0
11	353	0.5	0	0	0	0	0	0	0.5	0
12	313	0.5	0	0	0	0	0	0	0.5	0
13	353	0.5	30.841	0	4.546	7.545	0.565	0	0	0
14	353	0.5	30.841	0	4.546	7.545	0	0	0	0
15	353	0.5	4.5	1	0	0.159	0.091	0	0	0
16	353	0.5	3.556	1	0	0	0	0	0	0
17	365.54	0.101	4.556	0	0	0	1	0	0.5	0
18	546.71	0.5	4.556	0	0	0	1	0	0.5	0
18A	445.15	0.5	4.556	0	0	0	1	0	0.5	0
18B	426.58	0.5	4.556	0	0	0	1	0	0.5	0
19	417.21	0.101	0.439	1.282	0	0	0	0	0	0
19A	462.71	0.101	0.439	1.282	0	0	0	0	0	0
19B	574.75	0.101	0.439	1.282	0	0	0	0	0	0
19C	698.15	0.101	0.439	1.282	0	0	0	0	0	0
20	773.15	0.101	0.439	1.282	0	0	0	0	0	0
21	773.15	0.101	1.721	0	0	0	0	1.282	0	0
21A	1088.15	0.101	1.721	0	0	0	0	1.282	0	0
22	1123.15	0.101	1.721	0	0	0	0	1.282	0	0
23	1123.15	0.101	1.721	0	0	0	1	0.282	0.5	0
23A	803.26	0.101	1.721	0	0	0	1	0.282	0.5	0
23B	718.54	0.101	1.721	0	0	0	1	0.282	0.5	0
24	473.15	0.101	1.721	0	0	0	1	0.282	0.5	0
25	473.15	0.101	1.439	0.282	0	0	1	0	0.5	0

26	354.23	0.5	33.513	0	5.229	7.21	0	0	0	0
27	353.13	0.5	43.408	0	8.237	4.335	0	0	0	0
28	353	0.5	46.08	0	10.92	3	0	0	0	0
28A	353.18	1.17	46.08	0	10.92	3	0	0	0	0
29	412.15	1.17	46.08	0	10.92	3	0	0	0	0
30	422.23	1.17	46.08	0	8.92	4	0	0	0	0
30A	371.46	1.17	46.08	0	8.92	4	0	0	0	0
31	371.53	0.5	46.08	0	8.92	4	0	0	0	0
32	353	0.5	46.08	0	8.92	4	0	0	0	0
33	315.10	1.17	0	0	5	0	0	0	0	0
33A	633.15	1.17	0	0	5	0	0	0	0	0
33B	646.15	1.17	0	0	5	0	0	0	0	0
33C	694.55	1.17	0	0	5	0	0	0	0	0
34	723	1.17	0	0	5	0	0	0	0	0
35	723	1.17	0	0	3	1	0	0	0	1
36	723	1.17	0	0	3	1	0	0	0	0
36A	666.15	1.17	0	0	3	1	0	0	0	0
36B	468.42	1.17	0	0	3	1	0	0	0	0
37	723	1.17	0	0	0	0	0	0	0	1
38	723.63	0.101	0	0	0	0	0	0	0	1
38A	654.67	0.101	0	0	0	0	0	0	0	1
39	313	0.101	0	0	0	0	0	0	0	1

2.3.2 Analysis of the internal heat exchange network

From Figure 2-9, it can be seen that the designed internal heat exchange network consists of nine heat exchangers (i.e., IHE1 to IHE9), and most of them are located in the H_2SO_4 and HI sections. The detailed heat exchange processes inside these nine internal heat exchangers are shown in Figs. 2-10 to 2-12 and Table 2-10.

The IHE1 is located in the Bunsen section and its main task is to heat the cold water fed to the BUNSEN reactor (see Figure 2-9). Since the top distillate from the H_2SO_4 distillation column (H2SO4DST) needs to be cooled before entering the BUNSEN reactor (see Figure 2-2), it is used as the hot fluid of IHE1 (Stream 18A, see Figure 2-9). The complete heat exchange process inside IHE1 is presented in Figure 2-10. It is seen that the heat duty of IHE1 is very small, only about 4.13 kW (see Table 2-10), and the heat transfer temperature difference (ΔT) is always large (larger than $90^\circ C$). In this situation, the heat transfer process inside IHE1 can proceed smoothly.

There are four internal heat exchangers (i.e., IHE2 to IHE5) located in the H_2SO_4 concentration and decomposition section (see Figure 2-9), and the complete heat exchange processes inside them are shown in Figure 2-11. The main purpose of

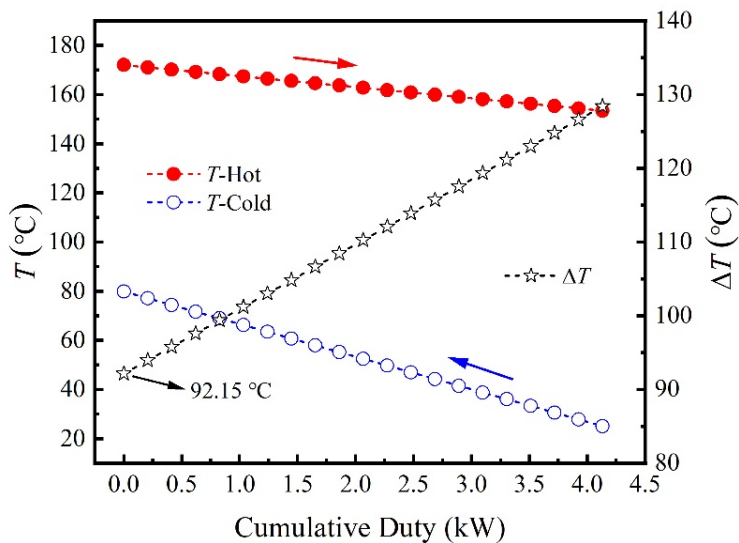


Figure 2-10. Heat exchange process of IHE1.

Table 2-10. Detailed operating data of the designed internal heat exchange network.

Components	Heat duty (kW)	Inlet temperature of hot fluid (°C)	Outlet temperature of hot fluid (°C)	Inlet temperature of cold fluid (°C)	Outlet temperature of cold fluid (°C)
IHE1	4.13	172	153.43	25.02	79.85
IHE2	22.93	273.56	172	144.06	189.56
IHE3	35.92	445.39	200	189.56	301.6
IHE4	13.12	530.11	445.39	425	500
IHE5	52.12	850	530.11	500	815
IHE6	292.32	149.08	98.31	80.03	139
IHE7	50.31	393	195.27	41.95	360
IHE8	2.04	450.48	381.52	360	373
IHE9	7.64	449.85	393	373	421.4

setting IHE2, IHE3, and IHE4 is to heat the high-concentration H_2SO_4 solution fed to the H_2SO_4 decomposition reactor ($\text{H}_2\text{SO}_4\text{DEC}$), while IHE5 is used to preheat the $\text{H}_2\text{SO}_4\text{DEC}$ products (Stream 21) which are sent to the SO_3 decomposition reactor (SO_3DEC) for oxygen production, as shown in Figure 2-9. As mentioned earlier, in this work, the internal heat exchange network is designed based on the energy cascade utilization principle. Given that the SO_3DEC outflow (Stream 23) is the hot stream with the highest exothermic temperature, it should be first used to heat the $\text{H}_2\text{SO}_4\text{DEC}$ products (Stream 21) with the highest endothermic temperature, and then used to heat the high-concentration H_2SO_4 solution with a moderate

endothermic temperature. Therefore, the SO₃DEC products (Stream 23) flow sequentially through IHE5, IHE4, and IHE3 as the hot fluid (see Figure 2-9), and its temperature gradually decreases from 850°C to 200°C, as shown in Figure 2-11B-D and Table 2-10. According to the simulation results, a total of about 101 kW of waste heat is recovered using these three internal heat exchangers. Furthermore, by placing IHE2 between the H₂SO₄ distillation column (H₂SO₄DST) and IHE3 (see Figure 2-9), about 22.9 kW of waste heat is also recovered from the top distillate of H₂SO₄DST, as shown in Figure 2-11A and Table 2-10.

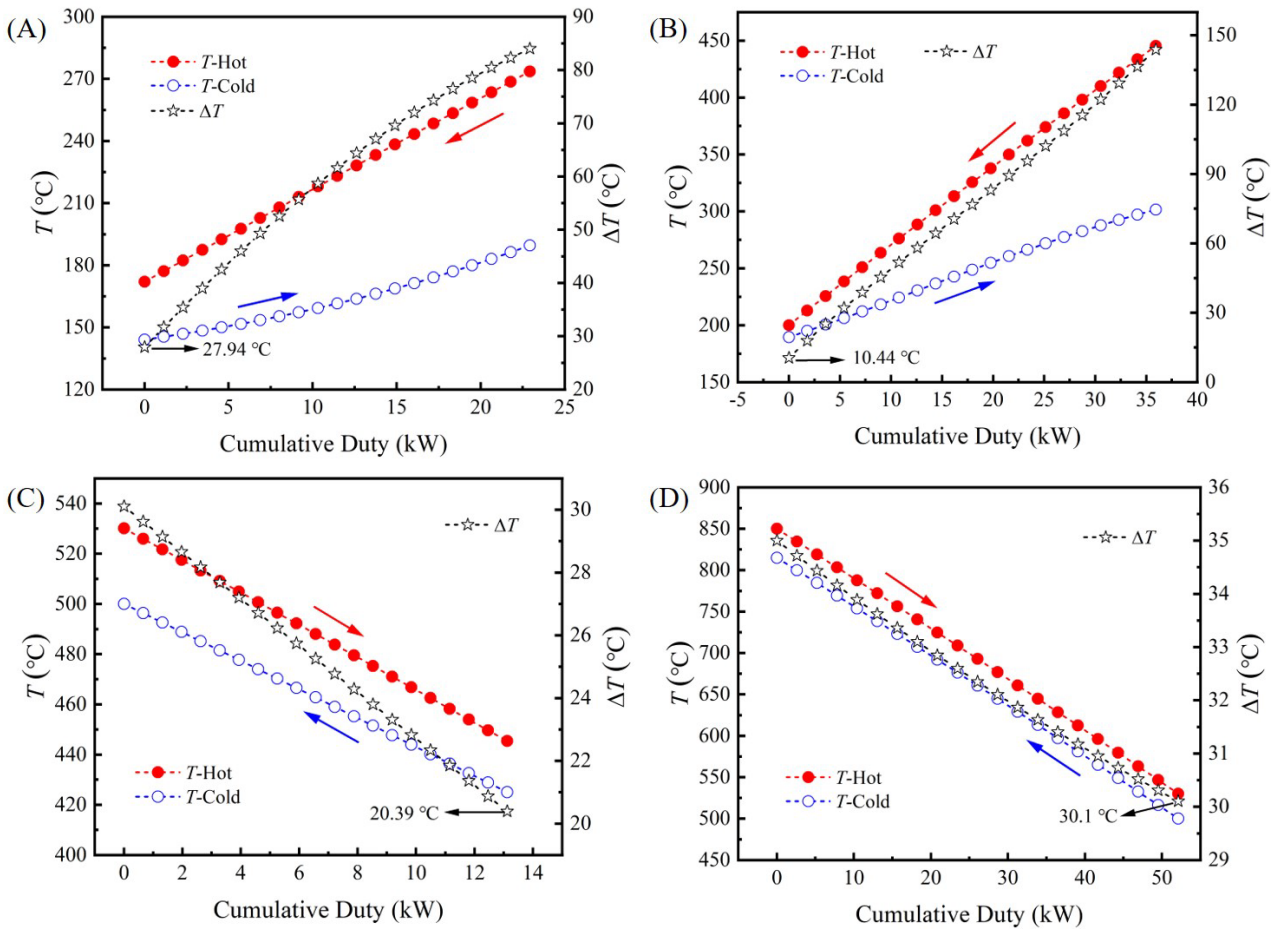


Figure 2-11. Heat exchange processes of (A) IHE2, (B) IHE3, (C) IHE4, and (D) IHE5.

From Figure 2-11, it can also be seen that the minimum heat transfer temperature differences of these four internal heat exchangers are equal to 27.94°C, 10.44°C, 20.39°C, and 30.1°C, respectively, which are all occurring at the terminal location of the heat exchanger. By comparing these temperature difference data with the minimum values set in Table 2-8, it can be concluded that all four internal heat exchangers satisfy the current heat transfer constraints.

Similarly, there are also four internal heat exchangers (i.e., IHE6 to IHE9) located in the HI concentration and decomposition section (see Figure 2-9), and the complete heat exchange processes inside them are shown in Figure 2-12. For IHE6, its main mission is to heat the over-azeotropic HI solution fed to the HI distillation column (HIDST), reducing the heat consumption of the reboiler of HIDST. The bottom HI solution of HIDST (Stream 30) is used as the hot fluid, and the detailed heat

exchange process inside IHE6 is shown in Figure 2-12A. It is seen that the heat duty of IHE6 is very large and is equal to about 292.3 kW (see Table 2-10). This result is considered to be mainly caused by the large material flow of the HI distillation process (Streams 28-32, see Table 2-9). Compared with the conversion rate of the H_2SO_4 decomposition reaction, the conversion rate of the HI decomposition reaction is much lower, which means that more high-purity HI distillate needs to be sent to the HI decomposition reactor (HIDEC) for compensating the shortboard of low HI conversion rate. To achieve this objective, the more over-azeotropic HI solution needs to be fed to the HI distillation column (HIDST), causing a large material flow in the HI distillation process. In addition, it can also be seen in Figure 2-12A that the minimum heat transfer temperature difference of IHE6 is equal to 10.01°C , which meets the low-temperature ($\leq 200^\circ\text{C}$) heat transfer constraint listed in Table 2-8.

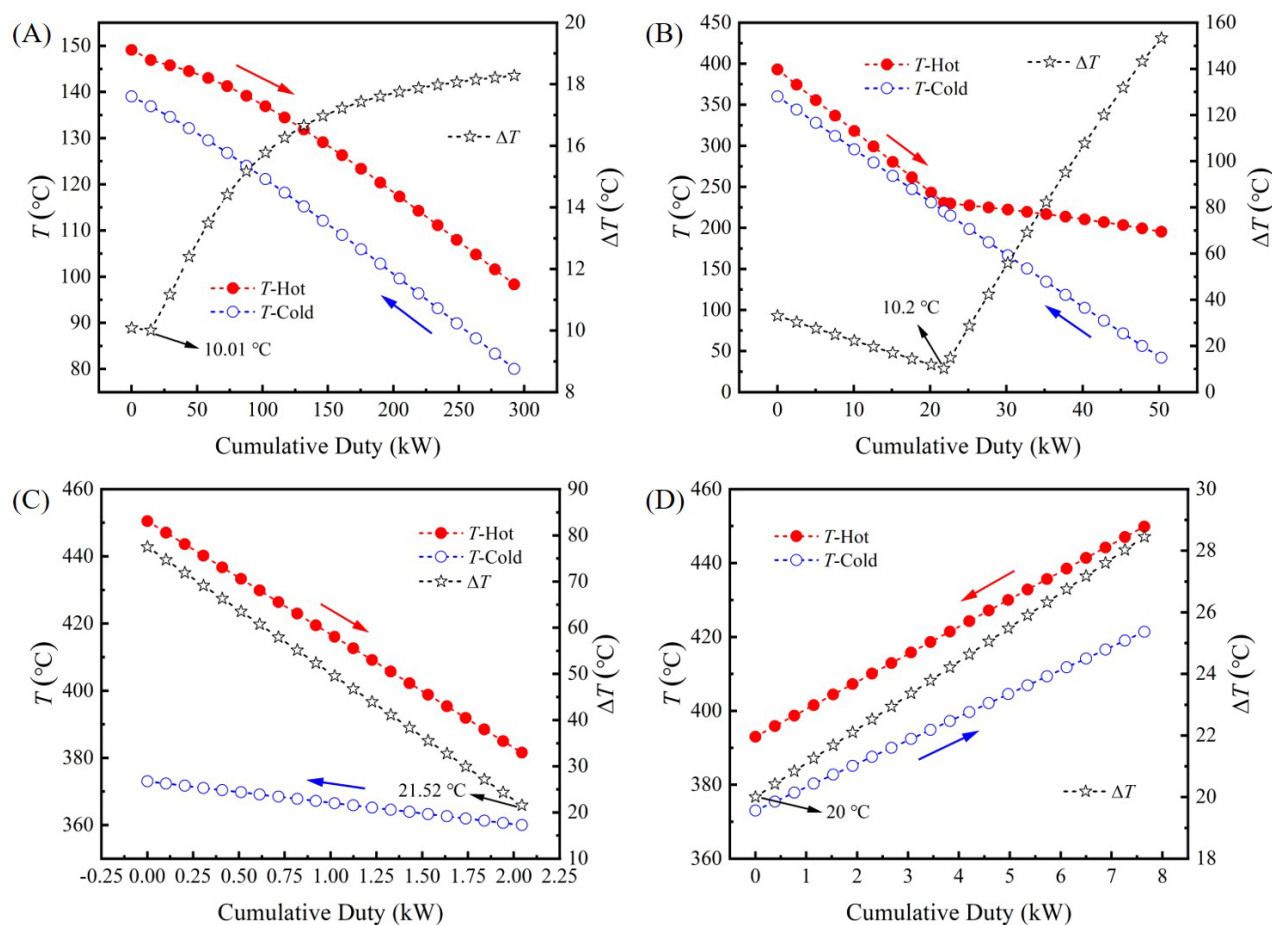


Figure 2-12. Heat exchange processes of (A) IHE6, (B) IHE7, (C) IHE8, and (D) IHE9.

For IHE7, IHE8, and IHE9, their main task is to heat the high-purity HI fed to the HI decomposition reactor (HIDEC), as shown in Figure 2-9. Due to the good temperature match, the HIDEC products (Streams 36 and 37) are used as the hot fluid of these three internal heat exchangers. The complete heat exchange processes inside IHE7, IHE8, and IHE9 are presented in Figure 2-12B-D. It can be seen that when the cold fluid (i.e., the high-purity HI) flows sequentially through IHE7, IHE8, and IHE9, it absorbs a total of about 60 kW of waste heat, which improves its temperature from 41.95°C to 421.4°C (see Table 2-10). Besides, it can also be seen in

Figure 2-12B-D that the minimum heat transfer temperature differences of IHE7, IHE8, and IHE9 are equal to 10.2°C, 21.52°C, and 20°C, respectively. For IHE8 and IHE9, their minimum heat transfer temperature differences are both appearing at the terminal location of the heat exchanger, but for IHE7, that is occurring inside the heat exchanger (at this time, the pinch point temperature difference constraint should be considered, which emphasizes the necessity of analyzing the complete heat transfer process inside the heat exchanger at the design stage). Anyway, by comparing these temperature difference values with the minimum values set in Table 2-8, it can be concluded that all three internal heat exchangers satisfy the current heat transfer constraints.

As mentioned in Section 2.2, the energy consumption (or thermal efficiency) of the S-I hydrogen production system is dependent on many factors, such as the process flowsheet, operating parameters, and system assumptions. For the S-I system without an internal heat exchange network (see Figure 2-2), it is calculated that producing 1 mol of hydrogen requires consuming about 1579.3 kJ of heat and about 151.4 kJ of electricity (see Table 2-6). If the heat consumption of the purification process is not considered (or assuming that the H₂SO₄ phase and the Hlx phase can be perfectly separated by the liquid-liquid separator), the heat consumption value will become 1468.5 kJ. If the designed internal heat exchange network is used, this value will be further reduced to 1046.5 kJ (according to the obtained calculation results, about 422 kJ of waste heat can be effectively recovered per mol of hydrogen produced via using the current internal heat exchange network). Given that the distillation processes of two acid solutions (or the reboilers of two distillation columns) consume a large amount of low-grade thermal energy (see Figure 2-5(b)), in some previous studies, the heat released by the condenser of the distillation column is assumed to be completely recovered for supplying part of the distillation heat [108]. If this assumption is also adopted in this work, the above heat consumption value will be reduced from 1046.5 kJ to 544.3 kJ. It is seen that the heat consumption of the entire system is reduced by 502.2 kJ, which means that the waste heat recovery from the distillation process also plays a key role in reducing the total heat consumption of the S-I system (or improving the thermal efficiency of the S-I system). In addition, according to Ref. [115], electric conversion efficiency of 15% can be considered to recover the remaining waste heat with temperatures higher than 313 K further (note that only the waste heat released by the heat exchanger is recyclable [95]). As a result, about 46 kJ of electricity can be generated by recovering this part of waste heat. At this time, the electricity consumption of the system for 1 mol of hydrogen production is decreased from 151.4 kJ to 105.4 kJ. In summary, the energy consumption of the S-I hydrogen production system is strongly dependent on the adopted system assumptions. The above analysis results of the energy consumption of the S-I system are summarized in Table 2-11.

It should be pointed out that in this section, the internal heat exchange network is designed only from the perspective of thermodynamic feasibility while the economic performance is not considered. Given that several internal heat exchangers (such as IHE1, IHE8, and IHE9) have relatively small heat duties (see Table 2-10) but lead to additional investment and maintenance costs, it is necessary to further make a layout optimization or improvement on the basis of the current design scheme. This work will be presented in Chapter 4.

Table 2-11. Several different analysis results of the S-I system's energy consumption.

Systems (adopted waste heat recovery measures or system assumptions)	Heat demand (kJ/mol·H ₂)	Electricity demand (kJ/mol·H ₂)
Original S-I system (without waste heat recovery)	1579.3	151.4
Original S-I system (without considering the heat consumption of the purification process)	1468.5	151.4
Improved S-I system (with an internal heat exchange network)	1046.5	151.4
Improved S-I system (with an internal heat exchange network and a 100% distillation heat recovery)	544.3	151.4
Improved S-I system (with an internal heat exchange network, a 100% distillation heat recovery and a feasible electricity recovery)	544.3	105.4

2.4 Summary of this chapter

In this chapter, a S-I thermochemical hydrogen production system was first designed and simulated using Aspen Plus software. Then, the energy consumption distribution and thermal efficiency of the S-I system were analyzed to investigate the operating characteristic and performance of the system. Finally, an internal heat exchange network was designed to reduce the energy consumption and improve the hydrogen production efficiency of the S-I system.

The performance analysis results of the S-I thermochemical hydrogen production system show that more than 90% of the energy consumption of the S-I cycle is caused by the concentration and decomposition process of the two acid solutions (i.e., H₂SO₄ and HI solutions), and the energy consumption of the Bunsen section is very small. Thus, it is concluded that optimizing the process flow and operating parameters of the H₂SO₄ section and HI section will be an efficient way to reduce the energy consumption of the S-I hydrogen production system. The efficiency analysis results of the S-I hydrogen production process show that the internal heat recovery situation has a great influence on the thermal efficiency of the S-I cycle, and the thermal efficiency of the designed S-I hydrogen production process is estimated to be in the range of 15%-42%. In addition, it is found that with a feasible internal heat exchange network, about 422 kJ of waste heat can be recovered per mole of hydrogen production, and about 502 kJ of heat consumption can be saved after recovering all the waste heat from the condensers of the two distillation columns (i.e., H₂SO₄ distillation column and HI distillation column). Thus, it is concluded that both the employment of an efficient internal heat exchange network and the recovery of waste heat from the distillation process will play a key role in improving the thermal efficiency of the S-I hydrogen production system.

Chapter 3

Design and analysis of the GSCC power conversion system

In this chapter, the conventional GSCC power conversion system was first introduced and was modeled based on the first and second laws of thermodynamics. Then, the thermodynamic performance of the conventional system under different operating conditions was analyzed and the weak links of the system were revealed. Lastly, a new system layout was proposed to improve the thermodynamic performance of the conventional system. This chapter aims to provide a theoretical foundation for understanding the thermodynamic characteristics of the VHTR and S-I cycle-based nuclear hydrogen production system with GSCC as the power conversion unit.

3.1 Description and modeling of the conventional GSCC power conversion system

3.1.1 System description

Figure 3-1 shows a schematic diagram of the conventional VHTR and S-I cycle-based nuclear hydrogen production system with GSCC as the power conversion unit. It is seen that the conventional system consists of four main parts, namely the VHTR, the IHX, the S-I hydrogen production system, and the GSCC power conversion system. Besides, it can be seen that the S-I hydrogen production system and the GSCC power conversion system are arranged in parallel. In more detail, the high-temperature helium at the outlet of VHTR is divided into two branches, and one stream is sent to the IHX for supplying heat to the S-I hydrogen production system, while another is sent to the GSCC for electricity generation. By adjusting the mass flow rate ratio x (see Figure 3-1), the amount of the heat input to the S-I system (or the combined cycle power conversion system) can be easily controlled (in other words, the hydrogen-electricity ratio of the system can be easily controlled by adjusting the mass flow rate ratio), which is a major advantage of the parallel system.

One major problem of the parallel system shown in Figure 3-1 is that the reactor inlet temperature might be unstable when the hydrogen production load is changed. Since the IHX's primary side helium outlet temperature ($T_{\text{out,ps,IHX}}$) is usually higher than the reactor inlet temperature and the Gas Compressor's (GC's) outlet

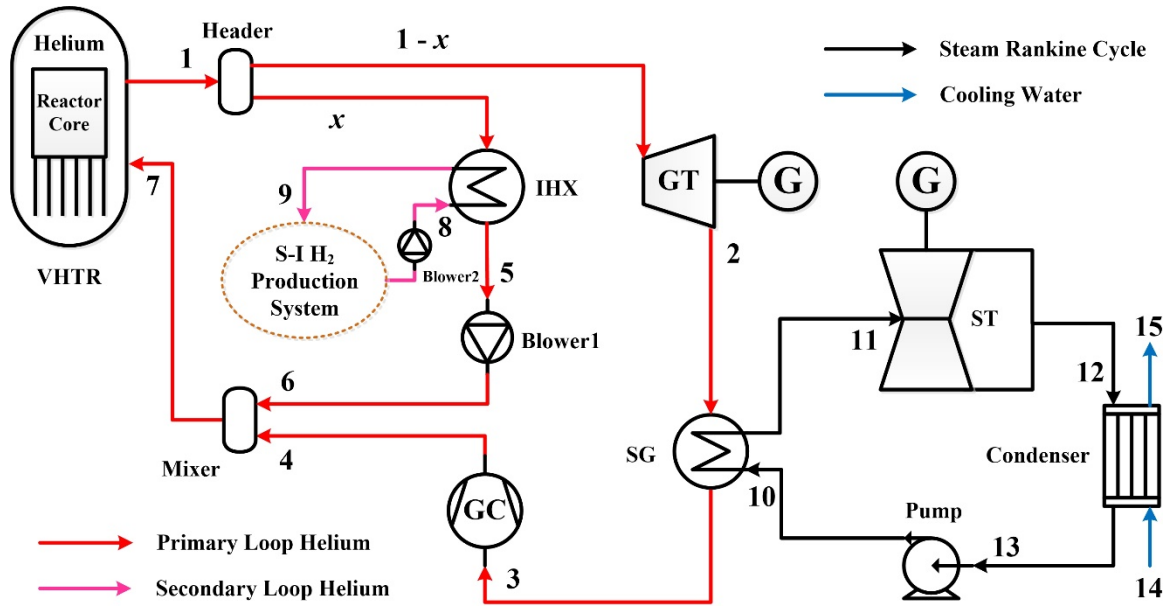


Figure 3-1. Schematic of the conventional VHTR and S-I cycle-based nuclear hydrogen production system with GSCC as the power conversion unit (Modified from Ref. [87]).

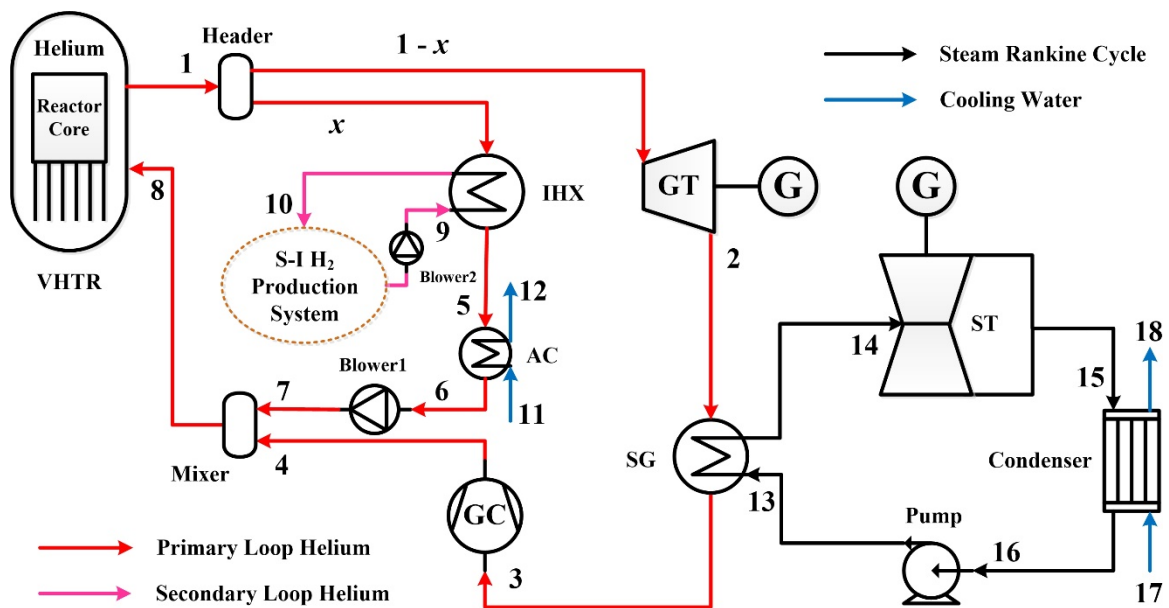


Figure 3-2. Schematic of the improved VHTR and S-I cycle-based nuclear hydrogen production system with GSCC as the power conversion unit.

temperature is always a constant, the reactor inlet temperature will increase with the increase of the mass flow rate ratio x (or the hydrogen production load). In other words, as the hydrogen production load increases, the more high-temperature helium should be sent to the IHX, causing the reactor inlet temperature to rise. At this time, it is necessary to place an accessional heat exchanger behind the IHX to release the excess heat. Therefore, an improved system is proposed, as shown in Figure 3-2. It is seen that in the improved system, a heat exchanger named Auxiliary Cooler (AC) is

added after the IHX, whose main function is to keep the temperature of the helium returning to the reactor constant. Besides, when the S-I hydrogen production system and the combined cycle power conversion system are simultaneously encountering operation accidents, the AC newly added can also be used as an emergency cooler to remove the reactor heat and ensure the system safety. However, it should be noted that when the IHX's primary side helium outlet temperature is very high and the outlet flow rate is very large, this device will result in huge energy loss, which greatly reduces system efficiency. At this time, it is very necessary to develop a new system layout to improve system performance (this work will be presented in Section 3.3).

3.1.2 Thermodynamic modeling

The energy and exergy analysis methods based on the first and second laws of thermodynamics are used in this work to model the improved system presented in Figure 3-2. To simplify the modeling process, several common operating assumptions are adopted [105], as follows:

- The system runs at the steady-state.
- The changes in kinetic and gravitational energies are ignored.
- The pressure drops of working fluids in connecting components and pipes are negligible.
- The heat losses of system components other than IHX and Steam Generator (SG) are ignored.
- The working fluid at the outlet of the Condenser is saturated water.
- The temperature of the cooling water flowing through the Condenser is increased by 10°C.

Before modeling, all system components are classified into the following three types: heat exchangers (including IHX, AC, SG, and Condenser), power conversion components (including GT, GC, Steam Turbine (ST), Pump, and Blower), and independent modules (including VHTR, S-I system, and Generator (G)).

Energy model

The energy analysis method based on the first law of thermodynamics focuses on the energy conversion process from the perspective of energy quantity, which can directly reflect the external energy losses of the system. Each component in the improved system can be regarded as an open steady-state control volume and its mass and energy conservation equation can be expressed as:

$$\begin{cases} \sum \dot{m}_{in,cv} = \sum \dot{m}_{out,cv} \\ \dot{Q}_{cv} = \sum (\dot{m}h)_{out,cv} - \sum (\dot{m}h)_{in,cv} + \dot{W}_{cv} \end{cases}, \quad (3-1)$$

where the subscript cv represents control volume; symbols \dot{m} , \dot{Q} , \dot{W} , and h are mass flow rate, heat flow rate, mechanical power, and specific enthalpy, respectively.

For heat exchangers, the above energy conservation equation can be expressed as:

$$\dot{Q}_{\text{he}} = \dot{m}_{\text{cf}} (h_{\text{out,cf}} - h_{\text{in,cf}}) = \dot{m}_{\text{hf}} (h_{\text{in,hf}} - h_{\text{out,hf}}) \cdot \eta_{\text{he}}, \quad (3-2)$$

where subscripts cf, hf, and he represent cold fluid, hot fluid, and heat exchanger, respectively; η_{he} is the heat exchanger efficiency.

For power generation components (GT and ST) and power consumption components (GC and Pump), the energy conservation equation can be respectively expressed as:

$$\dot{W}_{\text{gen},i} = \dot{m}_i (h_{\text{in},i} - h_{\text{out},i}) = \dot{m}_i (h_{\text{in},i} - h_{\text{out,is},i}) \cdot \eta_{\text{is},i}, \quad (3-3)$$

$$\dot{W}_{\text{con},j} = \dot{m}_j (h_{\text{out},j} - h_{\text{in},j}) = \dot{m}_j (h_{\text{out,is},j} - h_{\text{in},j}) / \eta_{\text{is},j}, \quad (3-4)$$

where $\dot{W}_{\text{gen},i}$ and $\dot{W}_{\text{con},j}$ represent the mechanical power generated by the i -th component and consumed by the j -th component, respectively; η_{is} denotes isentropic efficiency.

The mechanical power consumption of the Blower, $\dot{W}_{\text{con,Blower}}$, can be calculated by:

$$\dot{W}_{\text{con,Blower}} = \frac{\dot{V}_{\text{Blower}} \cdot \Delta p_{\text{Blower}}}{\eta_{\text{Blower}} \cdot \eta_{\text{m}}}, \quad (3-5)$$

where \dot{V}_{Blower} and Δp_{Blower} represent the volumetric flow rate and pressure difference of the Blower, respectively; η_{Blower} and η_{m} are Blower efficiency and mechanical efficiency, respectively.

The VHTR is essentially a heat exchanger and its “hot fluid” is the fissionable nuclear fuel in the graphite reactor core. The energy conservation equation of VHTR can be expressed as:

$$\dot{Q}_{\text{VHTR}} \cdot \eta_{\text{VHTR}} = \dot{m}_{\text{VHTR}} (h_{\text{out,VHTR}} - h_{\text{in,VHTR}}), \quad (3-6)$$

Due to the good thermal insulation of the reactor pressure vessel, the heat loss of the reactor can be neglected, which means the reactor efficiency (η_{VHTR}) is equal to 1 [118].

For the S-I system, its energy conservation equation can be expressed by Eq. (2-7) (or Eq. (2-8), if some waste heat recovery measures are adopted).

Given that the GT and GC are usually coaxial, the net electrical power output of the system, \dot{E}_{net} , can be approximately calculated by:

$$\dot{E}_{\text{net}} = \left[(\dot{W}_{\text{gen,GT}} - \dot{W}_{\text{con,GC}}) + \dot{W}_{\text{gen,ST}} \right] \cdot \eta_{\text{m}} \cdot \eta_{\text{G}} - \frac{(\dot{W}_{\text{con,Pump}} + \dot{W}_{\text{con,Blowers}})}{\eta_{\text{m}} \cdot \eta_{\text{M}}} - \dot{E}_{\text{con,S-I}}, \quad (3-7)$$

where η_{G} and η_{M} are Generator efficiency and Motor efficiency, respectively.

Thus, the thermal efficiency of the system, η_{th} , can be calculated by:

$$\eta_{\text{th}} = \frac{\dot{n}_{\text{H}_2} \cdot \Delta H_{\text{HHV,H}_2} + \dot{E}_{\text{net}}}{\dot{Q}_{\text{VHTR}}}, \quad (3-8)$$

where \dot{Q}_{VHTR} is the thermal power of the VHTR.

Exergy model

The exergy analysis method based on the first and second laws of thermodynamics focuses on the energy conversion process from the perspective of energy quantity and energy quality, which can reflect not only the external energy losses of the system, but also the internal exergy destructions of the system. Therefore, the exergy analysis method can better reveal the weak links of the system. For an open steady-state control volume, its exergy conservation equation can be expressed as:

$$\dot{E}x_{\dot{Q}_{cv}} = \sum (\dot{m} \cdot ex)_{out,cv} - \sum (\dot{m} \cdot ex)_{in,cv} + \dot{W}_{cv} + \dot{E}x_{loss,cv}, \quad (3-9)$$

where $\dot{E}x_{\dot{Q}_{cv}}$ and $\dot{E}x_{loss,cv}$ represent the heat exergy flow rate and exergy loss rate of the control volume, respectively; ex means specific exergy.

The heat exergy, Ex_Q , can be calculated by:

$$Ex_Q = \int \left(1 - \frac{T_0}{T}\right) dQ = Q - T_0 \cdot \Delta s, \quad (3-10)$$

where T_0 and Δs are the ambient temperature and the entropy change during heat transfer, respectively.

Neglecting the potential and kinetic exergies [84], the specific exergy (ex) in Eq. (3-9) can be calculated by:

$$ex = ex_{ph} + ex_{ch} = h - h_0 - T_0(s - s_0) + ex_{ch}, \quad (3-11)$$

where ex_{ph} and ex_{ch} are specific physical exergy and specific chemical exergy, respectively.

For component i , its exergy loss rate ($\dot{E}x_{loss,i}$) and exergy efficiency ($\eta_{ex,i}$) can be respectively calculated by:

$$\dot{E}x_{loss,i} = \dot{E}x_{input,i} - \dot{E}x_{output,i}, \quad (3-12)$$

$$\eta_{ex,i} = \frac{\dot{E}x_{output,i}}{\dot{E}x_{input,i}}, \quad (3-13)$$

where $\dot{E}x_{input,i}$ and $\dot{E}x_{output,i}$ represent the exergy flow input and exergy flow output of component i , respectively. The exergy loss equation and exergy efficiency equation of each component in the system are listed in Table 3-1.

Further, the exergy loss coefficient of component i , $\varepsilon_{loss,i}$, can be defined as:

$$\varepsilon_{loss,i} = \frac{\dot{E}x_{loss,i}}{\dot{E}x_{input,VHTR}} = \frac{\dot{E}x_{loss,i}}{\dot{E}x_{fuel}}, \quad (3-14)$$

where $\dot{E}x_{fuel}$ is the exergy flow rate of the nuclear fuel fission process (i.e., the exergy flow input of the reactor, $\dot{E}x_{input,VHTR}$) and can be calculated by Eq. (3-15).

Table 3-1. Exergy loss equation and exergy efficiency equation of each component in the system.

Components	Exergy loss equations	Exergy efficiency equations
IHX and SG	$\dot{E}x_{\text{loss},i} = \dot{m}_{\text{hf},i} (ex_{\text{in,hf},i} - ex_{\text{out,hf},i}) - \dot{m}_{\text{cf},i} (ex_{\text{out,cf},i} - ex_{\text{in,cf},i})$	$\eta_{\text{ex},i} = \frac{\dot{m}_{\text{cf},i} (ex_{\text{out,cf},i} - ex_{\text{in,cf},i})}{\dot{m}_{\text{hf},i} (ex_{\text{in,hf},i} - ex_{\text{out,hf},i})}$
AC and Condenser ^a	$\dot{E}x_{\text{loss},i} = \dot{m}_{\text{hf},i} (ex_{\text{in,hf},i} - ex_{\text{out,hf},i})$	$\eta_{\text{ex},i} = 0$
GT and ST	$\dot{E}x_{\text{loss},i} = \dot{m}_i (ex_{\text{in},i} - ex_{\text{out},i}) - \dot{W}_{\text{gen},i}$	$\eta_{\text{ex},i} = \frac{\dot{W}_{\text{gen},i}}{\dot{m}_i (ex_{\text{in},i} - ex_{\text{out},i})}$
GC, Pump, and Blower	$\dot{E}x_{\text{loss},i} = \dot{W}_{\text{con},i} - \dot{m}_i (ex_{\text{out},i} - ex_{\text{in},i})$	$\eta_{\text{ex},i} = \frac{\dot{m}_i (ex_{\text{out},i} - ex_{\text{in},i})}{\dot{W}_{\text{con},i}}$
VHTR	$\dot{E}x_{\text{loss},\text{VHTR}} = \dot{E}x_{\text{fuel}} - \dot{m}_{\text{VHTR}} (ex_{\text{out,VHTR}} - ex_{\text{in,VHTR}})$	$\eta_{\text{ex},\text{VHTR}} = \frac{\dot{m}_{\text{VHTR}} (ex_{\text{out,VHTR}} - ex_{\text{in,VHTR}})}{\dot{E}x_{\text{fuel}}}$
The S-I system	$\dot{E}x_{\text{loss},\text{S-I}} = \dot{E}x_{\dot{Q}_{\text{con},\text{S-I}}} + \dot{E}_{\text{con},\text{S-I}} - \dot{n}_{\text{H}_2} \cdot ex_{\text{ch},\text{H}_2}$	$\eta_{\text{ex},\text{S-I}} = \frac{\dot{n}_{\text{H}_2} \cdot ex_{\text{ch},\text{H}_2}}{\dot{E}x_{\dot{Q}_{\text{con},\text{S-I}}} + \dot{E}_{\text{con},\text{S-I}}}$
Generator ^b	$\dot{E}x_{\text{loss},\text{G}} = \left[(\dot{W}_{\text{gen},\text{GT}} - \dot{W}_{\text{con},\text{GC}}) + \dot{W}_{\text{gen},\text{ST}} \right] \cdot (1 - \eta_{\text{m}} \cdot \eta_{\text{G}})$	$\eta_{\text{ex},\text{G}} = \eta_{\text{m}} \cdot \eta_{\text{G}}$

^a The valid exergy outputs of AC and Condenser are considered to be 0 as the heat released by AC and Condenser is directly discharged to the environment.

^b The shaft coupling is considered part of the Generator.

$$\dot{E}x_{\text{fuel}} = \sum_{k=1}^m \left(\frac{\dot{Q}_{\text{VHTR}} b_{\text{fis},k}}{e_{\text{fis},k}} \cdot \left[\frac{\varphi_k e_{\text{fis},k}}{\sum_{k=1}^m (\varphi_k e_{\text{fis},k})} \right] \right), \quad (3-15)$$

where $b_{\text{fis},k}$, $e_{\text{fis},k}$, and φ_k represent the fission exergy, fission energy, and fractional fission of the fissionable element k , respectively. In this work, the nuclear fuel parameters of the HTR-10 (an experimental high-temperature gas-cooled reactor built in China) are used, which are summarized in Table 3-2.

Table 3-2. Main fuel parameters of the HTR-10.

Fissionable elements	Fission energy (MeV/nucleon)	Fission exergy (MeV/nucleon)	Fractional fission (%)
U ₂₃₅	203.0	192.9	85.59
Pu ₂₃₉	208.9	198.5	12.71
Pu ₂₄₁	210.8	200.3	1.49

Thus, the exergy efficiency of the system, η_{ex} , can be calculated by:

$$\eta_{\text{ex}} = \frac{\dot{n}_{\text{H}_2} \cdot ex_{\text{ch,H}_2} + \dot{E}_{\text{net}}}{\dot{E}x_{\text{fuel}}} = 1 - \sum \varepsilon_{\text{loss},i} = 1 - \varepsilon_{\text{loss,tot}}, \quad (3-16)$$

where $ex_{\text{ch,H}_2}$ and $\varepsilon_{\text{loss,tot}}$ represent the molar standard chemical exergy of hydrogen (236.1 kJ/mol [84]) and the total exergy loss coefficient of the system, respectively.

The above thermodynamic models are built and executed using MATLAB [119], and the thermodynamic properties of working fluids are retrieved from the NIST REFPROP database [120].

3.2 System simulation and performance analysis

3.2.1 System simulation

The key operating parameters of the system are listed in Table 3-3. In this work, the reactor operating parameters are determined according to the reactor concept of NGTCC (i.e., Nuclear Gas Turbine Combined Cycle) which is a helium cooled, graphite moderated modular VHTR with the process steam supply capability for cogeneration operation [121]. It is assumed that helium is used as the secondary loop heat carrier which enters and exits the IHX at 350°C [35,105] and 880°C [105,123], respectively. To avoid nuclear accidents and ensure reactor safety, the hydrogen production plant should be built away from the nuclear reactor. Therefore, the pressure loss of helium in the secondary loop pipeline cannot be ignored. In this study,

a pressure drop coefficient of 0.05 is used to roughly calculate this pressure loss [105]. Since the main task of this chapter is to figure out the thermodynamic characteristics of the nuclear hydrogen production system with GSCC as the power conversion unit, the S-I hydrogen production system is treated as a “black box” module consuming heat and electricity. According to the simulation results obtained in the previous chapter, when several waste heat recovery measures or assumptions (e.g., internal heat exchange network, distillation heat recovery, and electricity recovery) are applied to the S-I system, producing 1 mol of hydrogen will consume about 544.3 kJ of heat and about 105.4 kJ of electricity (see Table 2-11 and Ref. [124]). Therefore, these two values are used to represent the energy requirements of the S-I system for the reason of model simplification (it should be noted that the actual energy requirements of the S-I system may be larger due to the inevitable energy loss during waste heat recovery). Besides, given the high safety standards of nuclear power systems, the subcritical SRC is used in this work to avoid over-high operating pressures and ensure the absolute safety of the system.

Table 3-3. Key operating parameters of the system.

Parameters (Unit)	Value	Refs.
Ambient temperature, T_0 (°C)	25	[105]
Ambient pressure, p_0 (atm)	1	[105]
Reactor primary circuit		
Reactor thermal power (MWth)	350	[121]
Reactor inlet/outlet temperatures (°C)	400/950	[121]
Maximum system pressure (i.e., reactor inlet pressure) (MPa)	7.1	[121]
Primary loop pressure ratio (-)	1.94 ^a	[121]
Pressure drop coefficient of helium in the reactor (-)	0.022	[122]
Pressure drop coefficient of helium in the heat exchanger (-)	0.01	[122]
The S-I hydrogen production system		
Secondary loop helium supply temperature (°C)	880	[105,123]
Secondary loop helium return temperature (°C)	350	[35,105]
Pressure drop coefficient of helium in the secondary loop pipeline (-)	0.05	[105]
Blower efficiency, η_{Blower} (-)	0.85	[105]
Heat consumed to produce 1 mol of hydrogen (kJ)	544.3	[124]
Electricity consumed to produce 1 mol of hydrogen (kJ)	105.4	[124]
The GSCC power conversion system		
SRC main steam temperature (°C)	566	[18]
SRC main steam pressure (MPa)	13.9	[18]

SRC condensation pressure (i.e., SRC low pressure) (kPa)	10	[125]
Pressure drop coefficient of water/steam in the heat exchanger (-)	0.05	[122]
Isentropic efficiency of the GT, $\eta_{is,GT}$ (-)	0.92	[122]
Isentropic efficiency of the ST, $\eta_{is,ST}$ (-)	0.90	[122]
Isentropic efficiency of the GC, $\eta_{is,GC}$ (-)	0.90	[122]
Isentropic efficiency of the Pump, $\eta_{is,Pump}$ (-)	0.85	[122]
Efficiency of the heat exchanger, η_{he} (-)	0.98	[118]
Mechanical efficiency, η_m (-)	0.998	[118]
Motor efficiency, η_M (-)	0.95	[118]
Generator efficiency, η_G (-)	0.992	[118]

^a In this work, this value is considered to be the pressure (expansion) ratio of GT.

Figure 3-3 shows the flowchart of the model solving procedure. After entering all known system parameters, the first step is to set up the mass flow rate ratio (α) and the IHX's primary side helium outlet temperature ($T_{out,ps,IHX}$). Once these two parameters are specified, the heat input to the S-I hydrogen production system can be determined and the hydrogen production rate can be calculated. Then, an iterative calculation regarding the GC's inlet temperature begins, which uses a maximum absolute error of 0.001 in the GC's isentropic efficiency ($\eta_{is,GC}$) as the convergence criterion. If the calculated isentropic efficiency ($\eta_{is,GC}$) under the assumed GC's inlet temperature fails to satisfy the convergence criterion, a new round of calculations will be performed by changing the GC's inlet temperature by 0.01°C.

Once the convergence criterion is met, the other unknown operating parameters of the reactor primary circuit can be solved and the heat input to the SRC ($\dot{Q}_{input,SRC}$, namely the SG's heat flow rate, \dot{Q}_{SG}) can be calculated. Next, the outlet parameters of the Condenser and Pump can be easily calculated according to the known SRC condensation pressure and main steam pressure (see Table 3-3). Lastly, the mass flow rate of water (\dot{m}_{water}) in the SRC can be calculated according to the energy conservation law or Eq. (3-2).

After obtaining the mass flow rate of water, all operating parameters in the SRC can be solved. In order to ensure the feasibility and safety of the system operation, several key operation checks are carried out in this work. For instance, to ensure the smooth heat transfer process in the SG, the terminal heat transfer temperature difference ($\Delta T_{ter,SG}$) and pinch point temperature difference ($\Delta T_{pp,SG}$) of the SG should not be lower than 30°C and 15°C, respectively [126]; To keep the ST running safely, the turbine exhaust dryness (q_{ST}) should not be lower than 0.85 [17]. When all these operating constraints are fulfilled, the thermodynamic performance parameters of the entire system (i.e., hydrogen production rate, net electrical power output, thermal efficiency, and exergy efficiency) will be calculated and exported.

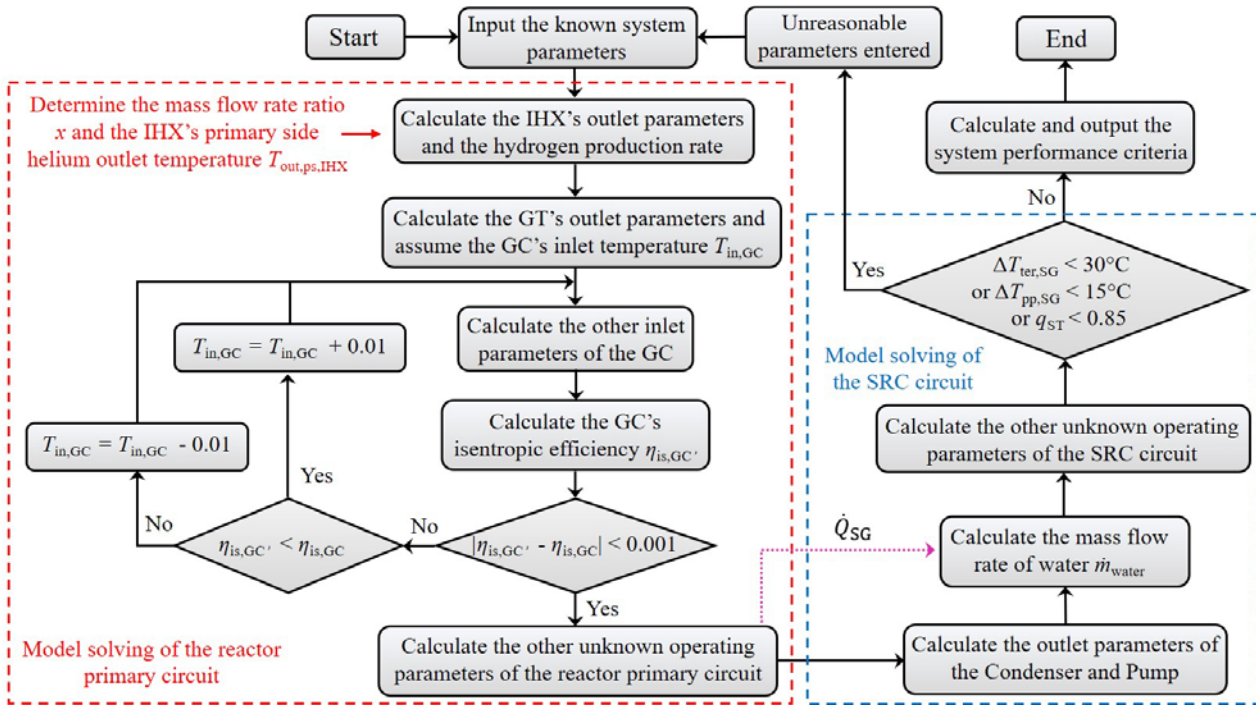


Figure 3-3. Flowchart of the model solving procedure.

Given that an actual VHTR-based nuclear hydrogen production system has not yet been built until now, the model validation can only be done by comparing the current simulation results with the data reported in the relevant literature. The model validation of the S-I hydrogen production system has been presented in the previous chapter (see Tables 2-4 and 2-5), so the remaining work is to verify the reliability of the simulation results of the GSCC power conversion system. Obviously, when the mass flow rate ratio (α) is set to 0, the system shown in Figure 3-2 will become a GSCC nuclear power system. Table 3-4 shows the model validation results of this system. It can be seen that under the same reactor thermal power and primary loop pressure ratio, the obtained simulation results are in good agreement with the results reported in the published literature. Therefore, the current thermodynamic models can be used to obtain some reliable analysis results.

Table 3-4. Model validation of the GSCC nuclear power system.

Parameters (Unit)	Ref. [105]	This work	Ref. [122]	This work
Reactor thermal power (MW)	350	350	600	600
Primary loop pressure ratio (-)	2.48	2.48	2.5	2.5
Net electrical power output \dot{E}_{net} (MW)	172.8	173.97	303.54	298.9
Thermal efficiency η_{th} (%)	49.36	49.71	50.59	49.82
Exergy efficiency η_{ex} (%)	51.94	52.31	—	52.43

3.2.2 Performance analysis

As shown in Figure 3-3, the mass flow rate ratio (x) and the IHX's primary side helium outlet temperature ($T_{\text{out,ps,IHX}}$) are two key operating parameters that determine the energy distribution of the system. Obviously, the mass flow rate ratio is related to the size of the hydrogen production load, and in theory, it can be set to a value in the range of 0 to 1. The IHX's primary side helium outlet temperature is related to both the IHX's secondary side helium inlet temperature (this temperature determines the lower limit of $T_{\text{out,ps,IHX}}$) and the IHX's heat exchange performance (this factor determines the temperature drop of the primary side helium flowing through IHX), and in this work, it is set to a value in the range of 400°C to 700°C. Keep other operating parameters (i.e., the operating parameters shown in Table 3-3) unchanged, the effects of different mass flow rate ratios and different IHX's primary side helium outlet temperatures on the thermodynamic performance of the system are obtained, as shown in Figure 3-4.

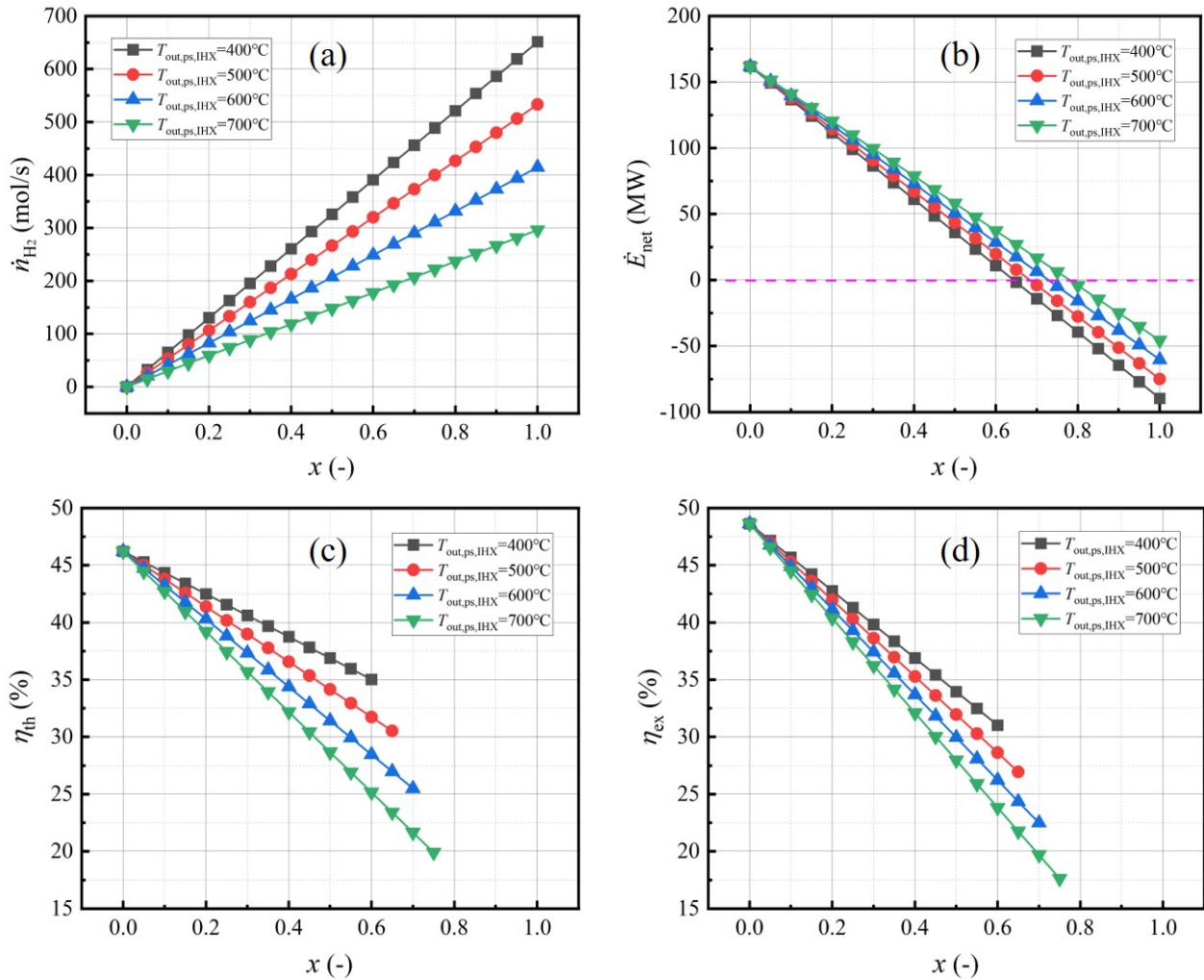


Figure 3-4. Thermodynamic performance of the system under different mass flow rate ratios and different IHX's primary side helium outlet temperatures: (a) Hydrogen production rate, (b) Net electrical power output, (c) Thermal efficiency, and (d) Exergy efficiency.

It can be seen from Figure 3-4(a) that when the IHX's primary side helium outlet temperature is kept unchanged, the hydrogen production rate will increase linearly with the increase of the mass flow rate ratio, and when the mass flow rate ratio is kept unchanged, the hydrogen production rate will decrease gradually with the increase of the IHX's primary side helium outlet temperature. Obviously, as the mass flow rate ratio increases or as the IHX's primary side helium outlet temperature decreases, both the heat duty of the IHX and the heat input to the S-I hydrogen production system will increase, causing the increase in the hydrogen production rate. From Figure 3-4(b), it can be seen that when the IHX's primary side helium outlet temperature is kept unchanged, the net electrical power output of the system will decrease linearly with the increase of the mass flow rate ratio, while when the mass flow rate ratio is kept unchanged, the net electrical power output will increase slightly with the increase of the IHX's primary side helium outlet temperature. As we all know, the heat input to the combined cycle power generation system will decrease as the mass flow rate ratio increases, which reduces the amount of power generation. On the other hand, the increase in the mass flow rate ratio results in the increase of the hydrogen production rate (see Figure 3-4(a)), which means that the S-I hydrogen production system will require consuming more electricity at this time. Accordingly, the net electrical power output of the system will decrease significantly as the mass flow rate ratio increases. Similarly, when the mass flow rate ratio is kept unchanged and the IHX's primary side helium outlet temperature is increased, the power generation of the combined cycle power conversion system will remain unchanged, while the electricity consumption of the S-I hydrogen production system will decrease (due to the reduced hydrogen production rate, see Figure 3-4(a)), that is why the net electrical power output of the system increases with the increase of the IHX's primary side helium outlet temperature.

From Figure 3-4(b), it can also be seen that when the mass flow rate ratio (or the hydrogen production rate) increases to exceed a certain value, the net electrical power output of the system will become a negative value. At this time, the electrical power generated by the combined cycle power conversion system cannot meet the electricity requirements of the S-I hydrogen production system, and part of electricity needs to be provided by external power sources such as electric grid. It should be noted that when the net electrical power output equals to a negative value, the definition equations of the system's thermal efficiency and exergy efficiency, namely Eqs. (3-8) and (3-16), are no longer applicable. Therefore, the thermal and exergy efficiencies of the system under some operating conditions are not shown in Figure 3-4(c) and (d).

From Figure 3-4(c) and (d), it can be seen that when one of the IHX's primary side helium outlet temperature and mass flow rate ratio remains unchanged, the thermal efficiency and exergy efficiency of the system will decrease with the increase of the other parameter. Obviously, when the mass flow rate ratio remains unchanged, the heat duty of the AC will increase as the IHX's primary side helium outlet temperature increases, and at this time, more reactor heat will be discharged to the environment (or cooling water) as heat loss. Thus, the thermal efficiency and exergy efficiency of the system will decrease with the increase of the IHX's primary side helium outlet temperature. Similarly, when the IHX's primary side helium outlet temperature remains unchanged and is higher than the reactor inlet temperature

(namely 400°C, see Table 3-3), the heat duty of the AC will also increase as the mass flow rate ratio increases, resulting in more heat losses (this is one of the reasons for the decreasing system efficiencies). Note that even when the IHX's primary side helium outlet temperature is equal to the reactor inlet temperature (400°C), the thermal efficiency and exergy efficiency of the system still decrease with the increase of the mass flow rate ratio (see Figure 3-4(c) and (d)). It is considered that this result is caused by the reason that the S-I cycle-based nuclear hydrogen production efficiencies are lower than the combined cycle-based nuclear power generation efficiencies. Take the thermal efficiency of nuclear hydrogen production (η_{th,H_2}) as an example, Figure 3-5 schematically shows a calculation diagram of the thermal efficiency of nuclear hydrogen production. It is known to us all that the reactor heat cannot be directly provided to the S-I system due to radioactivity and safety concerns. Therefore, an IHX is used, which brings a heat exchanger efficiency, η_{IHX} (in this work, it is set to 0.98, see Table 3-3). Besides this, it should also be noted that the VHTR is essentially a heat exchanger, except that its heat loss has been ignored in this work (as mentioned previously, η_{VHTR} is equal to 1 [118]). Therefore, the thermal efficiency of nuclear hydrogen production can be calculated by:

$$\eta_{th,H_2} = \frac{\dot{n}_{H_2} \cdot \Delta H_{HHV,H_2}}{\frac{\dot{Q}_{con,S-I}}{\eta_{IHX} \cdot \eta_{VHTR}} + \frac{\dot{E}_{con,S-I}}{\eta_{th,E}}}, \quad (3-17)$$

where $\eta_{th,E}$ represents the thermal efficiency of nuclear power generation.

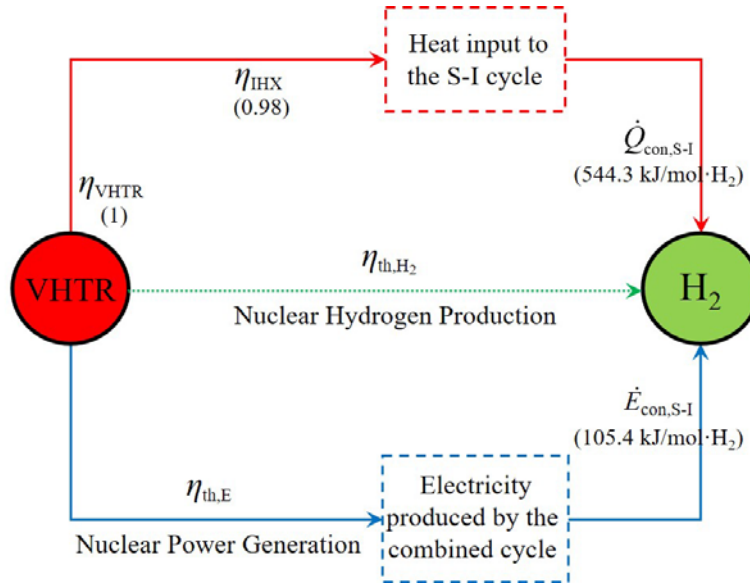


Figure 3-5. Schematic diagram of the calculation of the thermal efficiency of nuclear hydrogen production.

It is well-known that the thermal efficiency of the combined cycle-based nuclear power generation is usually larger than 45% (see Figure 3-4(c) for the case where the mass flow rate ratio x is equal to 0), and sometimes it can reach or exceed 50% after optimization (see Table 3-4). Assuming that the thermal efficiency of the combined

cycle-based nuclear power generation is in the range of 40%-50%, according to the above equation, the thermal efficiency of nuclear hydrogen production is calculated as:

$$\eta_{\text{th,H}_2} = \frac{285.83}{\frac{544.3}{0.98 \times 1} + \frac{105.4}{0.4 \sim 0.5}} \approx 0.349 \sim 0.373, \quad (3-18)$$

It is seen that the thermal efficiency of nuclear hydrogen production is equal to about 34.9%-37.3%, which is obviously lower than the thermal efficiency of the combined cycle-based nuclear power generation (the same is true for exergy efficiency). Therefore, as the mass flow rate ratio increases, more reactor heat is used to produce hydrogen at a lower efficiency, resulting in the decrease in the overall efficiency of the system, as shown in Figure 3-4(c) and (d).

It should be noted that, in the above equation, the energy consumption values to produce 1 mol of hydrogen (i.e., 544.3 kJ of heat and 105.4 kJ of electricity) are already the lowest energy consumption of the improved S-I system (see Table 2-11), which means that the calculated thermal efficiency of nuclear hydrogen production (i.e., 34.9%-37.3%) is somewhat overestimated (or the actual thermal efficiency of nuclear hydrogen production may be lower than the calculated value). If the S-I system is not improved or optimized, the thermal efficiency and exergy efficiency of the entire system will decrease in a faster rate as the mass flow rate ratio (or hydrogen production rate) increases.

In order to reveal the weak links of the system and provide directions for system optimization, the exergy analysis of the system under different IHX's primary side helium outlet temperatures (the mass flow rate ratio x remains unchanged at 0.5) are performed, as shown in Figure 3-6. It can be seen that for all operating conditions, the largest exergy loss occurs in the VHTR whose exergy efficiency and exergy loss coefficient are found to be about 70.65% and 29.35%, respectively. This result is reasonable because both the fuel fission process and the large temperature difference heat transfer process inside the reactor will lead to considerable irreversible energy loss (or exergy loss). It can also be seen that the exergy efficiency of the S-I system is very low, only about 50.8%, which means that it is very necessary and important to optimize the process flow and operating parameters of the S-I system when the hydrogen production load is large. As mentioned earlier (see Table 3-1), the heat released by the AC and Condenser (CON) is directly dumped to the environment (or cooling water) without being recovered, so the exergy efficiencies of these two components are considered to be 0. Different from the AC, the Condenser (CON) always has a low exergy loss coefficient (smaller than 2%, see Figure 3-6), which means that the exergy loss of the Condenser is not large. It is well-known that, for the SRC, to achieve the large steam enthalpy drop (or to generate more mechanical work), the turbine exhaust temperature is usually not high (slightly higher than the ambient temperature). In this situation, the specific exergy of the turbine exhaust is very small, so the exergy loss of the Condenser is not significant (similar to coal-fired power plants where the exergy loss of the Condenser is also small). However, for the AC, its exergy loss is dependent on the temperature difference between the IHX's primary side outlet and the reactor inlet. As shown in Figure 3-6, as the IHX's primary side helium outlet temperature increases (namely the temperature

difference between the IHX's primary side outlet and the reactor inlet is increasing), the exergy loss coefficient of the AC becomes larger and larger, and when the IHX's primary side helium outlet temperature is increased to 700°C, the exergy loss coefficient of the AC is equal to about 19% (only lower than the exergy loss coefficient of the VHTR, see Figure 3-6(d)). At this time, the exergy loss of the AC is quite large, and it is very necessary to improve the system layout or take some measures to recover the waste heat released by the AC.

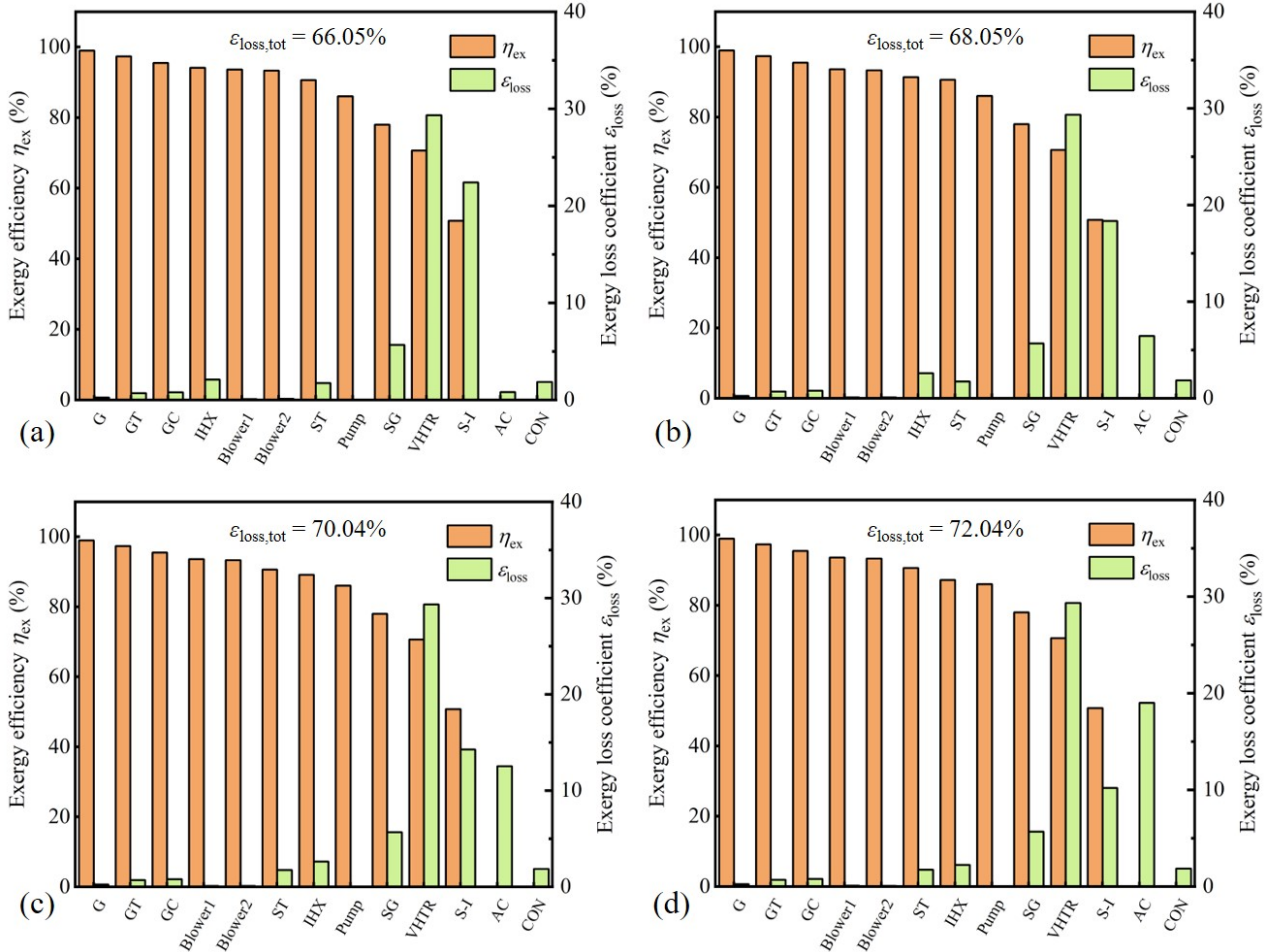


Figure 3-6. Exergy analysis results of the system under different IHX's primary side helium outlet temperatures ($x = 0.5$): (a) $T_{out,ps,IHX} = 400^\circ\text{C}$, (b) $T_{out,ps,IHX} = 500^\circ\text{C}$, (c) $T_{out,ps,IHX} = 600^\circ\text{C}$, and (d) $T_{out,ps,IHX} = 700^\circ\text{C}$.

From Figure 3-6, it can also be seen that when the mass flow rate ratio x remains unchanged at 0.5, the total exergy loss coefficient of the system ($\epsilon_{loss,tot}$) will increase with the increase of the IHX's primary side helium outlet temperature (according to Eq. (3-16), it can be concluded that the exergy efficiency of the system will decrease as the IHX's primary side helium outlet temperature increases). This result is in good agreement with the results shown in Figure 3-4(d), which again emphasizes that the exergy analysis results obtained are reasonable. In short, both the performance analysis results of Figure 3-4 and the exergy analysis results of Figure 3-6 indicate that when the IHX's primary side helium outlet temperature is very high and the hydrogen production load is large, it is necessary and important to recover the waste

heat of the AC to improve the thermodynamic performance of the entire hydrogen-power cogeneration system.

3.3 Design and analysis of a novel GSCC power conversion system

3.3.1 System design

As summarized in the previous section, when the IHX's primary side helium outlet temperature is very high, it is very necessary to improve the existing system layout to enhance the thermodynamic performance of the system. Figure 3-7 schematically shows three promising system layouts for the VHTR and S-I cycle-based nuclear hydrogen production system, and it is not difficult to see that the conventional GSCC power conversion system (see Figure 3-1 or Figure 3-2) adopts the parallel connection layout shown here. According to the series connection layout shown in Figure 3-7(a) and the mixed connection layout shown in Figure 3-7(c), the primary loop helium leaving the IHX can be further utilized by the PGS (i.e., Power Generation System) to generate electricity. Based on this idea, a new system is designed, as shown in Figure 3-8. It is seen that the proposed new system adopts a mixed connection layout, and in this layout, the primary loop helium leaving the IHX is sent to another SG (named SG2) to produce steam for power generation. Since the heat loss of the AC is avoided, the proposed new system is believed to be able to achieve better thermodynamic performance than the conventional system.

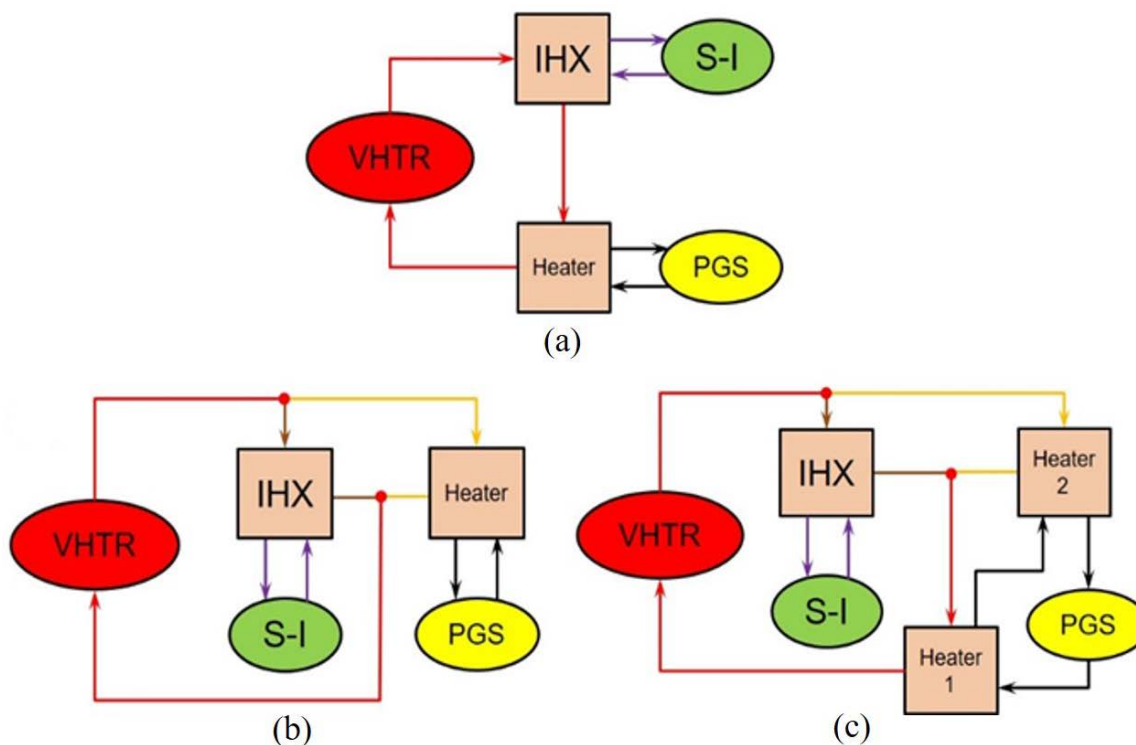


Figure 3-7. Three promising system layouts for the VHTR and S-I cycle-based nuclear hydrogen production system [127]: (a) The series connection layout, (b) The parallel connection layout, and (c) The mixed connection layout.

systems under the benchmark conditions are summarized in Tables 3-6 and 3-7, respectively). It can be seen that under the benchmark conditions, the two systems both achieve a hydrogen production rate of about 177.68 mol/s, but the net electrical power output of the conventional system is significantly less than that of the new system. This is because the heat wasted by the AC is recovered by the SG2 and finally converted into electricity by the turbine generator. Since the AC results in a considerable heat loss, the thermal efficiency and exergy efficiency of the conventional system are very low, only about 30.04% and 28.96%. By using the proposed new system layout, the thermal efficiency and exergy efficiency of the conventional system are improved by approximately 8.76% and 9.22%, respectively, as shown in Table 3-5.

Table 3-5. Performance data of the two systems under the benchmark conditions.

Performance parameters (Unit)	Conventional system	New system	Increment
Hydrogen production rate \dot{n}_{H_2} (mol/s)	177.68	177.68	0
Net electrical power output \dot{E}_{net} (MW)	54.36	85.02	30.66
Thermal efficiency η_{th} (%)	30.04	38.80	8.76
Exergy efficiency η_{ex} (%)	28.96	38.18	9.22

Table 3-6. State-point parameters of the conventional system (see Figure 3-2) under the benchmark conditions.

State points	Fluids	\dot{m} (kg/s)	T (K)	p (MPa)	h (kJ/kg)	s (kJ/kg·K)
1	Helium	122.6	1223.15	6.94	6376.6	26.559
2	Helium	61.3	961.41	3.58	5008.4	26.684
3	Helium	61.3	496.26	3.54	2593.4	23.272
4	Helium	61.3	673.15	7.1	3522.4	23.413
5	Helium	61.3	923.15	6.87	4819.3	25.119
6	Helium	61.3	659.98	6.81	3453.2	23.398
7	Helium	61.3	673.15	7.1	3522.4	23.413
8	Helium	122.6	673.15	7.1	3522.4	23.413
9	Helium	34.0	623.15	7.27	3263.5	22.962
10	Helium	34.0	1153.15	7.2	6014.0	26.178
11	Water	2003.8	298.15	0.101	104.9	0.367
12	Water	2003.8	308.15	0.101	146.7	0.505
13	Water	44.0	320.07	14.63	209.1	0.657
14	Steam	44.0	839.15	13.9	3504.3	6.620
15	Steam	44.0	319.96	0.0105	2242.4	7.058
16	Water	44.0	318.96	0.01	191.8	0.649

17	Water	2160.4	298.15	0.101	104.9	0.367
18	Water	2160.4	308.15	0.101	146.7	0.505

Table 3-7. State-point parameters of the proposed new system (see Figure 3-8) under the benchmark conditions.

State points	Fluids	\dot{m} (kg/s)	T (K)	p (MPa)	h (kJ/kg)	s (kJ/kg·K)
1	Helium	122.6	1223.15	6.94	6376.6	26.559
2	Helium	61.3	961.41	3.58	5008.4	26.684
3	Helium	61.3	496.26	3.54	2593.4	23.272
4	Helium	61.3	673.15	7.1	3522.4	23.413
5	Helium	61.3	923.15	6.87	4819.3	25.119
6	Helium	61.3	659.98	6.81	3453.2	23.398
7	Helium	61.3	673.15	7.1	3522.4	23.413
8	Helium	122.6	673.15	7.1	3522.4	23.413
9	Helium	34.0	623.15	7.27	3263.5	22.962
10	Helium	34.0	1153.15	7.2	6014.0	26.178
11	Water	68.9	320.07	14.63	209.1	0.657
12	Water	44.0	320.07	14.63	209.1	0.657
13	Water	24.9	320.07	14.63	209.1	0.657
14	Steam	68.9	839.15	13.9	3504.3	6.620
15	Steam	68.9	319.96	0.0105	2242.4	7.058
16	Water	68.9	318.96	0.01	191.8	0.649
17	Water	3382.5	298.15	0.101	104.9	0.367
18	Water	3382.5	308.15	0.101	146.7	0.505

The exergy analysis results of the two systems under the benchmark conditions are shown in Figure 3-9. It can be seen that, when the waste heat of the AC is used to produce the high temperature and pressure steam for power generation, the exergy loss coefficient of this component is decreased from about 15.73% to 4.36%, and the total exergy loss coefficient of the system ($\varepsilon_{\text{loss,tot}}$) is decreased from about 71.04% to 61.82% (this means that the system exergy efficiency is increased from 28.96% to 38.18% (according to Eq. (3-16)), as shown in Table 3-5). Therefore, it can be concluded that the proposed new system layout is an effective way to improve the thermodynamic performance of the conventional system.

Keeping the IHX's primary side helium outlet temperature unchanged (i.e., $T_{\text{out,ps,IHX}} = 650^\circ\text{C}$), the effects of the mass flow rate ratio (α) on system performance are shown in Figure 3-10. From Figure 3-10(a) and (b), it can be seen that as the mass flow rate ratio increases, the hydrogen production rate increases linearly (note that the

conventional system and the proposed new system have the same hydrogen yield), while the net electrical power output decreases linearly. As discussed in the previous section, the increase in the mass flow rate ratio means that part of the reactor heat previously used to generate electricity is now being used to produce hydrogen (so the hydrogen production rate is increasing, as shown in Figure 3-10(a)). On the other hand, the increase in the hydrogen yield means that the S-I system needs to consume more electricity. Therefore, the net electrical power output decreases gradually as the mass flow rate ratio increases. However, for the proposed new system, since the primary loop helium leaving the IHX still transfers some of the heat to the secondary loop water/steam for power generation, its net electrical power output is greater than that of the conventional system. And the larger the mass flow rate ratio, the greater the difference in net electrical power output, as shown in Figure 3-10(b). From Figure 3-10(c) and (d), it can be seen that for both systems, the thermal efficiency and exergy efficiency gradually decrease as the mass flow rate ratio increases, and the decreasing rate of the conventional system is faster than that of the proposed new system (this is because the heat loss of the AC of the conventional system is increasing). As explained in the previous section, the S-I cycle-based nuclear hydrogen production efficiencies are significantly lower than the combined cycle-based nuclear power generation efficiencies, so the thermodynamic efficiencies of the overall system will decrease when more hydrogen is produced.

Similarly, keeping the mass flow rate ratio unchanged (i.e., $x = 0.5$), the effects of the IHX's primary side helium outlet temperature ($T_{\text{out,ps,IHX}}$) on system performance are shown in Figure 3-11. It can be seen from Figure 3-11(a) and (b) that as the IHX's primary side helium outlet temperature increases, the hydrogen production rate decreases linearly (note that the conventional system and the proposed new system have the same hydrogen yield), while the net electrical power output increases linearly. As discussed in the previous section, the heat input to the S-I system decreases with the rise of the IHX's primary side helium outlet temperature, leading to a reduction in both hydrogen production and electricity consumption (this is why the net electrical power output of the conventional system gradually increases). In addition, for the proposed new system, the reduction in heat input of the S-I system means that more reactor heat is used to generate electricity, that is why the increasing rate of the net electrical power output of the new system is faster than that of the conventional system, as shown in Figure 3-11(b).

Because in this work, the thermal and exergy efficiencies of nuclear power generation are higher than those of nuclear hydrogen production, the thermodynamic efficiencies of the new system will increase when more reactor heat is used to generate electricity, as shown in Figure 3-11(c) and (d). However, as the IHX's primary side helium outlet temperature increases, the heat loss of the AC will also increase, so the thermal and exergy efficiencies of the conventional system become lower and lower, as presented in Figure 3-11(c) and (d). In a word, the proposed new system can achieve better thermodynamic performance than the conventional system, and this conclusion will be demonstrated again in the next chapter.

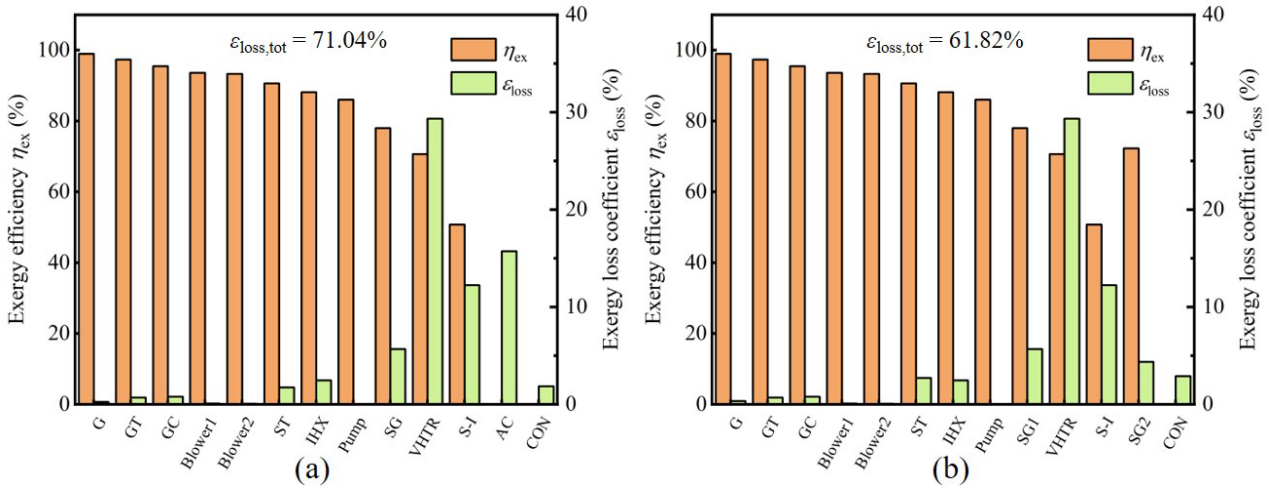


Figure 3-9. Exergy analysis results of the two systems under the benchmark conditions: (a) The conventional system and (b) The proposed new system.

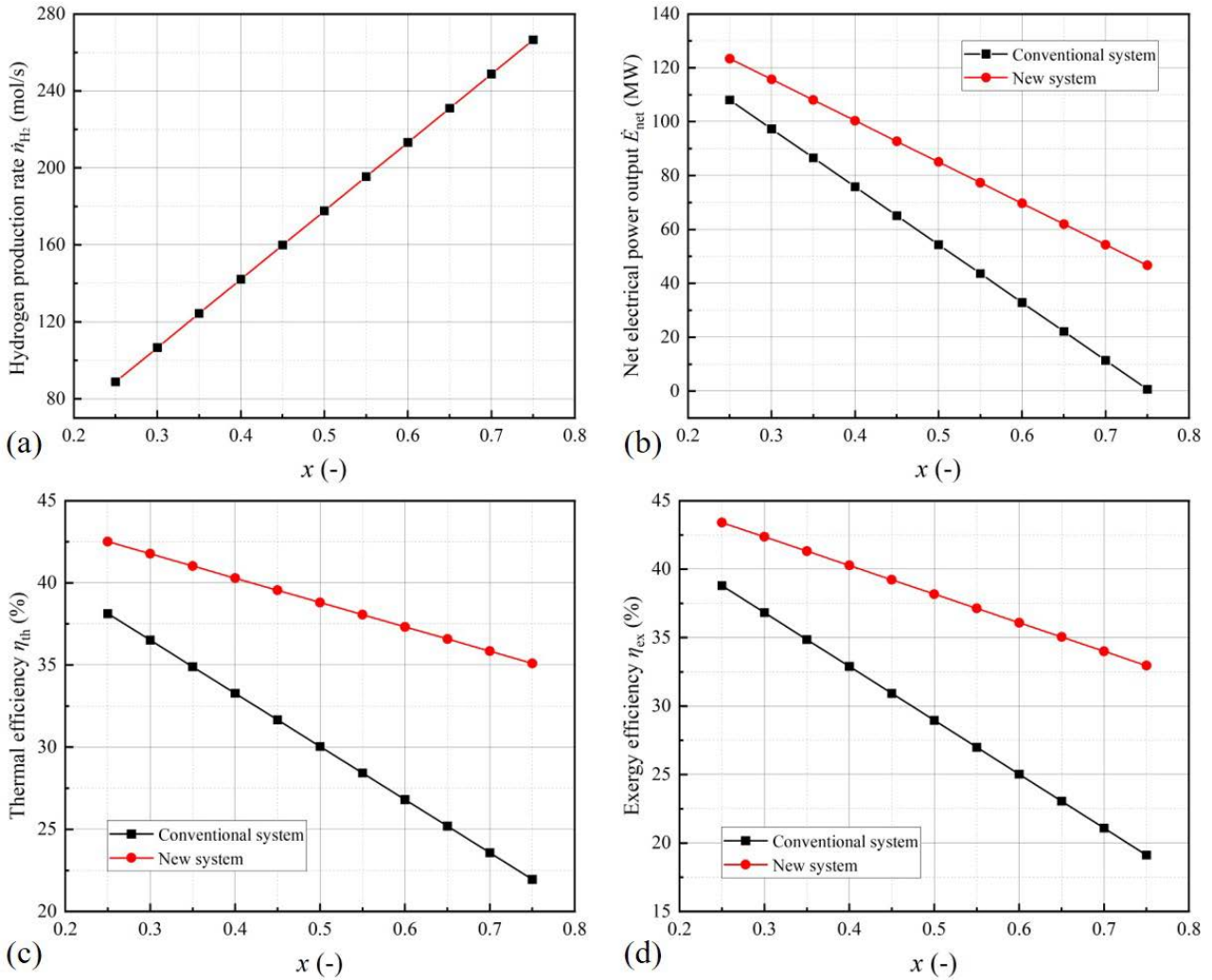


Figure 3-10. Effects of the mass flow rate ratio on system performance: (a) Hydrogen production rate, (b) Net electrical power output, (c) Thermal efficiency, and (d) Exergy efficiency.

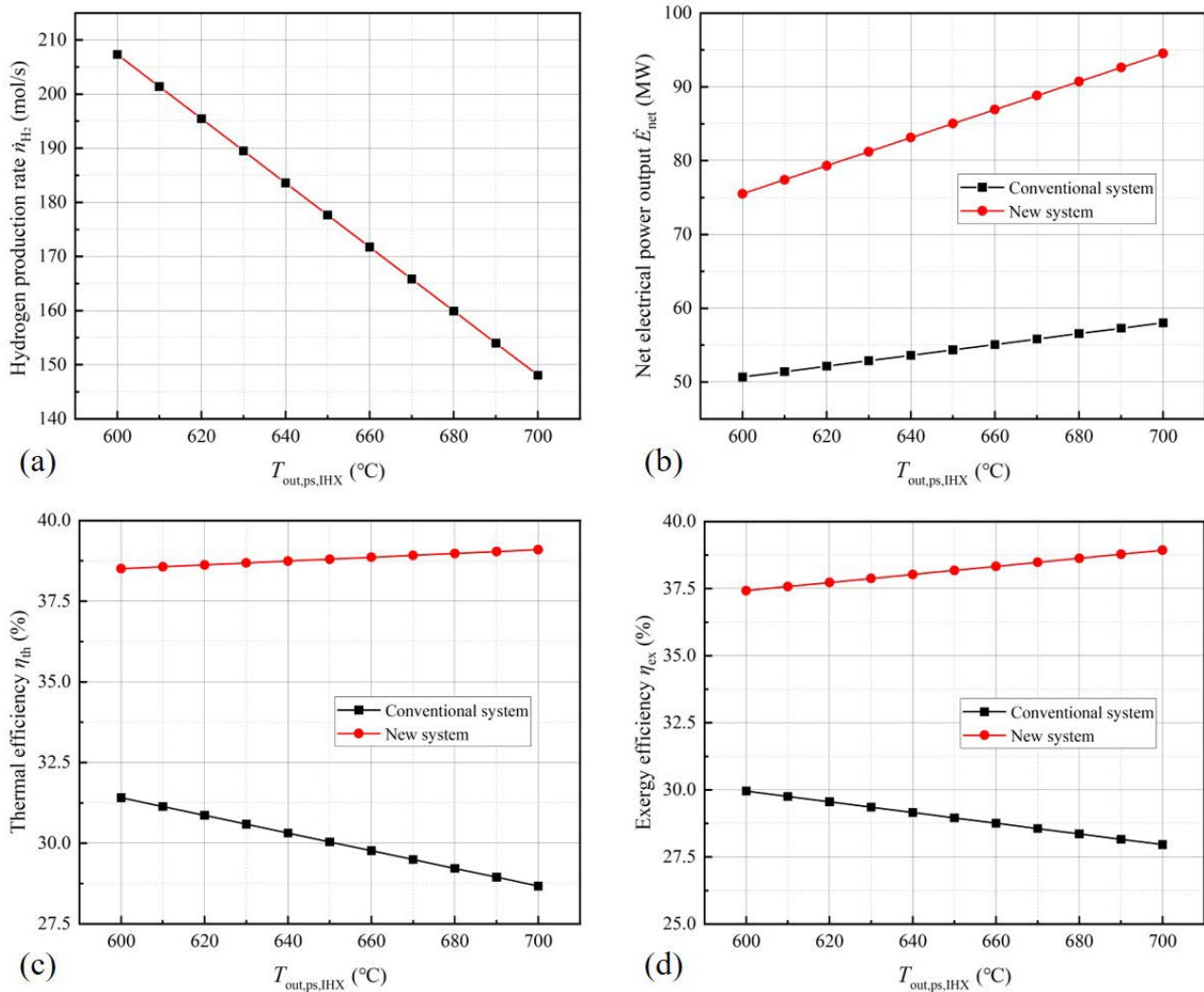


Figure 3-11. Effects of the IHX's primary side helium outlet temperature on system performance: (a) Hydrogen production rate, (b) Net electrical power output, (c) Thermal efficiency, and (d) Exergy efficiency.

3.4 Summary of this chapter

In this chapter, the conventional GSCC power conversion system was first modeled and analyzed based on the first and second laws of thermodynamics. Then, the thermodynamic performance of the conventional system under different operating conditions was studied and the weak links of the system were revealed. Finally, a new system layout was developed to elevate the thermodynamic performance of the conventional system.

The performance analysis results of the conventional VHTR-driven nuclear hydrogen production system using S-I cycle and GSCC show that with the increase of the mass flow rate ratio or the decrease of the IHX's primary side helium outlet temperature, the hydrogen production rate increases linearly, while the net electrical power output decreases linearly. It is also found that when more energy is used to produce

hydrogen, the overall thermodynamic efficiencies of the system (including thermal efficiency and exergy efficiency) will decrease significantly. Thus, it is concluded that the S-I cycle-based nuclear hydrogen production efficiencies are lower than the GSCC-based nuclear power generation efficiencies. Assuming that the thermal efficiency of the GSCC-based nuclear power generation is in the range of 40%-50%, the calculated thermal efficiency of the S-I cycle-based nuclear hydrogen production is only about 34.9%-37.3%. The exergy analysis results of the system show that the largest exergy loss of the system occurs in the nuclear reactor (i.e. VHTR), and its exergy efficiency and exergy loss coefficient are about 70.7% and 29.4%, respectively. The exergy efficiency of the S-I cycle is very low, only about 50.8%, which means that it is necessary to optimize the process flow and operating parameters of the S-I system when the hydrogen production load is large. Besides this, it is also found that the exergy loss coefficient of the Condenser is always very low, which means that the exergy loss of the Condenser is not significant. Finally, it is found that placing a SG at the primary side outlet of IHX is an effective way to improve the thermodynamic performance of the conventional nuclear hydrogen production system with S-I cycle and GSCC. In general, the obtained thermodynamic analysis results and the proposed new system layout not only provide a theoretical foundation for understanding the thermodynamic characteristics of the VHTR-driven nuclear hydrogen production system using S-I cycle and GSCC, but also point out a direction for the future engineering design of the system.

Chapter 4

System layout improvement and integrated design

In the previous two chapters, in order to simplify the system modeling process as much as possible, the preliminary conceptual designs of the S-I hydrogen production system and the GSCC power conversion system were carried out without considering some realistic operation requirements. Accordingly, the actual system characteristics cannot be fully demonstrated, and the obtained simulation results may not be used to guide actual engineering. Aiming at this problem, this chapter has carried out the system layout improvement and integration design, and finally formed two complete system design schemes. In addition, the thermodynamic performance of the two systems under different hydrogen production conditions was analyzed. This chapter aims to further refine the existing system design and calibrate the previously obtained simulation results.

4.1 System layout improvement

4.1.1 Overall system

Generally, when the Brayton cycle is used as the PGS, there are three main approaches considered for connecting the VHTR to the PGS and S-I cycle, as shown in Figure 4-1 (taking the parallel connection layout as an example). The first is the simplest and employs a direct PGS plus indirect S-I cycle (see Figure 4-1(a)), which is used in all systems studied in the previous chapter. The direct PGS means that the primary loop helium leaving the VHTR is sent directly to the GT for power generation, which may lead to contamination of the turbomachinery if significant care is not taken. The indirect gas-to-gas connection concept shown in Figure 4-1(b) helps to resolve this problem to a large extent because it effectively separates the primary loop radioactive helium from the secondary loop helium by using an IHX. Furthermore, if the gas pressure of the secondary loop remains higher than that of the primary loop, in the event of an IHX rupture, the radioactive helium will still be contained in the primary loop. Given the complexity of the S-I thermochemical hydrogen production process and the fact that hydrogen is a flammable and explosive gas, a tertiary heat transfer loop may be required to further isolate the nuclear reactor from potentially hazardous processes and avoid possible contamination, as

shown in Figure 4-1(c). Obviously, using such a loop will significantly improve the safety of the system. However, it is important to point out that any additional heat transfer loops will decrease the possibility of contamination in an accident, but will also result in additional components (or additional energy losses), reducing overall system efficiency and increasing system cost [87]. In this work, the second connection concept (i.e., the indirect gas-to-gas connection concept shown in Figure 4-1(b)) was finally chosen as a compromise between system safety, efficiency, and cost.

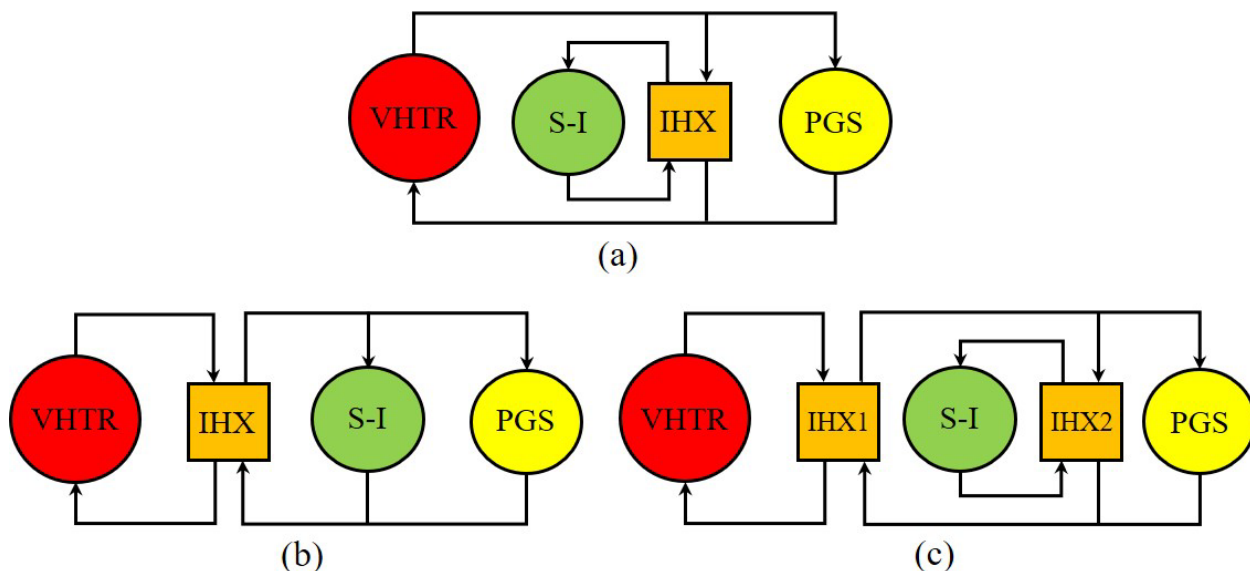


Figure 4-1. Three main nuclear reactor connection concepts for nuclear hydrogen production systems based on VHTR and S-I cycle: (a) direct PGS plus indirect S-I cycle, (b) indirect PGS and S-I cycle, and (c) indirect PGS plus double indirect S-I cycle.

4.1.2 S-I hydrogen production system

Based on the analysis results obtained in Chapter 2 and the principle of reducing system energy consumption while keeping the system layout as simple as possible, an improved S-I hydrogen production system was developed in Aspen Plus, as shown in Figure 4-2. It can be seen that, different from the previously designed S-I hydrogen production system with an internal heat exchange network (see Figure 2-9), the improved S-I hydrogen production system only uses three internal heat exchangers, namely E201, E301 and E302. To fully demonstrate the chemistry of hydrogen production, H₂SO₄DEC (i.e., the H₂SO₄ decomposition reactor) and SO₃ABS (i.e., the SO₃ absorber) are defined separately in the previous system flowsheet (see Figs. 2-2 and 2-9) to demonstrate the H₂SO₄ decomposition process and the SO₃ absorption process, respectively. Given that in actual engineering, these two processes occur automatically during heating or cooling, H₂SO₄DEC and SO₃ABS are no longer marked in the improved system layout. In other words, H₂SO₄DEC and SO₃ABS are now considered part of E202 and E201, respectively, as shown in Figure 4-2 (at this time, the heat released by the SO₃ absorption process is considered to be recoverable). To reduce the power consumption of the H₂SO₄ concentration & decomposition section, the generated O₂ is no longer sent to H₂SO₄DST (or C201). Instead, the

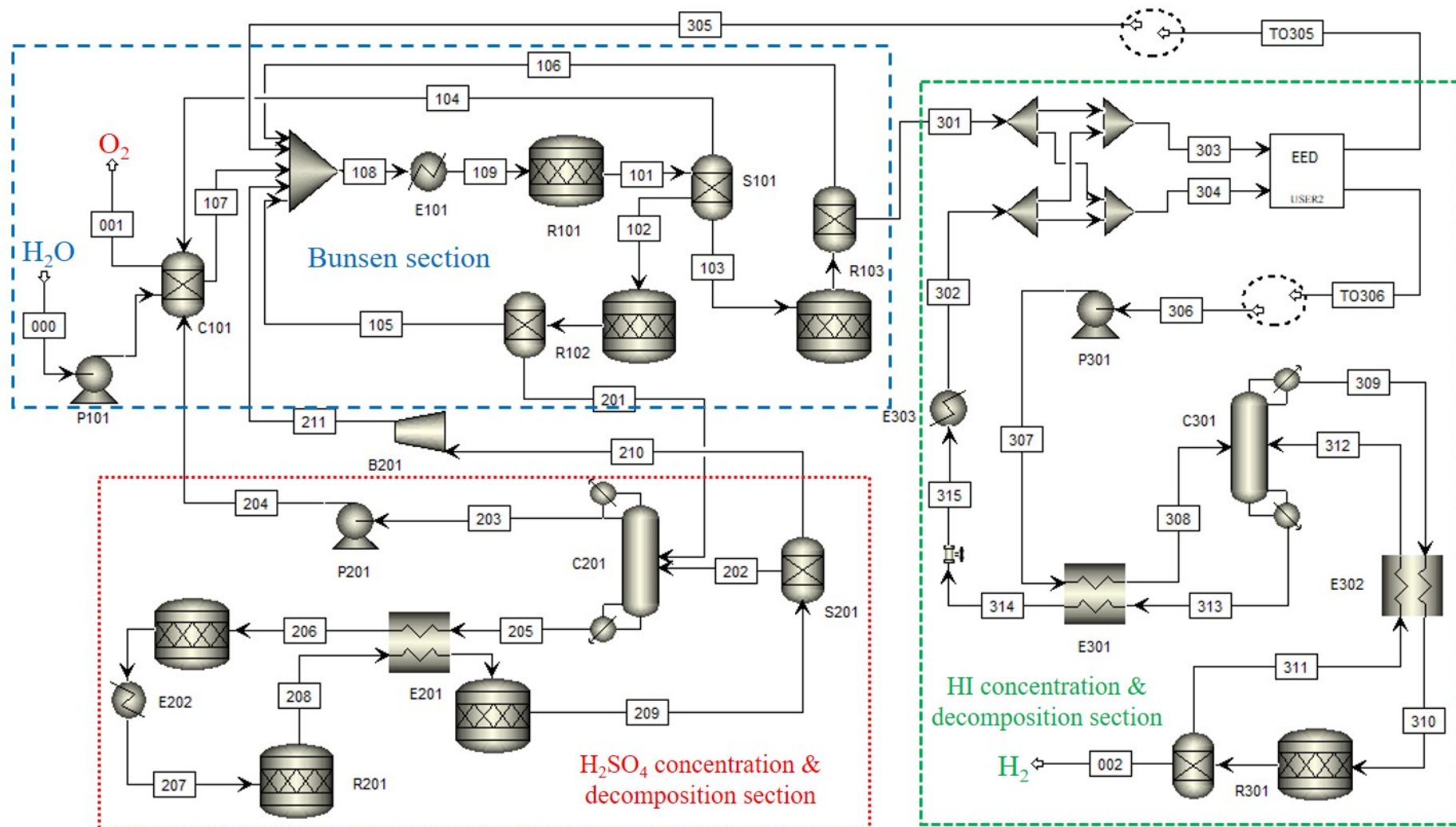


Figure 4-2. Schematic of the improved S-I hydrogen production system developed in Aspen Plus.

generated O₂ is separated by S201 and sent directly to the Bunsen section, as shown in Figure 4-2. In addition, to obtain pure O₂ as much as possible, the O₂ separated from S101 (i.e., Stream 104) is further sent to C101 (i.e., the O₂ scrubber) for water washing, as shown in Figure 4-2.

4.1.3 GSCC power conversion system

The previous chapter presents the conceptual design of the GSCC power conversion system, which roughly demonstrates the process of heat-to-power conversion. For conducting the thermodynamic analysis of the system, the conceptual design is already enough, since the critical system components or the indispensable system components are all included in the modeling process. However, for practical engineering applications, the conceptual design of the system is still insufficient due to the lack of some auxiliary system components such as Deaerator, Condensate Feed Pump (CFP), Low Pressure (LP) Heaters, etc. Therefore, the layout improvement of the combined cycle power conversion system carried out here is to add these missing auxiliary components to the previous system conceptual design.

4.2 System integrated design

According to the research results of the previous two chapters and the layout improvement measures introduced above, the integration design of two different nuclear hydrogen production systems based on VHTR, S-I cycle and combined cycle is carried out in this section.

4.2.1 Independent operating system

Although the conventional system shown in Figure 3-2 has poorer thermodynamic performance than the new system shown in Figure 3-8, it enables independent hydrogen production and power generation (due to the use of an auxiliary cooler (AC), the S-I hydrogen production process and the combined cycle power conversion process in the conventional system can operate independently). The independent hydrogen production and power generation promotes the simplification of system control and improves the safety of system operation to a certain extent. Based on this idea and the above layout improvement measures, an independent operating system based on VHTR, S-I cycle and combined cycle is finally developed, as shown in Figure 4-3.

It can be seen from Figure 4-3 that, in order to prevent the secondary loop components from being contaminated by the primary loop radioactive helium, an IHX is placed between the primary loop helium and the secondary loop helium, and the secondary loop helium enters the S-I cycle and the combined cycle in parallel for corresponding hydrogen production and power generation, as shown in Figure 4-1(b). It is not difficult to find that the S-I hydrogen production process shown in Figure 4-3 is exactly the improved version introduced in the previous section. In addition, it can be seen that the system configuration of the combined cycle power conversion system

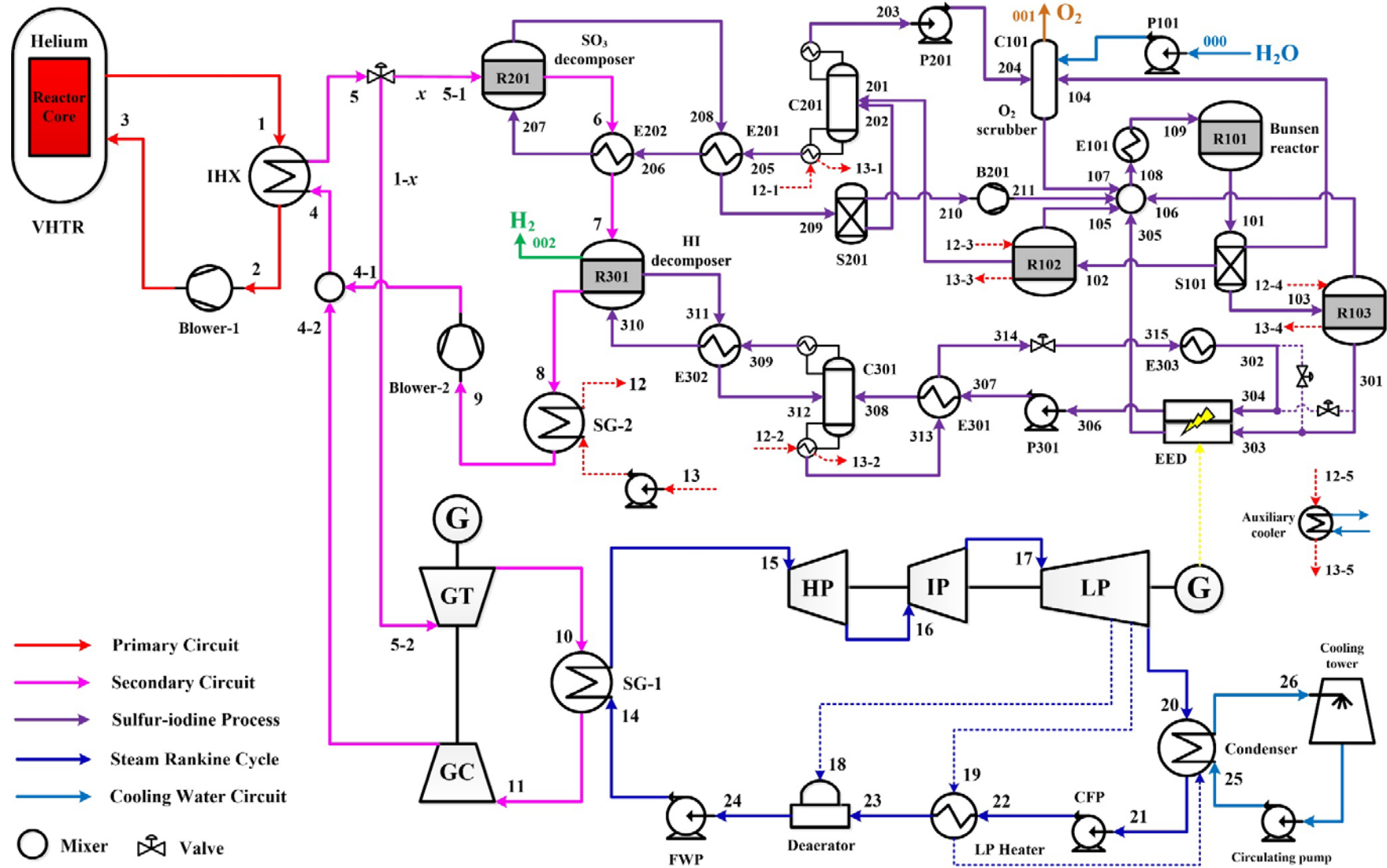


Figure 4-3. Schematic diagram of an independent operating system based on VHTR, S-I cycle and combined cycle.

is further refined, and several auxiliary components such as Deaerator, LP Heater, and CFP have been added to the system layout.

In the previous chapter, in order to simplify the system modeling process, the S-I hydrogen production system is treated as a "black box" module, and the details of how the secondary loop helium heat carrier flows through the S-I system are unknown. Therefore, one of the key tasks of this section is to determine the specific flow route of the helium heat carrier in the S-I system.

According to the energy cascade utilization principle and the heating requirements of the S-I hydrogen production system, a feasible flow route of helium heat carrier is proposed, as shown in Figure 4-3. It can be seen that part of the secondary loop helium heat carrier leaving the IHX is sent to the S-I hydrogen production system where it flows through R201, E202 and R301 in sequence to transfer heat for the decomposition of H_2SO_4 and HI. Figure 4-4 schematically shows the heat exchange process of the helium heat carrier flowing through these three components. In this work, the supply temperature of the helium heat carrier (i.e., the temperature of the helium heat carrier leaving the IHX (T_5 , see Figure 4-3)) is set to 880°C [105,123]. Assuming that the decomposition process of SO_3 is carried out in the temperature range of $800\text{--}850^\circ\text{C}$ and the pinch point temperature difference (ΔT_{pp}) is equal to 15°C , the temperature of the helium heat carrier leaving the HI decomposer (i.e., R301) or S-I system will be between 600°C and 700°C , as shown in Figure 4-4. It should be noted that this temperature is greatly affected by the supply temperature of the helium heat carrier, the decomposition temperature range of SO_3 , and the allowable minimum heat transfer temperature difference. For instance, when the supply temperature of the helium heat carrier was set to 890°C and the decomposition temperature range of SO_3 was set to be around $770\text{--}825^\circ\text{C}$, the temperature of the helium heat carrier leaving the S-I system would be about 440°C , as shown in Ref. [91].

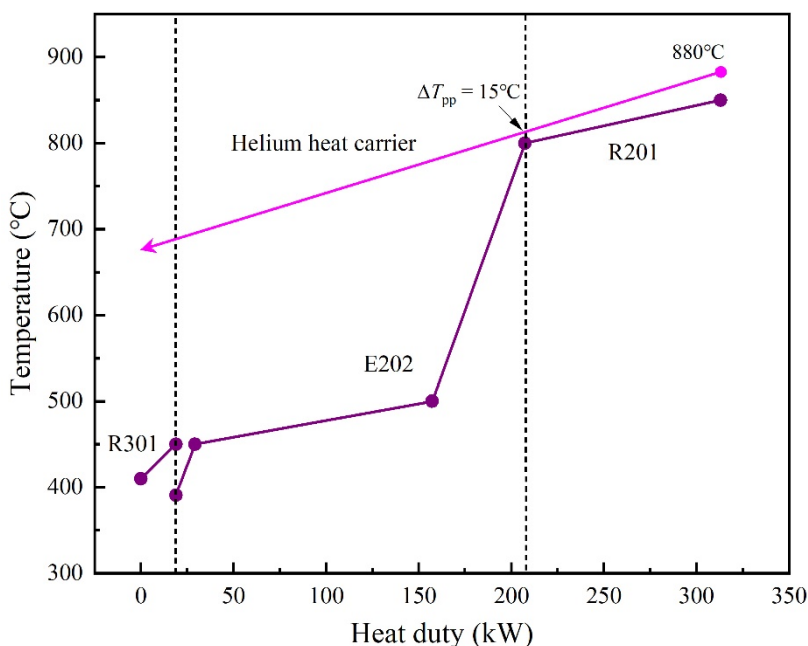


Figure 4-4. Schematic temperature-heat duty (1 mol H_2/s) diagram of the heat exchange process of the helium heat carrier flowing through R201, E202 and R301.

After leaving the HI decomposer (i.e., R301), the helium heat carrier is further sent to a steam generator called SG-2 to generate low-pressure steam, which is used to heat other heat-consuming parts of the S-I system such as the reboiler of H₂SO₄ distillation column (i.e., C201), the reboiler of HI distillation column (i.e., C301), the H₂SO₄ purification tower (i.e., R102), and the HI purification tower (i.e., R103), as shown in Figure 4-3. However, it should be noted that, in order to ensure the stable return temperature of the helium heat carrier (i.e., the helium outlet temperature of SG-2 (T_9 , see Figure 4-3)), the steam generated by SG-2 is usually in excess, and a part of the steam must be sent to an auxiliary cooler at this time (to release the excess heat), as shown in Figure 4-3. It is not difficult to see that the independent operating system is designed on the basis of the conventional system layout.

4.2.2 Coupled operating system

According to the new system layout proposed in the previous chapter, a coupled operating system is designed, as shown in Figure 4-5. It can be seen that in the coupled operating system, the helium heat carrier leaving the HI decomposer (i.e., R301) is still sent to the steam generator named SG-2 to produce steam, but the steam produced is sent to the turbine to generate mechanical work, instead of being sent to the S-I system to provide heat. To maintain the normal operation of the S-I system, some low-pressure steam will be extracted from the LP cylinder of the turbine and sent to the S-I system to heat the components that need to consume low-temperature heat (i.e., the reboiler of H₂SO₄ distillation column (C201), the reboiler of HI distillation column (C301), the H₂SO₄ purification tower (R102), and the HI purification tower (R103)), as shown in Figure 4-5. During the heat exchange process, the extracted low-pressure steam is gradually condensed into liquid water, which is finally collected together and sent to the Deaerator of the Rankine cycle (see Figure 4-5). The power generation process and the hydrogen production process are coupled together by means of extraction steam heating, which is why the system is called a coupled operating system.

Comparing Figure 4-5 and Figure 4-3, it is not difficult to find that the coupled operating system has more LP Heaters than the independent operating system. The essential reason for this result is that the mass flow rate of water (the working fluid of the Rankine cycle) in the coupled operating system is greater than that in the independent operating system. In more detail, in the coupled operating system, because the SG-2 also provides a part of the high-grade heat for the Rankine power conversion cycle (or the SG-2 also provides some steam for the Rankine power conversion cycle), the mass flow rate of water becomes larger, which further allows the feed water to enter the SG at a higher temperature. To explain this process clearly, a schematic T - S (temperature-entropy) diagram of the heat exchange process in SG is drawn, as shown in Figure 4-6. It is well-known that in SG, water is isobarically heated into steam (assuming a small and negligible pressure loss), and its temperature will remain unchanged during the phase transition, thereby resulting in a pinch point temperature difference (ΔT_{pp}) between helium (hot fluid) and saturated water (cold fluid), as shown in Figure 4-6. To reduce the energy loss (or exergy loss) in the heat transfer process and improve the system efficiency, in the system design stage, the pinch point temperature difference in SG should be as close

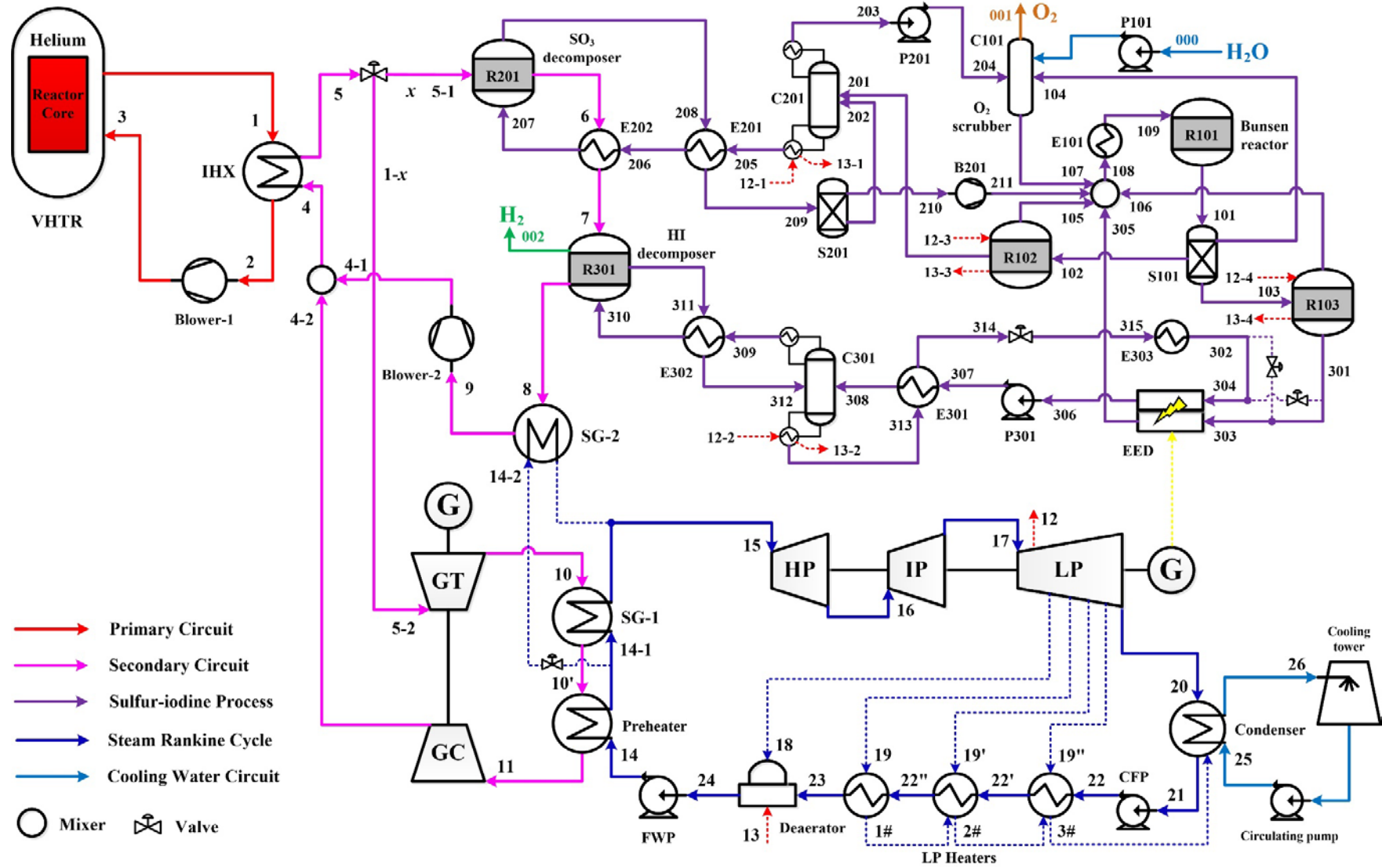


Figure 4-5. Schematic diagram of a coupled operating system based on VHTR, S-I cycle and combined cycle.

as possible to the minimum value (in this work, the minimum value is set to 15°C). Obviously, as the mass flow rate of water increases, the pinch point temperature difference also increases (that is, the pinch point moves from $A-B$ to $A'-B$, as shown in Figure 4-6). Since the helium inlet temperature ($T_{\text{in,helium}}$), helium outlet temperature ($T_{\text{out,helium}}$) and steam outlet temperature ($T_{\text{out,steam}}$, namely the main steam temperature) are all constants in this work, the only way to reduce the pinch point temperature difference (or the only way to get point A' back to point A) is to increase the feedwater temperature (or the inlet water temperature, $T_{\text{in,water}}$). Therefore, more LP Heaters are used in the coupled operating system to increase the feedwater temperature (to maintain a small pinch point temperature difference). This is why the coupled operating system has more LP Heaters than the independent operating system.

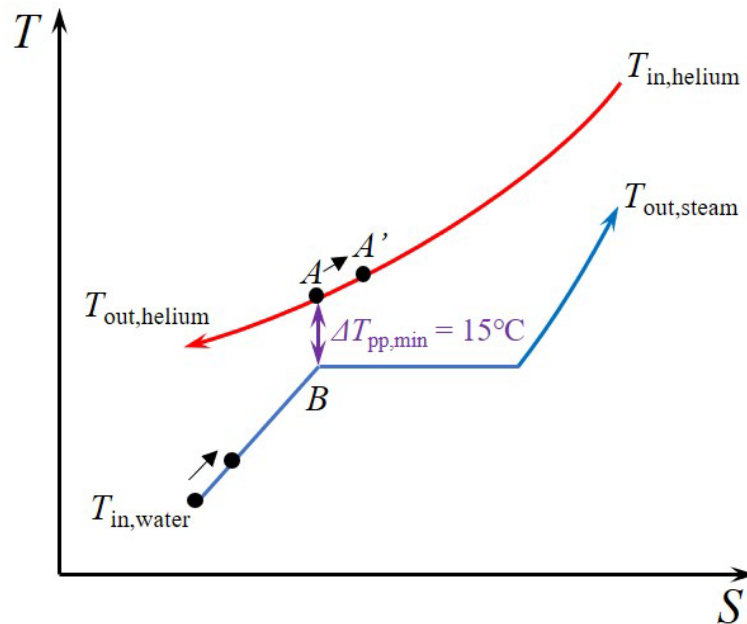


Figure 4-6. Schematic temperature-entropy diagram of the heat exchange process in SG.

In short, since the heat loss of the Auxiliary cooler no longer exists and the heat transfer temperature difference in SG is reduced (due to the increase in the feedwater temperature), the coupled operating system is anticipated to be able to achieve better thermodynamic performance (or higher thermodynamic efficiencies) than the independent operating system (this point will be discussed in detail in the next section). However, it should also be noted that in terms of system control and operational security, the independent operating system may perform better than the coupled operating system due to its simpler system layout and configuration.

4.3 System simulation and performance analysis

4.3.1 System simulation

Before performing system simulation, some operating parameters need to be adjusted or determined appropriately as the system layout has been updated. For the reactor, no matter which system layout is adopted, its operating parameters always remain unchanged, as shown in Table 3-3. For the IHX, similar to the previous parameter settings, assume that the secondary loop helium enters and exits the IHX at 350°C and 880°C, respectively. To prevent the primary loop radioactive helium from leaking into the secondary loop and contaminating the secondary loop components, the pressure of the secondary loop helium heat carrier is set to be slightly higher than the helium pressure of the reactor loop. In more detail, the secondary loop helium outlet pressure of IHX is set to 7.2 MPa, which is slightly higher than the maximum pressure in the reactor loop (i.e., the reactor inlet pressure of 7.1 MPa, see Table 3-3). For the S-I hydrogen production system, most of its operating parameters (such as chemical conversion rate, temperature, pressure, etc.) remain unchanged, as shown in Table 2-2. However, according to the analysis results shown in Figure 2-6, the reflux ratios of H₂SO₄DST and HIDST are adjusted to 0.1 and 1.0, respectively, to reduce the heat consumption of the distillation process as much as possible. In addition, the distillation parameter of H₂SO₄DST should also be modified since the O₂ produced is no longer sent to H₂SO₄DST. According to Ref. [101], the previous distillate rate of 6.056 mol/s (see Table 2-2) is now adjusted to a distillate-to-feed ratio of 0.72.

For the independent operating system, the pressure and temperature of the steam supplied to the S-I system (or the steam generated by SG-2) are set to 0.75 MPa and 200°C, respectively (in Ref. [18], these two values are equal to 1.0 MPa and 200°C, respectively). For the coupled operating system, the extraction steam pressure supplied to the S-I system is also set to 0.75 MPa, according to Ref. [84]. It is assumed that the steam supplied to the S-I system is eventually condensed into liquid water with a temperature of 165°C (in Ref. [84], this value is equal to 167.75°C, namely the saturation temperature of water at 0.75 MPa). The reason for using 165°C is that we think there should be a subcooling of about 2-3°C.

For the improved power generation system, the newly added components are mainly the LP Heater(s) and the Deaerator. For these components, the parameters that need to be determined are their extraction pressures. Table 4-1 lists the detailed turbine operating and extraction parameters for the two different systems.

Similarly, we first use Aspen Plus to simulate the improved S-I hydrogen production system with a hydrogen production rate of 1 mol/s (the detailed material flow data are shown in Table 4-2), and then the entire system can be simulated according to the obtained simulation results of the S-I system and the modeling approach described in the previous chapter. The state-point parameters of the two systems when the mass flow rate ratio (x) is equal to 0.5 are shown in Table 4-3 and Table 4-4, respectively.

It should be noted that for the coupled operating system, since part of the turbine

steam is extracted and sent to the S-I system for heat supply, it is considered to build the GSCC power conversion system near the S-I system (this means that the power conversion system is also built away from the nuclear reactor system). At this time, the pipeline pressure loss before the secondary loop helium enters the GT should also be considered. However, for the independent operating system, this pipeline pressure loss can be ignored since the power conversion system can be built close to the nuclear reactor system. This is why the operating parameters (i.e., the inlet parameters of GT) of state-point 5-2 in Table 4-3 and Table 4-4 are different. In addition, it can be seen from Table 4-3 and Table 4-4 that the mass flow rate of water (the working fluid of the Rankine cycle) in the coupled operating system is indeed much larger than that in the independent operating system, and the feedwater temperature in the coupled operating system is also higher than that in the independent operating system (see the operating parameters for state-point 14), as described in the previous section.

Table 4-1. Turbine operating and extraction parameters for two different systems.

Turbine parameters (Unit)	Independent operating system	Coupled operating system
Inlet steam temperature (°C)	566	566
Inlet steam pressure (MPa)	13.9	13.9
High Pressure (HP) cylinder exhaust steam pressure (MPa)	4	4
Intermediate Pressure (IP) cylinder exhaust steam pressure (MPa)	1	1
Low Pressure (LP) cylinder exhaust steam pressure (MPa)	0.01	0.01
Isentropic efficiency of steam turbine HP, IP and LP parts (-)	0.90, 0.92 and 0.87	0.90, 0.92 and 0.87
Deaerator extraction pressure (kPa)	100	680
1# LP Heater extraction pressure (kPa)	30	300
2# LP Heater extraction pressure (kPa)	—	100
3# LP Heater extraction pressure (kPa)	—	30

Table 4-2. Material flow data of the improved S-I system under a hydrogen production rate of 1 mol/s.

No.	T (K)	p (MPa)	Molar flow rate (mol/s)							
			H ₂ O	H ₂ SO ₄	HI	I ₂	SO ₂	SO ₃	O ₂	H ₂
000	298.15	0.101	1	0	0	0	0	0	0	0
001	353.18	0.5	0	0	0	0	0	0	0.5	0
002	723	1.17	0	0	0	0	0	0	0	1
101	353	0.5	34.029	1.656	5.858	7.048	0	0	0.5	0

102	353	0.5	4.318	1.091	0.182	0.068	0	0	0	0
103	353	0.5	29.711	0.565	5.676	6.98	0	0	0	0
104	353	0.5	0	0	0	0	0	0	0.5	0
105	353	0.5	0.944	0	0	0.159	0.091	0	0	0
106	353	0.5	0	0	0	0	0.565	0	0	0
107	353.18	0.5	5.556	0	0	0	0	0	0	0
108	363.03	0.5	37.341	0	2.546	8.704	1.656	0	0.5	0
109	353	0.5	37.341	0	2.546	8.704	1.656	0	0.5	0
201	353	0.5	3.556	1	0	0	0	0	0	0
202	425.15	0.101	1.490	0.282	0	0	0	0	0	0
203	371.15	0.101	4.556	0	0	0	0	0	0	0
204	371.19	0.5	4.556	0	0	0	0	0	0	0
205	414.27	0.101	0.490	1.282	0	0	0	0	0	0
206	629.06 ^a	0.101	0.490	1.282	0	0	0	0	0	0
207	1073.15	0.101	1.772	0	0	0	0	1.282	0	0
208	1123.15	0.101	1.772	0	0	0	1	0.282	0.5	0
209	425.15	0.101	1.490	0.282	0	0	1	0	0.5	0
210	425.15	0.101	0	0	0	0	1	0	0.5	0
211	603.36	0.5	0	0	0	0	1	0	0.5	0
301	353	0.5	30.841	0	4.546	7.545	0	0	0	0
302	353	0.5	46.08	0	8.92	4	0	0	0	0
303	354.23	0.5	33.513	0	5.229	7.21	0	0	0	0
304	353.13	0.5	43.408	0	8.237	4.335	0	0	0	0
305	353	0.5	30.841	0	2.546	8.545	0	0	0	0
306	353	0.5	46.08	0	10.92	3	0	0	0	0
307	353.18	1.17	46.08	0	10.92	3	0	0	0	0
308	413.15	1.17	46.08	0	10.92	3	0	0	0	0
309	315.29	1.17	0	0	5	0	0	0	0	0
310	683.15	1.17	0	0	5	0	0	0	0	0
311	723	1.17	0	0	3	1	0	0	0	0
312	468.07	1.17	0	0	3	1	0	0	0	0
313	423.50	1.17	46.08	0	8.92	4	0	0	0	0
314	372.72	1.17	46.08	0	8.92	4	0	0	0	0
315	372.26	0.5	46.08	0	8.92	4	0	0	0	0

^a This value is obtained without considering the heat recovered from the SO₃ absorption process. In fact, for the modified S-I system, the heat released by the SO₃ absorption process is used to heat the H₂SO₄ solution obtained from the H₂SO₄ distillation column (C201), in this case the temperature of Stream 206 is calculated to be about 664.07K.

Table 4-3. State-point parameters of the independent operating system when the mass flow rate ratio is equal to 0.5.

State points	Fluids	\dot{m} (kg/s)	T (K)	p (MPa)	h (kJ/kg)	s (kJ/kg ·K)
1	Helium	122.6	1223.15	6.94	6376.6	26.559
2	Helium	122.6	663.05	6.87	3469.4	23.401
3	Helium	122.6	673.15	7.1	3522.4	23.413
4	Helium	127.0	623.15	7.27	3263.5	22.962
5	Helium	127.0	1153.15	7.2	6014.0	26.178
5-1	Helium	63.5	1153.15	7.02	6013.5	26.230
5-2	Helium	63.5	1153.15	7.2	6014.0	26.178
6	Helium	63.5	1088.15	6.95	5675.9	25.950
7	Helium	63.5	972.18	6.88	5073.8	25.386
8	Helium	63.5	960.59	6.81	5013.4	25.344
9	Helium	63.5	594.93	6.74	3115.4	22.879
10	Helium	63.5	906.42	3.71	4723.3	26.303
11	Helium	63.5	461.84	3.67	2415.1	22.823
12	Steam	55.1	473.15	0.75	2842.5	6.852
12-1	Steam	15.1	473.15	0.75	2842.5	6.852
12-2	Steam	15.6	473.15	0.75	2842.5	6.852
12-3	Steam	1.5	473.15	0.75	2842.5	6.852
12-4	Steam	9.0	473.15	0.75	2842.5	6.852
12-5	Steam	13.9	473.15	0.75	2842.5	6.852
13	Water	55.1	438.15	0.71	697.2	1.992
13-1	Water	15.1	438.15	0.71	697.2	1.992
13-2	Water	15.6	438.15	0.71	697.2	1.992
13-3	Water	1.5	438.15	0.71	697.2	1.992
13-4	Water	9.0	438.15	0.71	697.2	1.992
13-5	Water	13.9	438.15	0.71	697.2	1.992
14	Water	46.8	374.39	14.63	435.3	1.310
15	Steam	46.8	839.15	13.9	3504.3	6.620
16	Steam	46.8	648.09	4	3154.6	6.681
17	Steam	46.8	481.34	1	2847.9	6.737
18	Steam	3.13	372.76	0.1	2495.7	6.878
19	Steam	1.65	342.25	0.03	2346.7	6.956
20	Steam	42.0	318.96	0.01	2226.3	7.028
21	Water	43.7	317.957	0.01	187.6	0.636
22	Water	43.7	317.964	0.105	187.7	0.636

23	Water	43.7	337.25	0.1	268.4	0.882
24	Water	46.8	372.76	0.1	417.5	1.303
25	Water	2050.8	298.15	0.101	104.9	0.367
26	Water	2050.8	308.15	0.101	146.7	0.505

Table 4-4. State-point parameters of the coupled operating system when the mass flow rate ratio is equal to 0.5.

State points	Fluids	\dot{m} (kg/s)	T (K)	p (MPa)	h (kJ/kg)	s (kJ/kg·K)
1	Helium	122.6	1223.15	6.94	6376.6	26.559
2	Helium	122.6	663.05	6.87	3469.4	23.401
3	Helium	122.6	673.15	7.1	3522.4	23.413
4	Helium	127.0	623.15	7.27	3263.5	22.962
5	Helium	127.0	1153.15	7.2	6014.0	26.178
5-1	Helium	63.5	1153.15	7.02	6013.5	26.230
5-2	Helium	63.5	1153.15	7.02	6013.5	26.230
6	Helium	63.5	1088.15	6.95	5675.9	25.950
7	Helium	63.5	972.18	6.88	5073.8	25.386
8	Helium	63.5	960.59	6.81	5013.4	25.344
9	Helium	63.5	594.93	6.74	3115.4	22.879
10	Helium	63.5	906.42	3.62	4722.9	26.355
10'	Helium	63.5	594.93	3.58	3105.7	24.190
11	Helium	63.5	449.86	3.55	2352.5	22.760
12	Steam	42.1	453.55	0.75	2796.9	6.754
12-1	Steam	15.4	453.55	0.75	2796.9	6.754
12-2	Steam	15.9	453.55	0.75	2796.9	6.754
12-3	Steam	1.5	453.55	0.75	2796.9	6.754
12-4	Steam	9.2	453.55	0.75	2796.9	6.754
13	Water	42.1	438.15	0.71	697.2	1.992
13-1	Water	15.4	438.15	0.71	697.2	1.992
13-2	Water	15.9	438.15	0.71	697.2	1.992
13-3	Water	1.5	438.15	0.71	697.2	1.992
13-4	Water	9.2	438.15	0.71	697.2	1.992
14	Water	95.1	439.38	15.40	711.0	1.987
14-1	Water	43.76	547.37	14.63	1203.9	2.989
14-2	Water	51.36	547.37	14.63	1203.9	2.989
15	Steam	95.1	839.15	13.9	3504.3	6.620
16	Steam	95.1	648.09	4	3154.6	6.681

17	Steam	95.1	481.34	1	2847.9	6.737
18	Steam	3.5	444.55	0.68	2780.3	6.760
19	Steam	3.2	406.67	0.3	2650.7	6.809
19'	Steam	2.7	372.76	0.1	2495.7	6.878
19''	Steam	1.6	342.25	0.03	2346.7	6.956
20	Steam	42.0	318.96	0.01	2226.3	7.028
21	Water	49.5	317.957	0.01	187.6	0.636
22	Water	49.5	318.02	0.79	188.6	0.637
22'	Water	49.5	337.25	0.75	268.9	0.882
22''	Water	49.5	367.76	0.72	396.9	1.245
23	Water	49.5	401.67	0.68	540.4	1.619
24	Water	95.1	436.93	0.68	691.9	1.980
25	Water	2053.9	298.15	0.101	104.9	0.367
26	Water	2053.9	308.15	0.101	146.7	0.505

4.3.2 Performance analysis

For the two operating systems, the net electrical power output, \dot{E}_{net} , can be approximately calculated by:

$$\dot{E}_{\text{net}} = \left[(\dot{W}_{\text{gen,GT}} - \dot{W}_{\text{con,GC}}) + \dot{W}_{\text{gen,ST}} \right] \cdot \eta_m \cdot \eta_G - \frac{(\dot{W}_{\text{con,FWP}} + \dot{W}_{\text{con,CFP}} + \dot{W}_{\text{con,cp}} + \dot{W}_{\text{con,Blowers}})}{\eta_m \cdot \eta_M} - \dot{E}_{\text{con,S-I}} \quad (4-1)$$

The mechanical power consumption of the Feed Water Pump (FWP) and CFP can be calculated according to Eq. (3-4). The mechanical power consumption of the circulating pump, $\dot{W}_{\text{con,cp}}$, can be calculated based on the following formula:

$$\dot{W}_{\text{con,cp}} = \frac{\dot{m}_{\text{cw}} g H_{\text{cp}} \times 10^{-3}}{\eta_{\text{cp}}}, \quad (4-2)$$

where \dot{m}_{cw} , g , H_{cp} , and η_{cp} are the mass flow rate of cooling water, gravitational acceleration ($9.8 \text{ m}\cdot\text{s}^{-2}$), circulating pump head (set to 20 m [128,129]), and circulating pump efficiency (set to 0.80 [129]), respectively.

Assuming that all recoverable waste heat is used for power generation under an electric conversion efficiency of 15% [115], the maximum net electrical power output, $\dot{E}_{\text{net,max}}$, can be calculated by:

$$\dot{E}_{\text{net,max}} = \dot{E}_{\text{net}} + 0.15 \times \dot{Q}_{\text{rec}}, \quad (4-3)$$

where \dot{Q}_{rec} is the recoverable thermal power. For the independent operating system, the recoverable thermal power mainly comes from five components, namely E101,

E303, C201, C301 (these four components are located in the S-I system, see Figure 4-3), and auxiliary cooler. For the coupled operating system, the auxiliary cooler does not exist, and the recoverable thermal power comes from only the four components of the S-I system.

The thermodynamic efficiencies (i.e., thermal and exergy efficiencies) of the two operating systems can be calculated according to Eq. (3-8) and Eq. (3-16).

Figure 4-7 shows the performance parameters of the two operating systems under different mass flow rate ratios (or different hydrogen production conditions). From Figure 4-7(a) and (b), it can be seen that for both operating systems, as the mass flow rate ratio increases, the hydrogen production rate increases linearly, while the net electrical power output decreases linearly. Under the same mass flow rate ratio, the hydrogen production rate of the two operating systems is the same, but the net electrical power output of the coupled operating system is significantly greater than that of the independent operating system. As mentioned earlier, the secondary loop helium leaves the HI decomposer (i.e., R301) at a relatively high temperature, and in the coupled operating system, the high-grade thermal energy carried by this part of helium is effectively used by the steam Rankine cycle for power generation (but in the independent operating system, this part of high-grade thermal energy is used to generate low-pressure steam for heating). Accordingly, the coupled operating system can better fulfill the principle of energy cascade utilization, which is why this operating system has better thermodynamic performance than the independent operating system, as shown in Figure 4-7(b), (c) and (d).

From Figure 4-7(c) and (d), it can be found that the thermodynamic efficiencies of both operating systems decrease with the increase of the mass flow rate ratio (or hydrogen production rate). As explained in the previous chapter, in this work, the S-I cycle-based nuclear hydrogen production efficiencies are significantly lower than the combined cycle-based nuclear power generation efficiencies. Therefore, as the mass flow rate ratio increases, more nuclear heat is used to produce hydrogen, resulting in the decrease in the overall system efficiencies.

It should be noted that for the current two operating systems, when the mass flow rate ratio reaches 0.7 and 0.9, respectively, the net electrical power output will become negative (at this time, the electricity generated by the power generation system cannot meet the electricity demand of the hydrogen production system), and the definition equations for thermal efficiency and exergy efficiency are no longer applicable. This is why the mass flow rate ratios for the two operating systems only increased to 0.65 and 0.85, as shown in Figure 4-7. In addition, for the coupled operating system, when the mass flow rate ratio drops to a certain value, the system configuration should also be adjusted appropriately. As mentioned in Section 4.1, an obvious difference between the independent operating system and the coupled operating system is that the coupled operating system has more LP Heaters. Since the SG-2 in the coupled operating system is also used to generate high-pressure steam for power generation, the mass flow rate of water (i.e., the working fluid of the Rankine cycle) increases, enabling a higher feedwater temperature (the specific reason has been given in Section 4.1, see Figure 4-6 and the corresponding explanation). As the mass flow rate ratio decreases, the heat load of SG-2 decreases, and the increase in the mass flow rate of water also decreases. When the mass flow

rate ratio decreases to a certain value, the increase in the mass flow rate of water is not significant anymore, and at this time, the feedwater temperature has to be decreased to ensure a smooth heat transfer process in the SG. An effective way to decrease the feedwater temperature is to reduce the number of LP Heaters.

Specifically, for the current coupled operating system, when the mass flow rate ratio is reduced to 0.3, the pinch point temperature difference in the SG will be lower than 15°C (note that the minimum pinch point temperature difference considered in this work is 15°C). At this time, if the mass flow rate ratio continues to be reduced without decreasing the feedwater temperature, the heat transfer process in the SG will not proceed normally. This is why the minimum mass flow rate ratio for the coupled operating system is only equal to 0.3, as shown in Figure 4-7. However, it should also be pointed out that when the mass flow rate ratio is very small, the performance difference between the two operating systems is not significant (because of the small heat load of SG-2). At this point, it does not make much sense to distinguish between independent and coupled operating systems.

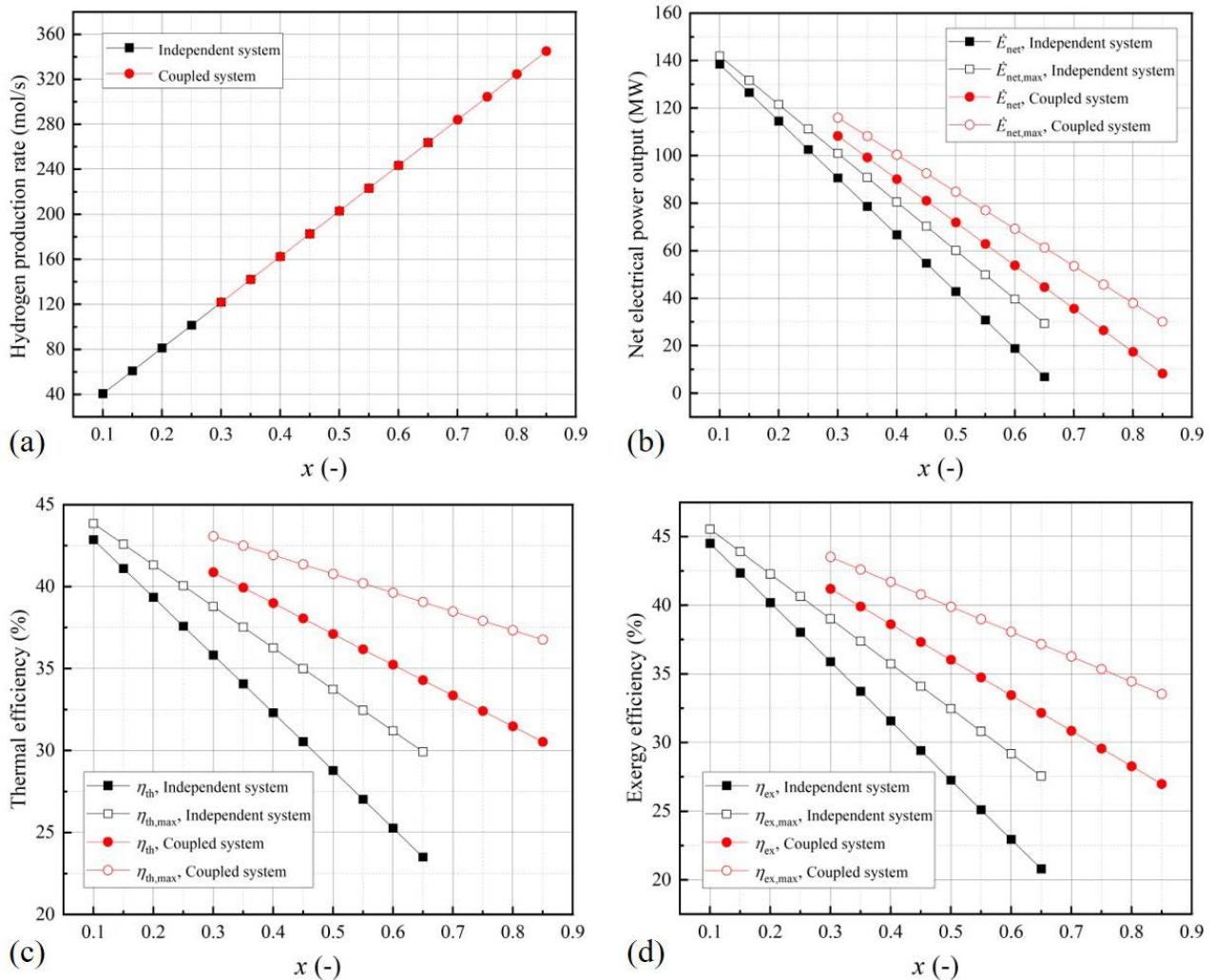


Figure 4-7. Performance parameters of the two operating systems under different mass flow rate ratios: (a) Hydrogen production rate, (b) Net electrical power output, (c) Thermal efficiency, and (d) Exergy efficiency.

In addition, it can also be seen from Figure 4-7 that for both operating systems, taking some effective measures to recover waste heat will be very important for improving system performance. Taking the mass flow rate ratio of 0.5 as an example, Table 4-5 shows the performance improvement effects of the two operating systems through adopting effective waste heat recovery. It can be seen that by adopting effective waste heat recovery, the net electrical power output, thermal efficiency, and exergy efficiency of the independent operating system are increased by about 17.3 MW, 4.94%, and 5.2%, respectively. And for the coupled operating system, these values are found to be 12.83 MW, 3.66%, and 3.85%, respectively.

Table 4-5. Performance parameters of the two operating systems when the mass flow rate ratio is equal to 0.5.

Performance parameters (Unit)	Independent operating system	With waste heat recovery	Increment
Hydrogen production rate (mol/s)	202.86	202.86	0
Net electrical power output (MW)	42.75	60.05	17.3
Thermal efficiency (%)	28.78	33.72	4.94
Exergy efficiency (%)	27.26	32.46	5.2
Performance parameters (Unit)	Coupled operating system	With waste heat recovery	Increment
Hydrogen production rate (mol/s)	202.86	202.86	0
Net electrical power output (MW)	71.89	84.72	12.83
Thermal efficiency (%)	37.11	40.77	3.66
Exergy efficiency (%)	36.02	39.87	3.85

4.4 Summary of this chapter

In this chapter, the system layout improvement and integration design were implemented and two complete system design schemes (namely independent operating system and coupled operating system) were proposed. The state-point parameters of the two systems under a typical operating working condition (i.e., the mass flow rate ratio is equal to 0.5) were simulated, and finally, the thermodynamic performance of the two systems under different hydrogen production conditions were analyzed and compared.

The performance analysis results of the two systems show that under the same operating working conditions, the two systems have the same hydrogen production rate, but the coupled operating system can obtain a greater net electrical power output and higher system efficiencies than the independent operating system. In other words, the coupled operating system can achieve better thermodynamic performance than the independent operating system. For example, when the mass

flow rate ratio is set to 0.5 (corresponding to a hydrogen production rate of 202.86 mol/s), the independent operating system and the coupled operating system can achieve net electric power of 42.75 MW and 71.89 MW, thermal efficiencies of 28.78% and 37.11%, and exergy efficiencies of 27.26% and 36.02%, respectively. However, the independent operating system may be more secure than the coupled operating system due to its simpler system controls.

In summary, this chapter formulates two complete system design schemes on the basis of the research results of the previous two chapters. Different from the previous conceptual design, the system design presented in this chapter is closer to the actual engineering design due to the consideration of some design details. Consequently, the simulation results obtained in this chapter can be used as some reference data for future engineering applications. In the next chapter, an economic evaluation of the two system designs will be carried out from the perspective of unit hydrogen production cost, and the development potential of the system will be further explored.

Chapter 5

System economic evaluation

Conducting economic evaluation work is an important and necessary step before building a pilot plant for any industrial processes. This chapter performed an economic analysis of the two VHTR-driven nuclear hydrogen production systems introduced in the previous chapter. Firstly, the cost composition of a thermochemical hydrogen production plant is presented, providing a framework for the subsequent economic modeling process. Then, a complete economic model was developed to calculate the unit hydrogen production cost, based on some existing equipment investment cost equations and the six-tenths-factor rule (a scaling method). Finally, the cost distribution of the system was analyzed and some parametric studies (e.g., different reactor thermal powers, mass flow rate ratios, cost capacity factors, electricity prices, etc.) were performed. This chapter aims to figure out the economic characteristics and cost-influencing mechanism of the VHTR-driven nuclear hydrogen production system using S-I thermochemical cycle and GSCC.

5.1 Cost composition of a thermochemical hydrogen production plant

For a thermochemical hydrogen production plant, its cost composition mainly includes two parts, namely the total capital investment and the total product cost.

5.1.1 The total capital investment

Generally, the cost invested before an industrial plant can be put into operation is called capital investment. The total capital investment consists of the fixed capital investment and the working capital investment. The fixed capital investment refers to the capital required for manufacturing and plant facilities, while the working capital investment refers to the capital needed for the ongoing operation of the plant [130].

The fixed capital investment can be further subdivided into the direct fixed capital investment and the indirect fixed capital investment (or subdivided into the manufacturing fixed capital investment and the non-manufacturing fixed capital investment [131]). The direct fixed capital investment (or manufacturing fixed capital investment) refers to the capital required for the installed process components with

all auxiliaries that are necessary for the complete process operation [130]. Expenses for system equipment purchase and installation, piping, instrumentation and controls, electrical, buildings, land and service facilities are general examples of costs included in the direct fixed capital investment. The indirect fixed capital investment is the cost needed for construction overhead that is not directly related to the process operation. Engineering and supervision expenses, miscellaneous construction expenses, contractor's fees and contingencies are general examples of costs included in the indirect fixed capital investment.

The working capital investment is the total cash available for payment of expenses related to the plant operation. Specifically, the working capital of an industrial plant consists of the following cash investments [130]:

- accounts receivable;
- accounts payable;
- raw materials and supplies in stock;
- finished goods in stock and semi-finished products in the manufacturing process;
- cash on hand for monthly payment of operating expenses, e.g., salaries, rents, and raw material purchases; and
- taxes payable.

The working capital investment of a chemical plant can be roughly estimated using the ratio defined as the working capital investment to the total capital investment. For most chemical plants, the working capital investment is between 10% and 20% of the total capital investment [130]. However, for factories or companies producing products that are in seasonal demand, this percentage may increase to 50% or more due to the necessity to maintain large inventories for a considerable period of time [130]. Since hydrogen is not a seasonal demand product, in this work it is assumed that the working capital investment of the S-I thermochemical hydrogen production system is approximately 15% of its total capital investment (this also means that the fixed capital investment of the S-I system accounts for about 85% of its total capital investment, as described in Refs. [130,131]).

Depending on the stage of development of the project, estimates of the capital investment for a process can vary significantly (e.g., from a rough design estimate based on very limited information except the size/capacity of the project, to a detailed estimate based on complete engineering drawings and specifications), resulting in varying accuracy of estimates [130]. The American Association of Cost Engineers has summarized five different estimation methods and the corresponding estimation accuracy, as shown in Table 5-1.

Since the actual data available for the S-I thermochemical hydrogen production system are very limited, it is currently difficult for us to perform a contractor's estimate or a project control estimate. In addition, the data required for a scope estimate are also insufficient. In this case, this work will adopt a ratio estimate to roughly calculate equipment costs by scaling up/down the cost data that were previously reported by Brown et al. [89] for a nuclear-powered S-I thermochemical hydrogen production plant. The ratio estimate performed is based on a scaling method known as the six-tenths-factor rule, which calculates a result when the new

equipment is similar to one with another capacity for which cost data are available [130,131] (a detailed description of the six-tenths-factor rule will be presented in the next section). After estimating all equipment costs, the fixed capital investment, working capital investment, and total capital investment can be determined accordingly.

Table 5-1. Five different estimation methods and their accuracy [130].

No.	Name	Core of the estimate	Accuracy
1	Ratio estimate	Based on similar previous cost data	About $\pm 30\%$
2	Factored estimate	Based on knowledge of major items of equipment	About $\pm 30\%$
3	Scope estimate	Based on sufficient data to permit an estimate to be budgeted	About $\pm 20\%$
4	Project control estimate	Based on almost complete data, but still before the completion of drawings and specifications	Within $\pm 10\%$
5	Contractor's estimate	Based on complete engineering drawings, specifications and site surveys	About $\pm 5\%$

5.1.2 The total product cost

The total product cost (or total production cost) refers to the costs associated with operating the plant and selling the products. The total product cost generally consists of the manufacturing costs and general expenses. The manufacturing costs are also known as the operating or production costs [130], which include three parts, namely direct production cost, fixed charges, and plant overhead cost. And general expenses are divided into four categories: administrative expenses, distribution and marketing expenses, research and development expenses, and financing expenses. Table 5-2 gives a detailed description of the manufacturing costs and general expenses.

Generally, the total product cost can be calculated in one of three ways: daily cost basis, annual cost basis, and unit-of-product cost basis. And among these three ways, the annual cost basis is often used because it has obvious advantages in eliminating the effects of seasonal variations, considering plant start-up time and equipment operation factors, achieving a rapid calculation of operating costs at less than full capacity, and providing a convenient way to include infrequent but large expenses [130]. Therefore, in this work, the total product cost of the nuclear hydrogen production system is calculated on an annual cost basis. It should be noted that the calculation of individual production cost is completed by adopting a certain proportion of the total product cost, total capital investment, and fixed capital investment (the specific calculation process and the used proportions/percentages will be introduced in the next section).

Figure 5-1 shows a schematic diagram of the cost structure of a typical chemical plant. After calculating the total capital investment and the total product cost, the total cost of the nuclear hydrogen production system can be obtained, and the unit hydrogen production cost can be calculated accordingly.

Table 5-2. Description of the manufacturing costs and general expenses [130].

Categories	Expenses	Description
Manufacturing costs	Direct production cost	Expenses that directly connected with the manufacturing operation, such as expenses for raw materials, fuel, utilities, catalysts, operating labor, supervisory and clerical labor, maintenance and repairs, operating supplies, patents, royalties, etc.
	Fixed charges	Expenses that remain nearly constant and do not vary significantly with changes in the production rate, such as expenses for depreciation, insurance, taxes and rent.
	Plant overhead cost	Expenses for various services (medical, restaurant, etc.), safety and production, general plant overhead, payroll overhead (pensions, vacation allowances, social welfare and security, life insurance, etc.), packaging, plant superintendence, property protection, special employee benefits, etc.
General expenses	Administrative expenses	Expenses for executive and clerical wages, engineering and legal support, office supplies, upkeep on office buildings and general communications.
	Distribution and marketing expenses	Expenses that incurred in the process of selling and distributing the products, such as expenses for materials handling, containers, shipping, advertising, etc.
	Research and development expenses	Expenses that incurred in developing new processes and technologies, such as salaries (for researchers), expenses for special equipment and research facilities, consultant fees, etc.
	Financing expenses	Extra expenses that involved in procuring the funds required for capital investment, such as loan interest.

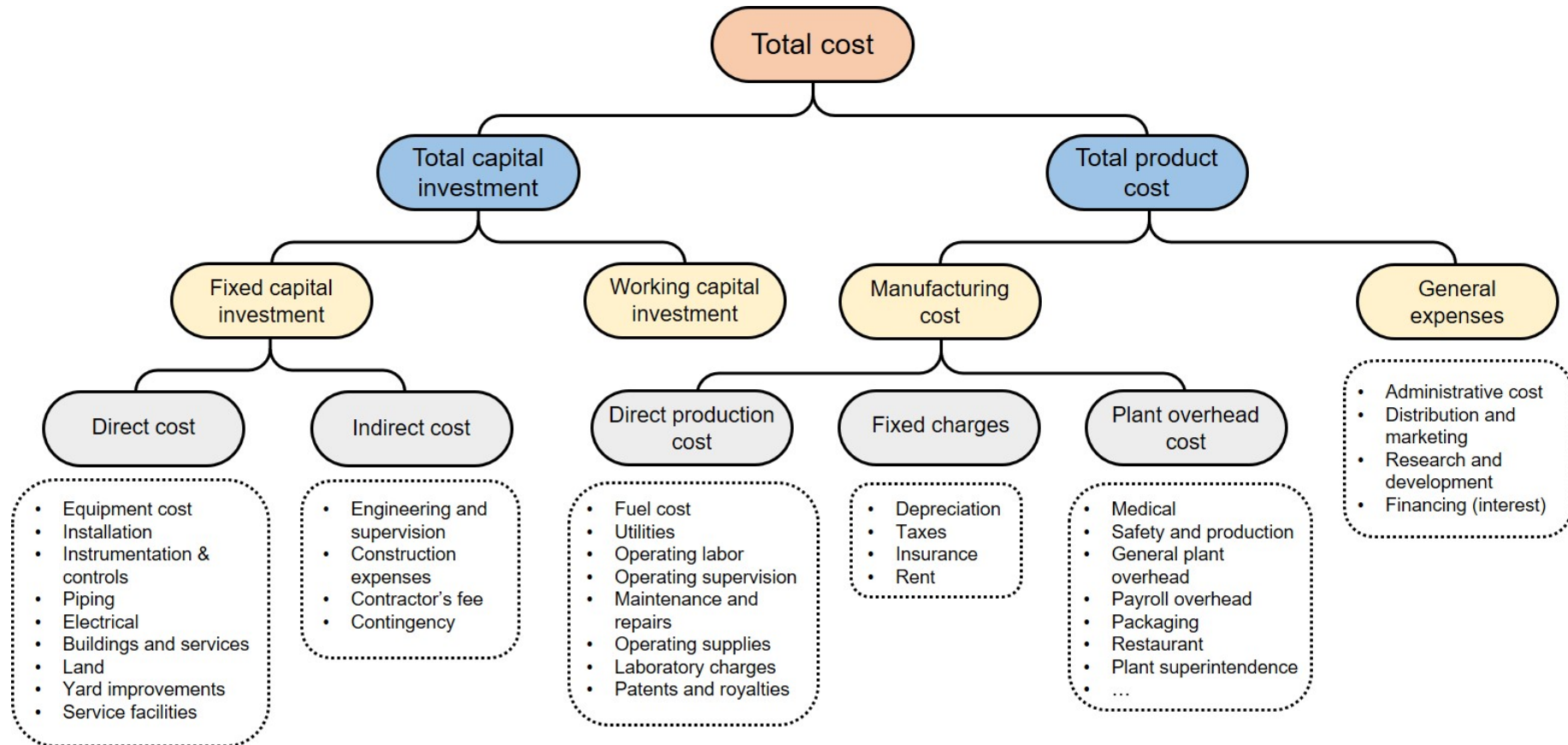


Figure 5-1. Schematic diagram of the cost structure of a typical chemical plant (Reproduced from Ref. [130]).

5.2 Economic modeling of the nuclear hydrogen production system

For the nuclear hydrogen production system studied in this work, its economic modeling process mainly consists of two parts: economic modeling of the S-I thermochemical hydrogen production plant and economic modeling of the nuclear power system.

5.2.1 Economic modeling of the S-I hydrogen production plant

As mentioned in the previous section, in this work, the economic estimate of the S-I thermochemical hydrogen production plant is based on a ratio estimate which adopts a scaling method called the six-tenths-factor rule to roughly calculate the cost of similar equipment at different capacities. Specifically, the six-tenths-factor rule can be expressed by the following formula:

$$\text{Cost of equipment a'} = \text{Cost of equipment a} \times \left(\frac{\text{Capacity of equipment a'}}{\text{Capacity of equipment a}} \right)^\sigma, \quad (5-1)$$

where the symbol σ is the cost capacity factor that equals to 0.6.

Clearly, when the cost of a given equipment (marked as equipment a) at one capacity is known, the cost of a similar equipment (marked as equipment a') with another capacity can be approximately estimated using this formula.

It should be noted that the cost capacity factor of 0.6 used here is just a preliminary estimate since the actual values of the cost capacity factor may vary from less than 0.2 to greater than 1 [131]. In subsequent parametric studies, the effects of different cost capacity factors on the unit cost of hydrogen production will be performed.

For the S-I thermochemical hydrogen production plant proposed in this work, its system components can be divided into the following categories: power equipment (such as pump and blower), heat exchangers (such as heater, cooler, internal heat exchanger, condenser and reboiler), chemical reactors (such as Bunsen reactor, SO₃ decomposer and HI decomposer), tower equipment (such as distillation column and O₂ scrubber), and other components (such as EED, valve, separator and mixer).

For power equipment, the cost can be roughly calculated through several equipment investment cost equations introduced in the next section - Economic modeling of the GSCC power conversion system.

For heat exchangers, the cost can be roughly calculated using the six-tenths-factor rule described above and the corresponding cost data reported in Ref. [89]. However, it should be particularly pointed out that for a heat exchanger, when its structure and materials are determined, its cost is mainly dependent on the size of the heat exchange area. Therefore, when calculating the cost of a heat exchanger, the capacity shown in formula (5-1) refers to the heat exchange capacity (i.e., heat duty) of the heat exchanger. In addition, since the cost data reported in Ref. [89] were published

in 2003, the Chemical Engineering Plant Cost Index (CEPCI) is used in this work to reflect price volatility and cost inflation from year to year. So, formula (5-1) is further modified as:

$$\text{Cost of equipment a}' = \text{Cost of equipment a} \times \left(\frac{\text{Capacity of equipment a}'}{\text{Capacity of equipment a}} \right)^{0.6} \cdot \left(\frac{\text{CEPCI}_{2020}}{\text{CEPCI}_{\text{Ref}}} \right), \quad (5-2)$$

where the term $\text{CEPCI}_{\text{Ref}}$ represents the Chemical Engineering Plant Cost Index based on the reference year. Note that in this work, cost data for all system components are only updated to 2020.

Similarly, for chemical reactors, tower equipment and separators, the cost can also be calculated according to formula (5-2) and Ref. [89]. However, it should be noted that when calculating the costs of these components, the capacity shown in formulas (5-1) and (5-2) is defined as the hydrogen production capacity of the system, which is different from the capacity definition of a heat exchanger.

In Ref. [89], the reactive distillation method is used to concentrate the HI solution, which means that no EED cells are used, the cost data of which are unknown. Therefore, the cost of the EED unit used in this work has to be calculated by referring to other literatures. Generally, the capital cost of an electro dialysis unit mainly consists of membrane cost and stack cost, namely:

$$C_{\text{EED}} = C_{\text{mem}} + C_{\text{sta}}, \quad (5-3)$$

where the terms C_{EED} , C_{mem} , and C_{sta} represent the EED cost, membrane cost, and stack cost, respectively.

The membrane cost (C_{mem}) can be calculated by multiplying the membrane area of the EED unit by the membrane cost per unit area, as follows:

$$C_{\text{mem}} = A_{\text{mem}} \cdot c_{\text{mem}}, \quad (5-4)$$

where the terms A_{mem} and c_{mem} represent the membrane area and membrane cost per unit area, respectively. The membrane area can be roughly estimated based on the experimental study by Guo et al. [101], where the EED cell with an effective membrane area of 800 cm² was used to produce hydrogen at a rate of 10 NL/h (i.e., 0.45 mol/h). It was reported in Refs. [132,133] that the membrane cost per unit area (for ion exchange membranes) was typically around 100 to 150 \$/m². However, in a recent study, the membrane cost per unit area was reported to be about 25 \$/m² [134]. It is believed that the significant difference in membrane cost per unit area is mainly due to technological developments in membranes and materials. In this work, the membrane cost per unit area is set to 100 \$/m² [135] as an intermediate value between high and low prices.

The stack cost (C_{sta}) is typically taken 1.5 times of the membrane cost [133,135], expressed as:

$$C_{\text{sta}} = 1.5 \times C_{\text{mem}}. \quad (5-5)$$

In addition to the EED unit, the HI decomposer (R301) in this work is also a special equipment with a membrane module, which is significantly different from the device in Ref. [89]. As mentioned in Chapter 2, the membrane separation technology was applied to the HI decomposition process to increase the HI conversion rate, which means that the HI decomposer in this work is a membrane reactor with a H₂ separation membrane. In this case, the capital cost of the HI decomposer (R301) will consist of two parts: reactor cost and membrane module cost. The reactor cost can be roughly calculated based on Eq. (5-2) and the corresponding cost data reported in Ref. [89], and the membrane module cost can be roughly estimated based on Eq. (5-2) and the membrane cost data reported in Ref. [136] (in Ref. [136], the capital cost of a H₂ membrane separation module was reported to be around \$5105 at a H₂ production capacity of 15 m³/h).

Also, it should be noted that the costs of valves and mixers are ignored in this work, as these components are usually much less expensive than others [137].

Thus, the equipment investment cost of the S-I thermochemical hydrogen production plant, $C_{\text{equ,S-I}}$, can be calculated by:

$$C_{\text{equ,S-I}} = \sum_{i=1}^j C_{\text{equ},i}, \quad (5-6)$$

where the term $C_{\text{equ},i}$ represents the capital investment cost of equipment i and the letter j represents the total number of equipment in the S-I plant.

After calculating the equipment investment cost of the S-I plant, the fixed capital investment of the S-I plant, $C_{\text{fix-cap,S-I}}$, can be obtained by multiplying the equipment cost ($C_{\text{equ,S-I}}$) by some cost factors shown in Table 5-3.

Table 5-3. The S-I plant's fixed capital investment breakdown.

Categories	Expenses	Cost factors ^a
Direct cost	Equipment cost	1.00
	Installation	0.10
	Instrumentation and controls	0.15
	Piping	0.15
	Electrical	0.10
	Buildings and services	0.25
	Land	0.06
Indirect cost	Engineering and supervision	0.15
	Construction expenses	0.25
	Contractor's fee	0.20
	Contingency	0.15
Total	Fixed capital investment	2.56

^a Taken from Ref. [138].

As mentioned in Section 5.1.1, for most chemical plants, the working capital investment is between 10% and 20% of the total capital investment. In this work, the working capital investment of the S-I plant ($C_{\text{work-cap,S-I}}$) is considered to be 15% of the total capital investment of the S-I plant, $C_{\text{tot-cap,S-I}}$ (this means that the fixed capital investment, $C_{\text{fix-cap,S-I}}$, is equal to 85% of the total capital investment, $C_{\text{tot-cap,S-I}}$) [130,131]. Therefore, when the fixed capital investment of the S-I plant ($C_{\text{fix-cap,S-I}}$) is known, the working capital investment and total capital investment of the S-I plant can be calculated by:

$$\begin{cases} C_{\text{work-cap,S-I}} = 0.15 \times C_{\text{tot-cap,S-I}} \\ C_{\text{tot-cap,S-I}} = C_{\text{fix-cap,S-I}} \div 0.85 \end{cases} \quad (5-7)$$

Thus, the annual capital investment of the S-I plant, $C_{\text{ann-cap,S-I}}$, can be calculated by:

$$C_{\text{ann-cap,S-I}} = C_{\text{tot-cap,S-I}} \cdot CRF, \quad (5-8)$$

where the term CRF represents the Capital Recovery Factor, which can be calculated based on the following formula:

$$CRF = \frac{i_r(1+i_r)^l}{(1+i_r)^l - 1}, \quad (5-9)$$

where the symbols i_r and l denote the interest rate and the lifetime of the plant, respectively. In this work, the nominal values of these two parameters are set to 12% and 30 years [139,140], respectively, which means that the CRF is equal to approximately 0.124.

As mentioned in Section 5.1.2, the total product cost includes the manufacturing costs and general expenses, and it can be calculated on an annual cost basis. Table 5-4 shows the S-I plant's total product cost breakdown (calculated at annual cost). For the S-I plant, its raw material for hydrogen production is water, and its main utility components include heating medium, electricity and cooling medium. In this work, the cost of utility components is not considered because the main utilities of the S-I plant (e.g., heating helium and electricity) are provided directly by the reactor and power conversion system (in Ref. [89], the utility cost is also ignored). In addition, since in most cases nuclear hydrogen plants are considered to be built in remote areas (for safety reasons), the rent cost is also ignored (the same is true in Refs. [89,138]). However, it should be pointed out that, different from Refs. [89,138], in this work, the research and development expenses of the S-I plant are included in the total product cost, because the S-I thermochemical hydrogen production technology is still in the bench-scale or small-scale test stage and further research and development work is required to enable pilot-scale engineering applications.

Thus, the annual total cost of the S-I plant, $C_{\text{ann-tot,S-I}}$, can be calculated by:

$$C_{\text{ann-tot,S-I}} = C_{\text{ann-cap,S-I}} + C_{\text{ann-pro,S-I}}, \quad (5-10)$$

where the term $C_{\text{ann-pro,S-I}}$ represents the annual product cost of the S-I plant.

Table 5-4. The S-I plant's total product cost breakdown (calculated at annual cost).

Categories	Expenses	Basis [Ref(s).]	
Manufacturing costs	Raw materials (i.e., water)	1.00 \$/m ³ [89]	
	Utilities (heating, electricity, etc.)	Not considered ^a [89]	
	Operating labor	15 operators per shift on 4 rotating shifts at 80,000 \$/person/year [89]	
	Direct production cost	Supervisory and clerical labor	10% of operating labor [130,138]
		Maintenance and repairs	3% of fixed capital investment [130]
		Operating supplies	0.7% of fixed capital investment [130,138]
		Laboratory charges	10% of operating labor [130,138]
		Patents and royalties	None [89,130]
		Depreciation	Not considered [89,138]
	Fixed charges	Taxes	1% of fixed capital investment [130]
		Insurance	0.4% of fixed capital investment [130]
		Rent	Not considered ^b [89,138]
		Plant overhead cost	50% of operating labor [130]
	General expenses	Administrative cost	20% of operating labor [130]
Distribution and marketing		20% of operating labor [130]	
Research and development		50% of operating labor [130]	
Financing (interest)		1% of total capital investment [130]	
Total product cost	Manufacturing costs + General expenses		

^a This is because the heating and electrical utilities of the S-I plant are provided directly by the nuclear power system.

^b This is because in most cases nuclear hydrogen plants are built in remote areas where the land rent can be neglected.

5.2.2 Economic modeling of the nuclear power system

For the nuclear power system (or the reactor and power conversion system), its cost mainly consists of three parts: total capital investment cost, operating and maintenance cost, and fuel cost. The total capital investment cost of the nuclear power system ($C_{\text{tot-cap,NPS}}$) can be roughly calculated by multiplying the equipment investment cost ($C_{\text{equ,NPS}}$) by an amplification factor α (this factor is used to reflect other capital investment components other than equipment cost, such as Structures and Improvements, Construction Services, Engineering & Home Office Services, Field Supervision & Field Office Services, Contingencies, etc.). In this work, the amplification factor α is derived from the cost data reported in Ref. [89], and the equipment investment cost ($C_{\text{equ,NPS}}$) is calculated based on some existing equipment capital investment cost equations. Furtherly, the equipment investment cost of the nuclear power system ($C_{\text{equ,NPS}}$) can be expressed as:

$$C_{\text{equ,NPS}} = \sum_{k=1}^z C_{\text{equ,k,Ref}} \left(\frac{\text{CEPCI}_{2020}}{\text{CEPCI}_{\text{Ref}}} \right), \quad (5-11)$$

where the term $C_{\text{equ,k,Ref}}$ represents the capital investment cost of equipment k based on the reference year and the letter z represents the total number of equipment in the nuclear power system.

The detailed equipment investment cost equations of the nuclear power system are summarized in Table 5-5 [137,141,142], and the CEPCI indexes from 1985 to 2020 are given in Table 5-6. Due to the lack of actual cost data for Generation IV nuclear reactors, the cost of the VHTR is roughly estimated based on a typical nuclear reactor investment cost model [137,141]. It can be seen from Table 5-5 that the investment cost of the reactor is directly proportional to its thermal power capacity. As we all know, the investment cost of a heat exchanger depends largely on the type and heat transfer area of the heat exchanger. In this work, the IHX, SG and Preheater are considered as compact heat exchangers, while the Condenser and LP Heater(s) are considered as shell and tube heat exchangers. The heat transfer area of the heat exchanger can be calculated based on the Logarithmic Mean Temperature Difference (LMTD) method, which is expressed as:

$$\begin{cases} A = \frac{\dot{Q}}{K \cdot \Delta T_{\text{mn}}} \\ \Delta T_{\text{mn}} = \frac{\Delta T_{\text{max}} - \Delta T_{\text{min}}}{\ln\left(\frac{\Delta T_{\text{max}}}{\Delta T_{\text{min}}}\right)}, \end{cases} \quad (5-12)$$

where the terms K and ΔT_{mn} represent the overall heat transfer coefficient and the LMTD of the heat exchanger, respectively.

In this work, the overall heat transfer coefficient of the heat exchanger is set according to the fluid phase state on both sides of the heat exchanger. For instance, the overall heat transfer coefficient of the IHX is set to $0.7 \text{ kW/m}^2 \cdot \text{K}$ [142] as the

Table 5-5. Equipment investment cost equations of the nuclear power system [137,141,142].

Equipment	Capital investment cost equations	Reference year
VHTR	$C_{\text{VHTR,Ref}} = c \cdot \dot{Q}_{\text{VHTR}}, c = 283 \text{ \$/kW}_{\text{th}}$	2003
IHX	$C_{\text{IHX,Ref}} = 2681 \cdot A_{\text{IHX}}^{0.59}$	1986
GT	$C_{\text{GT,Ref}} = 479.34 \cdot \dot{m}_{\text{GT}} \cdot \left(\frac{1}{0.93 - \eta_{\text{GT}}}\right) \cdot \ln(\text{PRc}) \cdot (1 + \exp(0.036 \cdot T_{\text{in,GT}} - 54.4))$ ^a	1994
GC and Blowers	$C_{\text{k,Ref}} = 71.1 \cdot \dot{m}_{\text{k}} \left(\frac{1}{0.92 - \eta_{\text{k}}}\right) \cdot \text{PRc} \cdot \ln(\text{PRc})$ ^a	1994
Generator (Brayton)	$C_{\text{G,Brayton,Ref}} = 4 \times 10^6 \times \left(\frac{\dot{W}_{\text{gen,GT}} - \dot{W}_{\text{con,GC}}}{160000}\right)^{0.7}$	1991
SGs and Preheater	$C_{\text{SG,Ref}} = 2681 \cdot A_{\text{SG}}^{0.59}, C_{\text{Preheater,Ref}} = 2681 \cdot A_{\text{Preheater}}^{0.59}$	1986
ST	$C_{\text{ST,Ref}} = 4405 \cdot \dot{W}_{\text{gen,ST}}^{0.7}$	2005
Condenser	$C_{\text{CON,Ref}} = 2143 \cdot A_{\text{CON}}^{0.514}$	1986
LP Heater(s)	$C_{\text{LP Heater,Ref}} = C_{\text{CON,Ref}} \cdot \left(\frac{\dot{Q}_{\text{LP Heater}}}{\dot{Q}_{\text{CON}}}\right)^{0.6}$	1986
FWP, CFP and Circulating pump	$C_{\text{k,Ref}} = 1120 \cdot \dot{W}_{\text{con,k}}^{0.8}$	2005
Generator (SRC)	$C_{\text{G,SRC,Ref}} = 60 \times \dot{W}_{\text{gen,ST}}^{0.95}$	2005

^a The term PRc denotes the pressure ratio of the component (for GT, $\text{PRc} = p_{\text{in}} / p_{\text{out}}$; for GC and Blower, $\text{PRc} = p_{\text{out}} / p_{\text{in}}$).

Table 5-6. CEPCI indexes from 1985 to 2020.

Year	CEPCI	Year	CEPCI	Year	CEPCI
1985	325.3	1997	386.5	2009	521.9
1986	318.4	1998	389.5	2010	550.8
1987	323.8	1999	390.6	2011	585.7
1988	342.5	2000	394.1	2012	584.6
1989	355.4	2001	394.3	2013	567.3
1990	357.6	2002	395.6	2014	576.1
1991	361.3	2003	402.0	2015	556.8
1992	358.2	2004	444.2	2016	541.7
1993	359.2	2005	468.2	2017	567.5
1994	368.1	2006	499.6	2018	603.1
1995	381.1	2007	525.4	2019	607.5
1996	381.7	2008	575.4	2020	596.2

fluids on both sides are gaseous; a value of $1.6 \text{ kW/m}^2 \cdot \text{K}$ [141] is used as the overall heat transfer coefficient for the SG, since this component can be considered as an evaporator with a gas (helium) as the heating fluid; considering that the cooling fluid is a liquid (water), the overall heat transfer coefficient of the Condenser is set to $2.0 \text{ kW/m}^2 \cdot \text{K}$ [137,141].

It should be noted that in this work, the total heat transfer area of the SG consists of three parts: the heat transfer area of the subcooling zone, the heat transfer area of the two-phase zone, and the heat transfer area of the superheating zone. And for each zone, there will be a separate LMTD (ΔT_{mn}). However, the heat transfer coefficient for each zone is all set to $1.6 \text{ kW/m}^2 \cdot \text{K}$ because this value represents an overall average (since the Preheater is essentially a part of the SG subcooling zone, its overall heat transfer coefficient is also considered to be $1.6 \text{ kW/m}^2 \cdot \text{K}$, this is why the Preheater is placed together with the SG in Table 5-5). In addition, considering that the total heat transfer of the LP Heater is relatively small and the calculation of the heat transfer area is relatively complicated, in order to simplify the modeling process, the cost of the LP Heater is roughly calculated according to the Condenser's cost and the six-tenths-factor rule, as shown in Table 5-5 (in fact, the investment cost of the LP Heater is very small, or even negligible).

Also, it should be pointed out that in this work, the cost of the Deaerator (considered as a mixer) is ignored due to its small value (taking Ref. [143] as an example, it was reported that the investment cost of the Deaerator was less than 3% of the investment cost of the Turbine). And the investment cost of the Cooling tower is not considered either, since this component can be removed when the nuclear plant is built close to a lake or sea (which is the case in most cases).

Thus, the total capital investment ($C_{\text{tot-cap,NPS}}$) and the annual capital investment ($C_{\text{ann-cap,NPS}}$) of the nuclear power system can be calculated by:

$$\begin{cases} C_{\text{tot-cap,NPS}} = \alpha \cdot C_{\text{equ,NPS}} \\ C_{\text{ann-cap,NPS}} = C_{\text{tot-cap,NPS}} \cdot CRF \end{cases}, \quad (5-13)$$

where the amplification factor α is estimated to be about 2.09 (i.e., $\alpha = 1098026 / (695230-132133-38070)$, data from Ref. [89]).

The annual operating and maintenance cost of the nuclear power system, $C_{\text{ann-O\&M,NPS}}$, can be roughly estimated by multiplying the total capital investment ($C_{\text{tot-cap,NPS}}$) by the maintenance factor γ , namely:

$$C_{\text{ann-O\&M,NPS}} = \gamma \cdot C_{\text{tot-cap,NPS}}. \quad (5-14)$$

In this work, the maintenance factor γ is estimated to be about 0.0242 (i.e., $\gamma = 26540 / 1098026$, data from Ref. [89]).

The annual fuel cost, $C_{\text{ann-fuel}}$, can be calculated by:

$$C_{\text{ann-fuel}} = (\dot{Q}_{\text{VHTR}} \times 365 \times 24 \times LF \times 3600) \cdot c_Q = (\dot{Q}_{\text{VHTR}} \times N \times 3600) \cdot c_Q, \quad (5-15)$$

where the terms LF , N and c_Q denote the Load Factor, the annual operating hours and the nuclear fuel cost per unit thermal exergy of the reactor ($c_Q = 0.4$ \$/GJ [144]), respectively. In this work, the plant is assumed to run 8000 hours per year [137,141], which means that the load factor is about 0.913.

5.2.3 Unit hydrogen production cost and results comparison

The unit hydrogen production cost, c_{H_2} , can be calculated as:

$$c_{\text{H}_2} = \frac{C_{\text{ann-cap,S-I}} + C_{\text{ann-pro,S-I}} + C_{\text{ann-cap,NPS}} + C_{\text{ann-O\&M,NPS}} + C_{\text{ann-fuel}} - IN_{\text{ann-E}} - IN_{\text{ann-O}_2}}{M_{\text{ann-H}_2}}, \quad (5-16)$$

where the terms $IN_{\text{ann-E}}$, $IN_{\text{ann-O}_2}$, and $M_{\text{ann-H}_2}$ represent the annual income from electricity, annual income from oxygen, and annual hydrogen production capacity, respectively.

The annual income from electricity can be calculated by:

$$IN_{\text{ann-E}} = c_E \cdot \dot{E}_{\text{net}} \cdot N, \quad (5-17)$$

where the term c_E represents the unit electricity cost. It is well known that the unit electricity cost is not constant but varies with time and location (as shown in Ref. [145]). In this work, the nominal electricity price is set to 0.1 \$/kWh.

The annual income from oxygen can be calculated by:

$$IN_{\text{ann-O}_2} = c_{\text{O}_2} \cdot M_{\text{ann-O}_2}, \quad (5-18)$$

where the terms c_{O_2} and $M_{\text{ann-O}_2}$ represent the unit oxygen price and annual oxygen

production capacity, respectively. In this work, the unit oxygen price is set to 85.9 \$/ton [146].

It is not difficult to find that the above economic model is established with reference to many cost data reported in literature [89]. Therefore, the calculated results of this work were compared with the data reported in Ref. [89], as shown in Table 5-7. As mentioned earlier, there are many uncertainties in economic analysis, which may make the calculation results of different studies (or different cases) vary widely. Overall, the estimated unit hydrogen production cost is comparable to the value reported in Ref. [89], as shown in Table 5-7. This shows that the calculation results obtained in this work can be used as some data references for system economic evaluation.

Table 5-7. Comparison of results between this work and Ref. [89].

Parameters (Unit)	Ref. [89]	This work
Overall availability (or load factor), LF (-)	90% (or 0.90)	91.3% (or 0.913)
Capital Recovery Factor, CRF (-)	0.125	0.124
Annual hydrogen production, $M_{\text{ann-H}_2}$ (ton)	250073	250387 ^a
Daily hydrogen production, $M_{\text{day-H}_2}$ (ton) ^b	685	686
Unit hydrogen production cost, c_{H_2} (\$/kg)	1.57	1.54 ^c

^a This hydrogen production capacity is achieved by setting \dot{Q}_{VHTR} to 7500 MWth.

^b $M_{\text{day-H}_2} = M_{\text{ann-H}_2} / 365$.

^c For the coupled operating system (see Figure 4-5).

5.3 Cost distribution and parametric studies

Before conducting cost distribution analysis and parametric studies, it is necessary to clarify the system's benchmark conditions and parametric variables. Table 5-8 summarizes some important parametric variables studied in this work and their base values.

Table 5-8. Some important parametric variables and their base values.

Parametric variables (Unit)	Base values
Reactor thermal power, \dot{Q}_{VHTR} (MWth)	350
Mass flow rate ratio, x (-)	0.5
Cost capacity factor, σ (-)	0.6
Interest rate, i_r (-)	12%
Lifetime of the system, l (year)	30
Electricity price, c_E (\$/kWh)	0.1

5.3.1 Cost distribution

The cost data of the two operating systems under the benchmark conditions are summarized in Table 5-9. It can be seen that under the baseline conditions, both the independent operating system and the coupled operating system can achieve an annual hydrogen production of about 11685 tons (corresponding to a daily hydrogen production of about 32 tons), and the unit hydrogen production cost of the independent operating system and the coupled operating system is equal to about 6.94 \$/kg and 5.12 \$/kg, respectively. As discussed in the previous chapter, under the same operating conditions, the coupled operating system can achieve a much larger net electrical power output than the independent operating system. Therefore, the coupled operating system can obtain greater annual electricity revenue (see Table 5-9), which is why the unit hydrogen production cost of the coupled operating system is significantly lower than that of the independent operating system.

Table 5-9. Cost data of the two operating systems under the benchmark conditions.

Parameters (Unit)	Independent operating system	Coupled operating system
Annual capital investment of the S-I plant, $C_{\text{ann-cap,S-I}}$ (k\$)	37744	37744
Annual product cost of the S-I plant, $C_{\text{ann-pro,S-I}}$ (k\$)	28806	28806
Annual capital investment of the nuclear power system, $C_{\text{ann-cap,NPS}}$ (k\$)	44137	45845
Annual operating and maintenance cost of the nuclear power system, $C_{\text{ann-O\&M,NPS}}$ (k\$)	8593	8926
Annual fuel cost, $C_{\text{ann-fuel}}$ (k\$)	4032	4032
Annual electricity income, $IN_{\text{ann-E}}$ (k\$)	34201	57511
Annual oxygen income, $IN_{\text{ann-O}_2}$ (k\$)	8030	8030
Annual hydrogen production, $M_{\text{ann-H}_2}$ (ton)	11685	11685
Daily hydrogen production, $M_{\text{day-H}_2}$ (ton)	32	32
Unit hydrogen production cost, c_{H_2} (\$/kg)	6.94	5.12

Under the benchmark conditions, the economic cost distributions of the independent operating system and the coupled operating system are shown in Figures 5-2 and 5-3, respectively. From Figures 5-2(a) and 5-3(a), it can be seen that under the baseline conditions, the annual cost expenditure of the nuclear hydrogen production system is mainly caused by the annual capital investment of the nuclear power system, the annual capital investment of the S-I hydrogen production plant, and the annual product cost of the S-I hydrogen production plant, because the sum of these three items accounts for nearly 90% of the total annual cost expenditure of the system. In more detail, the annual capital investment of the nuclear power system is the largest

annual cost source, which accounts for about 36% of the total annual expenditure of the system. The annual capital investment and annual product cost of the S-I hydrogen production plant are the second and third largest annual cost sources, accounting for about 30% and 23% of the total annual expenditure of the system, respectively. Besides this, it is found that the annual fuel cost is the smallest annual cost source that accounts for only 3.2%-3.3% of the total annual expenditure of the system, as shown in Figures 5-2(a) and 5-3(a).

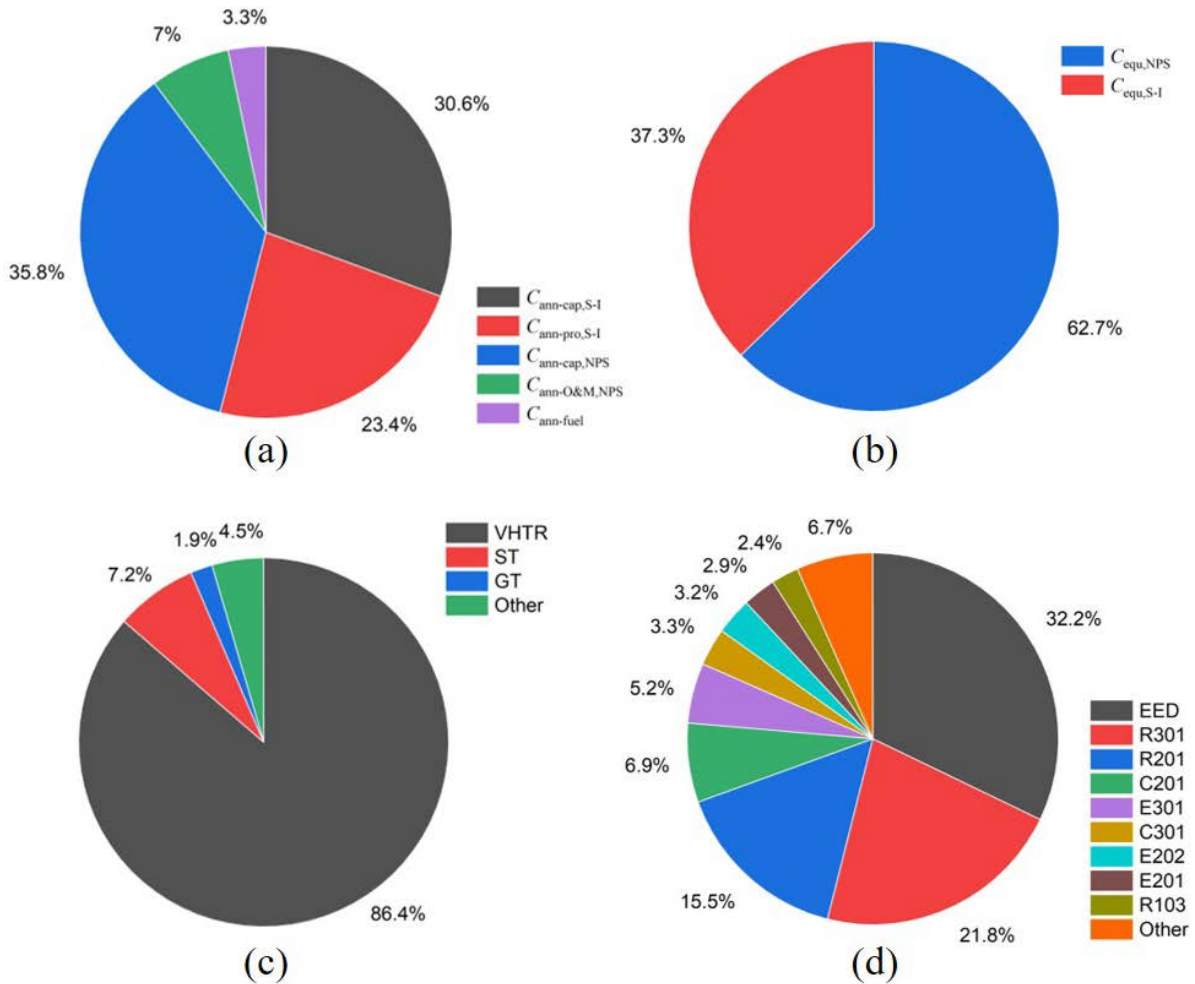


Figure 5-2. Economic cost distribution of the independent operating system under the benchmark conditions: (a) Annual cost distribution, (b) Equipment investment cost distribution of the overall system, (c) Equipment investment cost distribution of the nuclear power system, and (d) Equipment investment cost distribution of the S-I plant.

Obviously, the annual capital investment of the system is closely related to the equipment investment cost. From Figures 5-2(b) and 5-3(b), it can be seen that for both operating systems under the baseline conditions, more than 60% of the total equipment investment cost of the system is occupied by the nuclear power plant, and more than 35% is occupied by the S-I hydrogen production plant. For the nuclear power plant, most of the equipment investment cost is used for the construction of the reactor, since the equipment investment cost of the reactor is quite large and accounts for more than 80% of the total equipment investment cost of the nuclear

power system (see Figures 5-2(c) and 5-3(c)). For the S-I hydrogen production plant, the equipment investment cost is mainly used for the construction of the EED unit, HI decomposition reactor (R301), and SO₃ decomposition reactor (R201), because the sum of the equipment investment costs of these three components accounts for about 70% of the total equipment investment of the S-I hydrogen production plant, as shown in Figure 5-2(d) or 5-3(d) (note that the independent operating system and the coupled operating system have the same S-I hydrogen production unit, which is why Figure 5-2(d) is the same as Figure 5-3(d)). As mentioned in the previous section, the equipment investment cost of the EED device is largely dependent upon the membrane cost per unit area, while part of the equipment investment cost of the HI decomposition reactor (R301) is caused by the added H₂ separation membrane. In view of the relatively high equipment investment costs of these two components (as shown in Figure 5-2(d) or 5-3(d), more than half of the total equipment investment of the S-I plant is occupied by these two components), one possible way to reduce the equipment investment cost of the S-I hydrogen production plant is to decrease the membrane cost through the development of membrane science and technology.

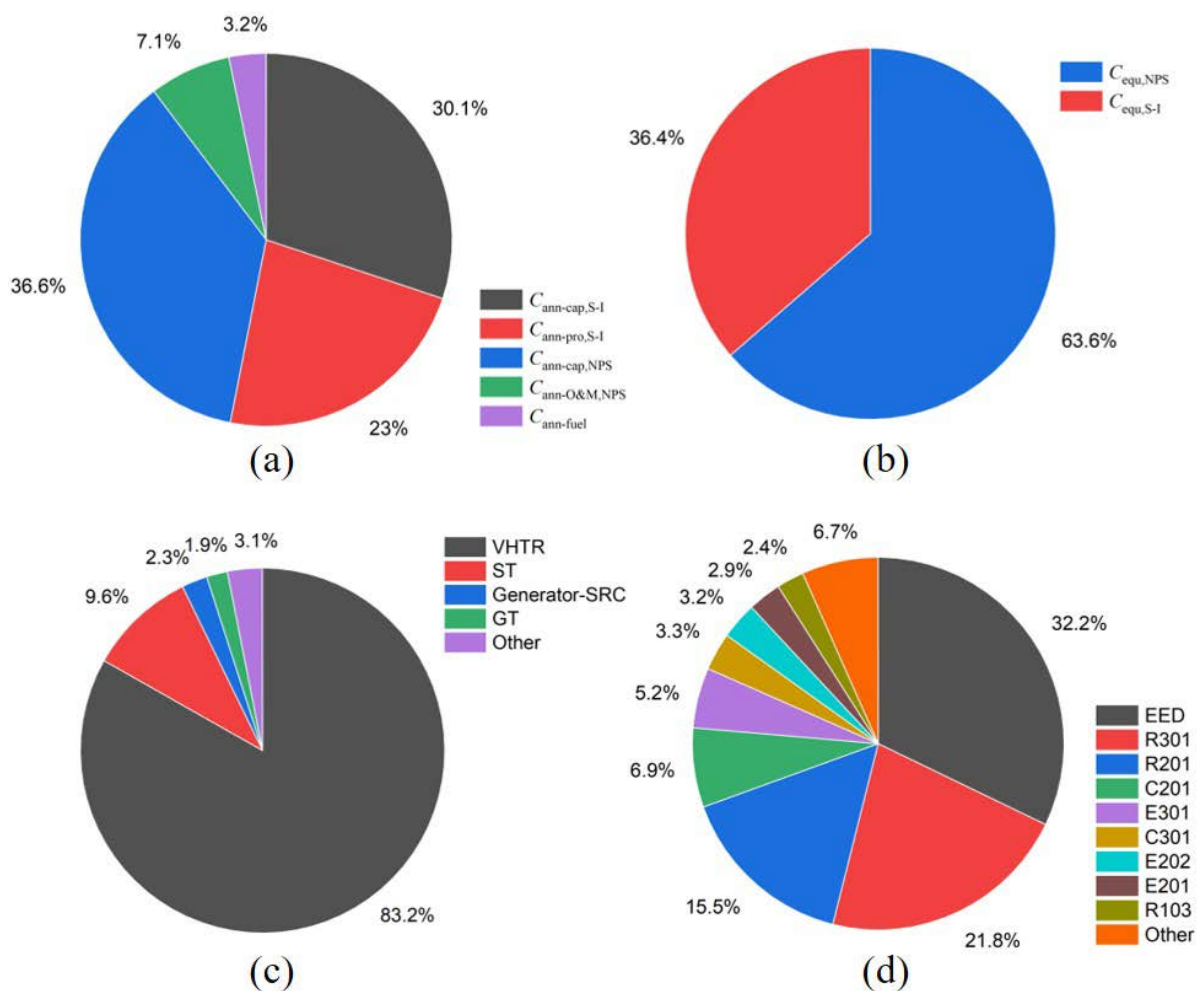


Figure 5-3. Economic cost distribution of the coupled operating system under the benchmark conditions: (a) Annual cost distribution, (b) Equipment investment cost distribution of the overall system, (c) Equipment investment cost distribution of the nuclear power system, and (d) Equipment investment cost distribution of the S-I plant.

Under the benchmark conditions, the detailed equipment investment cost data of the nuclear power system and the S-I hydrogen production plant are given in Table 5-10 and Table 5-11, respectively.

Table 5-10. Equipment investment cost data of the nuclear power system under the benchmark conditions.

Equipment	Investment cost (\$)	
	Independent operating system	Coupled operating system
VHTR	1.4690e+08	1.4690e+08
IHX	1.1033e+06	1.1033e+06
Blower-1	6.7291e+03	6.7291e+03
Blower-2	1.1660e+04	1.1660e+04
GT	3.2676e+06	3.2676e+06
GC	4.9423e+05	5.7183e+05
Generator (Brayton)	1.9531e+06	1.7529e+06
FWP	3.0929e+05	5.7733e+05
Preheater	—	3.2839e+05
SG-1	3.7219e+05	2.5551e+05
SG-2	1.2915e+05	2.4918e+05
ST	1.2228e+07	1.6900e+07
Generator (SRC)	2.5935e+06	4.0233e+06
Condenser	2.4640e+05	2.4660e+05
CFP	5.1429e+03	3.0566e+04
LP Heater(s)	3.6300e+04	1.4601e+05
AC	1.3065e+05	—
Circulating pump	2.0656e+05	2.0681e+05
Total	1.7000e+08	1.7658e+08

Table 5-11. Equipment investment cost data of the S-I hydrogen production plant under the benchmark conditions (hydrogen production rate of 202.86 mol/s).

Equipment	Description	Investment cost (\$)
P101	Feed water pump	2.2053e+03
C101	O ₂ scrubber	5.4479e+05
E101	External heat exchanger used to keep the inlet temperature of the Bunsen reactor constant	1.3377e+05
S101	Liquid-liquid separator	8.4585e+05
R101	Bunsen reactor	1.7980e+06
R102	H ₂ SO ₄ purification reactor	2.7292e+05

R103	HI purification reactor	2.4033e+06
P201	Water pump	7.6135e+03
B201	Blower for conveying O ₂ and SO ₂	7.3606e+05
C201	H ₂ SO ₄ distillation column	6.9499e+06
E201	Internal heat exchanger for heat recovery from SO ₃ decomposition products	2.9225e+06
E202	External heat exchanger used to keep the inlet temperature of the SO ₃ decomposer constant	3.2300e+06
S201	Vapor-liquid separator	8.3449e+04
R201	SO ₃ decomposer	1.5697e+07
P301	Feed pump of the HI distillation column	1.1899e+05
E301	Internal heat exchanger for heat recovery from the reboiler product of the HI distillation column	5.2758e+06
E302	Internal heat exchanger for heat recovery from HI decomposition products	1.9724e+06
E303	External heat exchanger used to keep the inlet temperature of the EED unit constant	2.0898e+05
EED	Electrodialysis unit for increasing HI concentration	3.2458e+07
C301	HI distillation column	3.3090e+06
R301	HI decomposer	2.1980e+07
Total	The independent operating system and the coupled operating system have the same S-I hydrogen production plant	1.0095e+08

5.3.2 Parametric studies

In this section, a series of parametric studies including the reactor thermal power, mass flow rate ratio, cost capacity factor, interest rate, system lifetime, and electricity price are performed to comprehensively explore the cost-influencing mechanism of the nuclear hydrogen production system based on S-I cycle and GSCC. It should be noted that in the parameter analysis process, the variable control method is adopted, that is, when examining the influence of a certain parameter on the economic performance of the system, other parameters remain unchanged.

Effects of the reactor thermal power

Under the condition that other parameters in Table 5-8 remain unchanged, the effects of the reactor thermal power on the daily hydrogen production capacity and unit hydrogen production cost of the two operating systems are shown in Figure 5-4. It can be seen that as the reactor thermal power increases, the daily hydrogen production of the two operating systems increases linearly (note that the two operating systems have the same hydrogen production capacity), while the unit

hydrogen production cost of the two operating systems first declines sharply and then decreases slightly. For example, when the thermal power of the reactor is increased from 100 MW to 1000 MW and from 1000 MW to 5000 MW, respectively, the unit hydrogen production cost of the independent operating system is reduced from about 11.84 \$/kg to 5.06 \$/kg and from about 5.06 \$/kg to 3.66 \$/kg. It is believed that the reduction in the unit hydrogen production cost is caused by the theory of economies of scale. In addition, it should be pointed out that the unit hydrogen production cost of the coupled operating system is always lower than that of the independent operating system due to its larger power generation (that is, the larger annual electricity revenue), as shown in Figure 5-4(b).

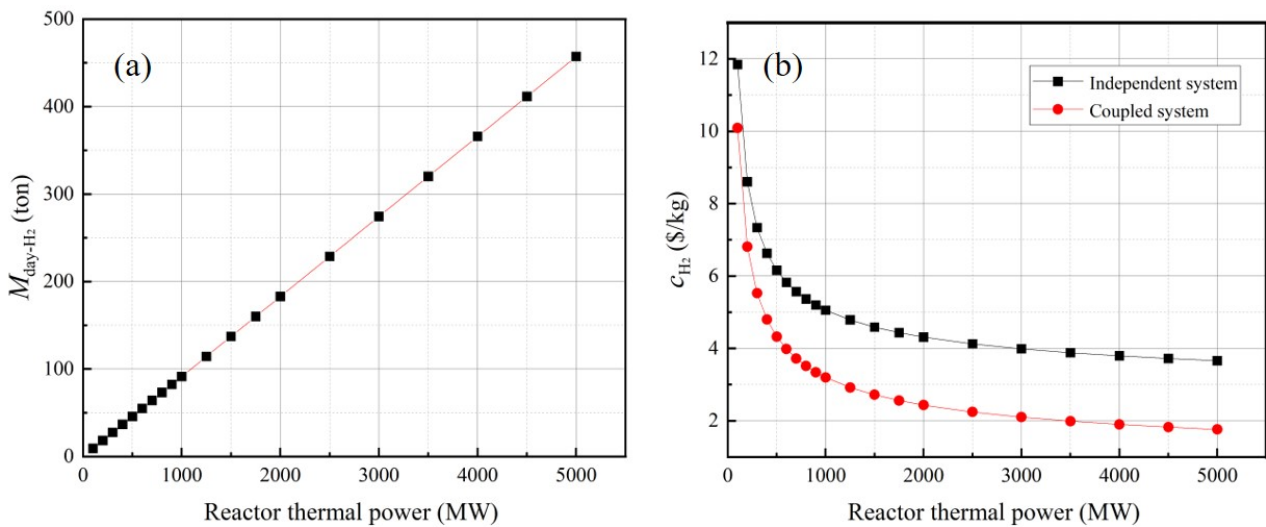


Figure 5-4. Effects of the reactor thermal power on (a) Daily hydrogen production and (b) Unit hydrogen production cost.

Effects of the mass flow rate ratio

Keeping the other parameters in Table 5-8 unchanged, the effects of the mass flow rate ratio on the daily hydrogen production capacity and unit hydrogen production cost of the two operating systems are illustrated in Figure 5-5. It can be seen that as the mass flow rate ratio increases, the daily hydrogen production of the two operating systems increases linearly (note that the two operating systems have the same hydrogen production capacity), while the unit hydrogen production cost of the two operating systems shows a parabolic growth. Different from the increase of the reactor thermal power, the increase in the mass flow rate ratio means that the proportion of hydrogen production is increasing and the proportion of power generation is decreasing. Although the hydrogen production capacity of the system increases with the increase of the mass flow rate ratio, the power generation and annual electricity revenue decrease significantly. At this time, the theory of economies of scale no longer applies. According to the analysis results in the previous chapter, the overall energy efficiencies of the two operating systems decrease as the mass flow rate ratio increases (see Figure 4-7(c) and (d)). In this circumstance, the reactor thermal energy is utilized inefficiently, which ultimately leads to an increase in the levelized cost of energy. Since the hydrogen energy produced is essentially

converted from the reactor thermal energy, the unit hydrogen production cost increases with the increase of the levelized cost of energy.

Similarly, it can be found from Figure 5-5(b) that under the same operating conditions, the unit hydrogen production cost of the coupled operating system is always lower than that of the independent operating system. In addition, it should be pointed out that when the mass flow rate ratio increases beyond a certain value, the net electrical power output will become negative, and at this time, the definition equation for unit hydrogen production cost (i.e., Eq. (5-16)) is no longer applicable. This is why the mass flow rate ratios for the two operating systems only increased to 0.65 and 0.85, as shown in Figure 5-5.

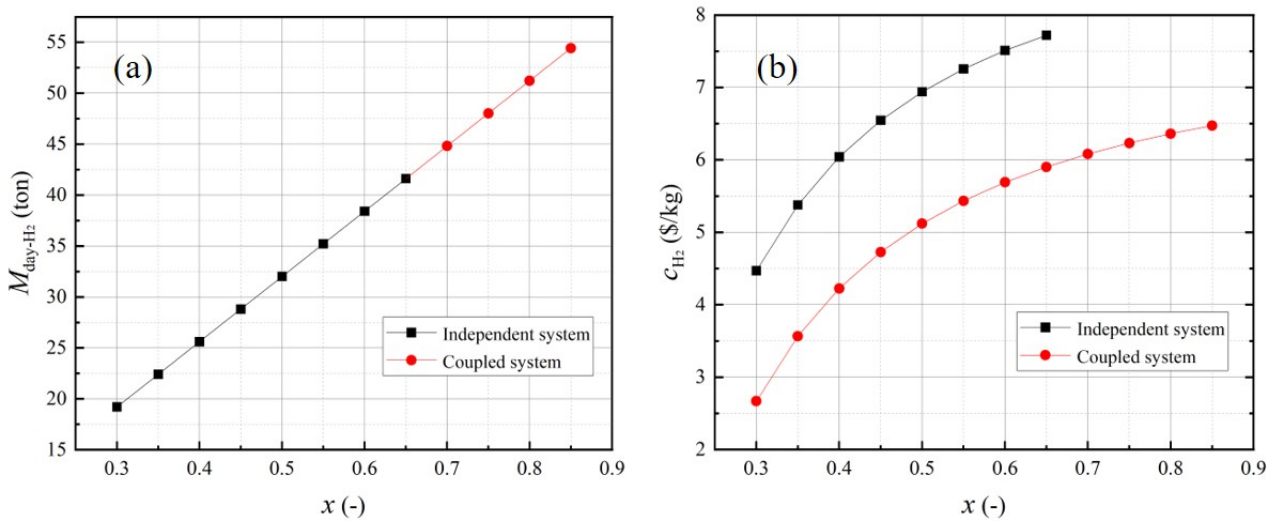


Figure 5-5. Effects of the mass flow rate ratio on (a) Daily hydrogen production and (b) Unit hydrogen production cost.

Effects of the cost capacity factor

Keeping the other parameters in Table 5-8 unchanged, the effects of the cost capacity factor on the S-I plant's equipment investment cost and the unit hydrogen production cost of the two operating systems are depicted in Figure 5-6. It can be seen that with the increase of the cost capacity factor, both the S-I plant's equipment investment cost and the unit hydrogen production cost gradually decrease (note that the equipment investment cost of the S-I plant for the independent operating system is the same as that for the coupled operating system). It can be seen from Eq. (5-1) that when the capacity of the new equipment a' is less than the capacity of the given equipment a (at this time, the capacity ratio of the new equipment a' to the given equipment a is between 0 and 1), the calculated equipment investment cost of the new equipment a' will decrease with the increase of the cost capacity factor. On the contrary, when the capacity of the new equipment a' is greater than that of the given equipment a (at this time, the capacity ratio of the new equipment a' to the given equipment a is greater than 1), the calculated equipment investment cost of the new equipment a' will increase with the increase of the cost capacity factor. It is already known that the equipment investment cost of the S-I plant in this work was estimated based on the cost data reported in Ref. [89], and the equipment investment

cost of the S-I plant in Ref. [89] was calculated at a hydrogen production rate of 4200 mol/s. Since the hydrogen production rate under the benchmark conditions is only about 202.86 mol/s (see Table 5-11), the capacity ratio of the new equipment to the given equipment is between 0 and 1, which is why the equipment investment cost of the S-I plant will decrease with the increase of the cost capacity factor, as shown in Figure 5-6(a). According to Table 5-3 and formulas (5-7) and (5-8), it is not difficult to infer that with the reduction of the equipment investment cost of the S-I plant, the annual capital investment of the S-I plant will also decrease, which will eventually lead to a decrease in the unit hydrogen production cost, as shown in Figure 5-6(b). In addition, it can also be seen from Figure 5-6(b) that under the same cost capacity factors, the unit hydrogen production cost of the coupled operating system is always lower than that of the independent operating system.

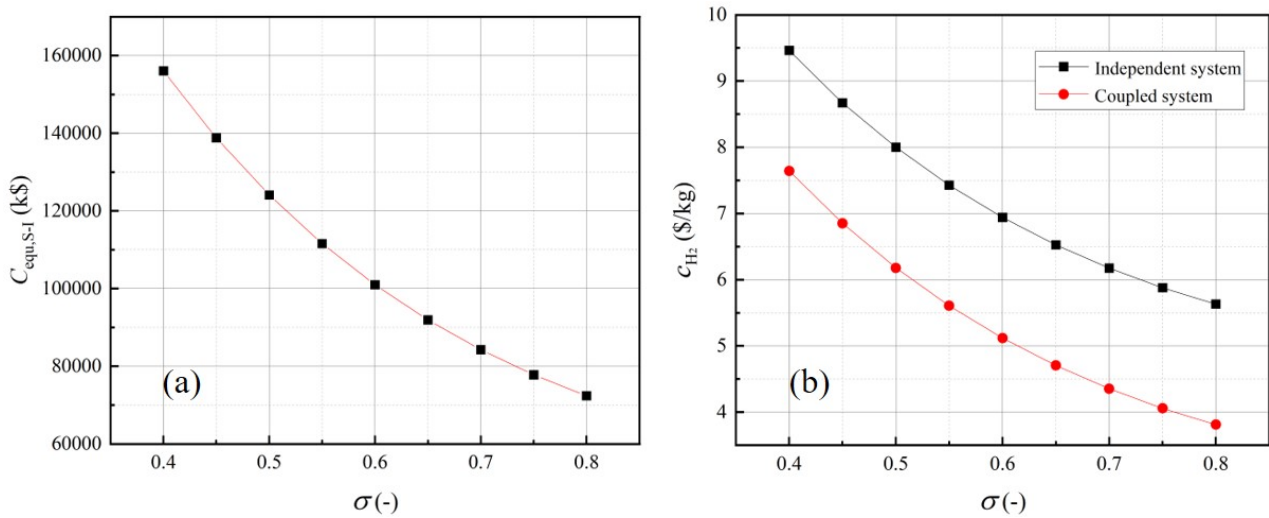


Figure 5-6. Effects of the cost capacity factor on (a) Equipment investment cost of the S-I plant and (b) Unit hydrogen production cost.

Effects of the interest rate and system lifetime

Keeping the other parameters in Table 5-8 unchanged, the effects of the interest rate on the CRF and unit hydrogen production cost of the two operating systems are shown in Figure 5-7. It can be seen that with the increase of the interest rate, both the CRF and the unit hydrogen production cost increase approximately linearly (note that the CRF is the same for both operating systems). Evidently, the CRF is only a function of interest rate and system lifetime (see formula (5-9)), and the annual capital investment of both the S-I plant and the nuclear power system will increase with the increase of the CRF (see formulas (5-8) and (5-13)). Thus, the unit hydrogen production cost will also increase with the increase of the CRF . Besides this, under the same interest rate, the unit hydrogen production cost of the coupled operating system is always lower than that of the independent operating system, as shown in Figure 5-7(b).

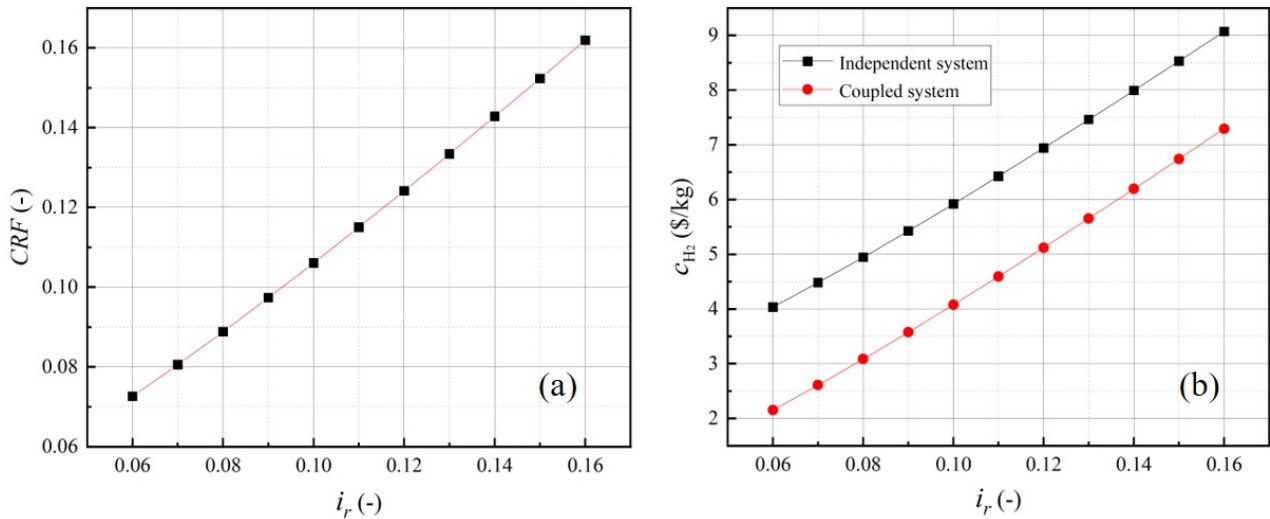


Figure 5-7. Effects of the interest rate on (a) Capital Recovery Factor and (b) Unit hydrogen production cost.

Similarly, keeping the other parameters in Table 5-8 unchanged, the effects of the system lifetime on the CRF and unit hydrogen production cost of the two operating systems are presented in Figure 5-8. It can be seen that as the system lifetime increases, the CRF first declines rapidly and then decreases slowly, and the unit hydrogen production cost shows a similar evolution process as the CRF . Taking the coupled operating system as an example, when the system lifetime is increased from 10 years to 30 years, the unit hydrogen production cost is reduced from about 8.16 \$/kg to 5.12 \$/kg. And when the system lifetime is increased from 30 years to 60 years, the unit hydrogen production cost is only reduced from about 5.12 \$/kg to 4.89 \$/kg. In addition, under the same system lifetime, the unit hydrogen production cost of the coupled operating system is still lower than that of the independent operating system, as shown in Figure 5-8(b).

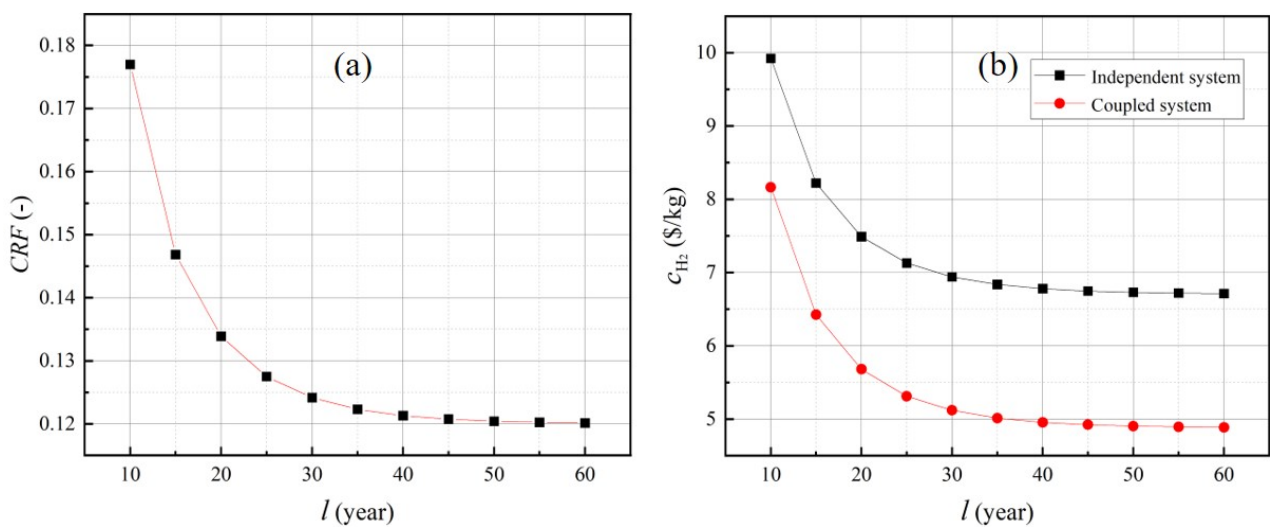


Figure 5-8. Effects of the system lifetime on (a) Capital Recovery Factor and (b) Unit hydrogen production cost.

Effects of the electricity price

Keeping the other parameters in Table 5-8 unchanged, the effects of the electricity price on the annual electricity income and unit hydrogen production cost of the two operating systems are shown in Figure 5-9. It can be seen that as the electricity price increases, the annual electricity revenue will increase linearly, and the unit hydrogen production cost will decrease linearly. Due to the larger net electrical power output, the coupled operating system can achieve a greater annual electricity revenue and a lower unit hydrogen production cost than the independent operating system. And the higher the electricity price, the greater the difference in economic performance between the two operating systems, as shown in Figure 5-9.

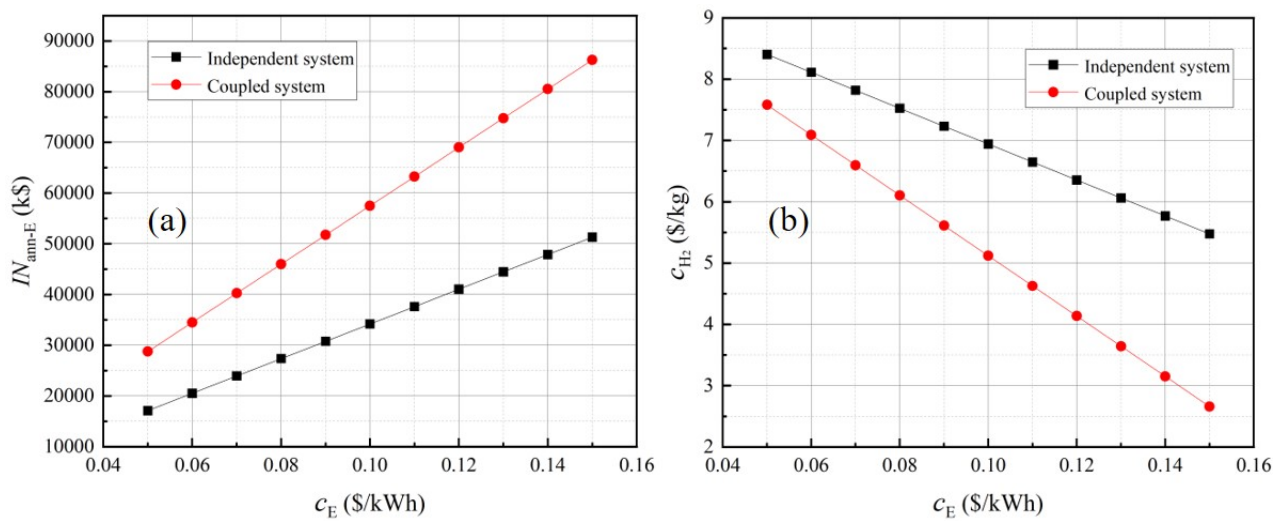


Figure 5-9. Effects of the electricity price on (a) Annual electricity income and (b) Unit hydrogen production cost.

From Figure 5-4 to Figure 5-9, it can be seen that the cost-influencing mechanism of the nuclear hydrogen production system based on S-I cycle and GSCC is very complex, and the economic performance of the system is affected by many factors. It is found that all the following means are able to reduce the unit hydrogen production cost: increasing the reactor thermal power, cost capacity factor, system lifetime and electricity price, and reducing the mass flow rate ratio and interest rate. Generally, the unit hydrogen production cost of the VHTR-driven nuclear hydrogen production system using S-I thermochemical cycle and GSCC is estimated to lay between 1.5 \$/kg and 12 \$/kg. In addition, the coupled operating system can achieve a lower unit hydrogen production cost than the independent operating system because of its greater annual electricity revenue.

5.4 Summary of this chapter

In this chapter, an economic study was performed to figure out the economic characteristics and cost-influencing mechanism of the VHTR-driven nuclear hydrogen production system using S-I cycle and GSCC. The cost composition of a common thermochemical hydrogen production plant was first introduced, and then, a complete economic model was developed based on the six-tenths-factor rule and some existing equipment investment cost equations. Finally, the cost distribution of the VHTR-driven nuclear hydrogen production system using S-I cycle and GSCC was analyzed and some parametric studies regarding the unit hydrogen production cost were performed.

The economic analysis results of the two operating systems show that nearly 90% of the annual cost expenditure of the nuclear hydrogen production system is caused by the annual capital investment of the nuclear power plant, the annual capital investment of the S-I hydrogen production plant, and the annual product cost of the S-I hydrogen production plant. The annual fuel cost is not large, accounting for only 3.2%-3.3% of the system's total annual expenditure. For the nuclear power plant, more than 80% of the equipment investment cost is used for the construction of the reactor, and for the S-I hydrogen production plant, about 70% of the equipment investment cost is used for the construction of the EED unit and two decomposition reactors. The parametric analysis results show that the cost-influencing mechanism of the nuclear hydrogen production system is very complex, and the economic performance of the system is affected by many factors. It is found that increasing the reactor thermal power, cost capacity factor, system lifetime and electricity price or reducing the mass flow rate ratio and interest rate are all helpful to reduce the unit hydrogen production cost of the system. In general, the unit hydrogen production cost of the VHTR-driven nuclear hydrogen production system using S-I cycle and GSCC is estimated to lay between 1.5 \$/kg and 12 \$/kg. In addition, it is found that the coupled operating system can always achieve a lower unit hydrogen production cost (that is, better economic performance) than the independent operating system.

Chapter 6

Conclusion and outlook

Under the background of energy shortage and climate crisis, nuclear energy, as a potential substitute for fossil energy, has attracted more and more attention from countries all over the world. At the same time, the development of hydrogen economy has become a common goal of many countries because of the multifunctional characteristics of hydrogen as a clean energy carrier. When linking nuclear energy with hydrogen, the first concept that comes to mind is hydrogen production from nuclear energy. At present, research on nuclear hydrogen production is being actively carried out in many countries, because this technology can not only realize large-scale hydrogen production without CO₂ emissions, but also improve the operational flexibility and economic competitiveness of nuclear power plants. Among various hydrogen production methods, the S-I thermochemical cycle is one of the most attractive hydrogen production processes, and it shows great potential in nuclear hydrogen production when coupled with a VHTR. However, the existing studies on the design and analysis of the VHTR and S-I thermochemical cycle-based nuclear hydrogen production system are insufficient, especially when the GSCC is integrated into the system as a power conversion unit.

To fill the above research gap, a S-I thermochemical hydrogen production process was first designed and analyzed using the Aspen Plus software, and then, the operating characteristics of the VHTR-driven nuclear hydrogen production system using S-I thermochemical cycle and GSCC were analyzed based on the first and second laws of thermodynamics. After obtaining some preliminary analysis results, the system layout improvement and the integrated design were further carried out, and finally two complete system design schemes were formed. In addition, to figure out the economic characteristics and cost-influencing mechanism of the nuclear hydrogen production system, a complete economic model was developed, and the unit hydrogen production cost under different operating scenarios was analyzed.

6.1 Conclusion

The performance analysis results of the S-I thermochemical hydrogen production process show that more than 90% of the energy consumption of the S-I cycle is caused by the concentration and decomposition process of two acid solutions (i.e., H₂SO₄ and HI solutions), and the energy consumption of the Bunsen section is very small. Thus, it can be concluded that optimizing the process flow and operating parameters of the

H₂SO₄ section and HI section will be an efficient way to reduce the energy consumption of the S-I hydrogen production system. The efficiency analysis results of the S-I hydrogen production process show that the internal heat recovery situation has a great influence on the thermal efficiency of the S-I cycle, and the thermal efficiency of the designed S-I hydrogen production process is estimated to be in the range of 15%-42%. In addition, it is also found that with a feasible internal heat exchange network, about 422 kJ of waste heat can be recovered per hydrogen production of one mole, and about 502 kJ of heat consumption can be saved after recovering all the waste heat from the condensers of the two distillation columns (i.e., H₂SO₄ distillation column and HI distillation column). Thus, it can be concluded that both the employment of an efficient internal heat exchange network and the recovery of waste heat from the distillation process will play a key role in improving the thermal efficiency of the S-I hydrogen production process.

By conducting the performance analysis of the VHTR-driven nuclear hydrogen production system using S-I thermochemical cycle and GSCC, it is found that with the increase of the mass flow rate ratio or the decrease of the IHX's primary side helium outlet temperature, the hydrogen production rate increases linearly, while the net electrical power output decreases linearly. It is also found that when more energy is used to produce hydrogen, the overall thermodynamic efficiencies of the system (including thermal efficiency and exergy efficiency) will decrease significantly. Thus, it is concluded that the S-I cycle-based nuclear hydrogen production efficiencies are lower than the GSCC-based nuclear power generation efficiencies. Assuming that the thermal efficiency of the GSCC-based nuclear power generation is in the range of 40%-50%, the calculated thermal efficiency of the S-I cycle-based nuclear hydrogen production is only about 34.9%-37.3%. The exergy analysis results of the system show that the largest exergy loss of the system occurs in the nuclear reactor (i.e. VHTR), and its exergy efficiency and exergy loss coefficient are about 70.7% and 29.4%, respectively. The exergy efficiency of the S-I cycle is very low, only about 50.8%, which means that it is necessary to optimize the process flow and operating parameters of the S-I system when the hydrogen production load is large. Besides this, it is also found that the exergy loss coefficient of the Condenser is always very low, which means that the exergy loss of the Condenser is not significant. Finally, it is found that placing a SG at the primary side outlet of IHX is an effective way to improve the thermodynamic performance of the conventional nuclear hydrogen production system based on S-I cycle and GSCC.

The thermodynamic analysis results of the two integrated operating systems show that under the same operating conditions, the two operating systems have the same hydrogen production rate, but the coupled operating system can obtain a greater net electrical power output and higher system efficiencies than the independent operating system. In other words, the coupled operating system can achieve better thermodynamic performance than the independent operating system. For example, when the mass flow rate ratio is set to 0.5 (corresponding to a hydrogen production rate of 202.86 mol/s), the independent operating system and the coupled operating system can achieve net electric power of 42.75 MW and 71.89 MW, thermal efficiencies of 28.78% and 37.11%, and exergy efficiencies of 27.26% and 36.02%, respectively. However, it should also be noted that the independent operating system may be more secure than the coupled operating system due to its simpler system

controls.

The economic analysis results of the two integrated operating systems show that nearly 90% of the annual cost expenditure of the nuclear hydrogen production system is caused by the annual capital investment of the nuclear power plant, the annual capital investment of the S-I hydrogen production plant, and the annual product cost of the S-I hydrogen production plant. The annual fuel cost is not large, accounting for only 3.2%-3.3% of the system's total annual expenditure. For the nuclear power plant, more than 80% of the equipment investment cost is used for the construction of the reactor, and for the S-I hydrogen production plant, about 70% of the equipment investment cost is used for the construction of the EED unit and two decomposition reactors. The parametric analysis results show that the cost-influencing mechanism of the nuclear hydrogen production system is very complex, and the economic performance of the system is affected by many factors. It is found that increasing the reactor thermal power, cost capacity factor, system lifetime and electricity price or reducing the mass flow rate ratio and interest rate are all helpful to reduce the unit hydrogen production cost of the system. In general, the unit hydrogen production cost of the VHTR-driven nuclear hydrogen production system using S-I thermochemical cycle and GSCC is estimated to lay between 1.5 \$/kg and 12 \$/kg. In addition, it is found that the coupled operating system can always achieve a lower unit hydrogen production cost (that is, better economic performance) than the independent operating system.

In conclusion, two promising VHTR-driven nuclear hydrogen production systems using S-I thermochemical cycle and GSCC were designed and analyzed in this thesis. The proposed system design ideas and the obtained analysis results not only provide some important data references for future engineering applications, but also lay a theoretical foundation for understanding the thermo-economic characteristics of the VHTR-driven nuclear hydrogen production system based on S-I thermochemical cycle and GSCC.

6.2 Outlook

Before the real VHTR-driven nuclear hydrogen production system using S-I thermochemical cycle and GSCC can be put into operation in the future, there are still many technical issues to be solved. As a forward-looking large-scale clean hydrogen production technology, almost every detail of this technology needs to be proved or verified, either by experiments or by simulations. Although there have been many numerical and experimental studies on the S-I thermochemical cycle, and the commercial HTR-PM has also been successfully commissioned, there is still little research on the nuclear hydrogen production system based on the integrated HTR (or VHTR) and S-I thermochemical cycle. From the perspective of technology landing, there are several aspects that need to be further investigated, as follows:

- (1) As stated in the conclusion, the recovery of waste heat from the distillation process is an important way to improve the thermal efficiency of the S-I hydrogen production process. Therefore, how to effectively recover the waste heat from the distillation process is considered to be one of my future research

works. Given that this part of waste heat belongs to low-temperature (or low-grade) thermal energy, several promising low-temperature heat recovery technologies, such as the ORC, the Organic Flash Cycle (OFC) [147], and the Trilateral Flash Cycle (TFC) [148], could be applied to the S-I hydrogen production system for efficiency improvement.

- (2) In addition to the GSCC and helium Brayton cycle, the Supercritical CO₂ Brayton Cycle (SCBC) is also a very promising thermodynamic cycle to replace the traditional SRC as the power cycle of a nuclear hydrogen production system. Due to the outstanding characteristics of high stability, simplicity, compactness, improved safety, high efficiency and less cost, the SCBC is considered as one of the most promising thermodynamic cycles applied to Generation IV nuclear power systems. It was reported that the VHTR system could achieve a power generation efficiency of approximately 52% when the SCBC was adopted [149]. Therefore, conducting the research on the VHTR-driven nuclear hydrogen production system based on S-I thermochemical cycle and SCBC will also be one of my future works.
- (3) In this work, the design and analysis of the nuclear hydrogen production system is carried out based on the assumption of steady-state operation. In the actual production process, the system will inevitably encounter some special operating conditions, such as reactor start-up and shutdown conditions, changes in hydrogen production load, abnormal operation or even accident conditions, etc., resulting in significant fluctuations or deviations of some key operating parameters. In such cases, it is essential to understand the dynamic operating characteristics of the system in order to achieve a better system control performance and ensure the system safety.
- (4) Due to limited time, only the overall layout and component configuration of the nuclear hydrogen production system are shown in this thesis, but the detailed structure, size and materials of the components are not given. Therefore, a major task of my future research is to collect and determine the detailed information of each system component. A more precise economic assessment can be made when details of all system components are available. In addition, the completion of the information collection of all system components also means that the Life Cycle Analysis or Life Cycle Assessment (LCA) of the nuclear hydrogen production system can be further carried out. Although the nuclear hydrogen production system based on S-I thermochemical cycle hardly emits CO₂ to the environment during the operation phase, its construction and dismantling process will cause certain CO₂ emissions. Thus, it is necessary to use a reliable method to comprehensively evaluate the environmental impact of the nuclear hydrogen production system throughout its lifespan. LCA is such an approach, as it can scientifically evaluate the environmental impact of a product or service from the perspective of the whole life cycle (i.e., from cradle to grave) [150].

Bibliography

- [1] Suman S. Hybrid nuclear-renewable energy systems: A review. *Journal of Cleaner Production* 2018;181:166-77.
- [2] Granovskii M, Dincer I, Rosen MA, et al. Performance assessment of a combined system to link a supercritical water-cooled nuclear reactor and a thermochemical water splitting cycle for hydrogen production. *Energy Conversion and Management* 2008;49(7):1873-81.
- [3] Şahin S, Şahin HM. Generation-IV reactors and nuclear hydrogen production. *International Journal of Hydrogen Energy* 2021;46(57):28936-48.
- [4] Yan XL, Hino R. *Nuclear hydrogen production handbook*. CRC Press; 2011.
- [5] Locatelli G, Mancini M, Todeschini N. Generation IV nuclear reactors: Current status and future prospects. *Energy Policy* 2013;61:1503-20.
- [6] Revankar ST. Chapter Four - Nuclear Hydrogen Production. *Storage and Hybridization of Nuclear Energy*, Academic Press; 2019.
- [7] Ji M, Wang J. Review and comparison of various hydrogen production methods based on costs and life cycle impact assessment indicators. *International Journal of Hydrogen Energy* 2021;46(78):38612-35.
- [8] Baykara SZ. Hydrogen: A brief overview on its sources, production and environmental impact. *International Journal of Hydrogen Energy* 2018;43(23):10605-14.
- [9] H2@Scale concept. 2017. US department of energy. <http://www.energy.gov/eere/fuelcells/h2scale>.
- [10] Safari F, Dincer I. A review and comparative evaluation of thermochemical water splitting cycles for hydrogen production. *Energy Conversion and Management* 2020;205:112182.
- [11] Sadeghi S, Ghandehariun S, Rosen MA. Comparative economic and life cycle assessment of solar-based hydrogen production for oil and gas industries. *Energy* 2020;208:118347.
- [12] *Hydrogen Scaling Up. A Sustainable Pathway for the Global Energy Transition*. Belgium: Hydrogen Council; 2017.
- [13] El-Emam RS, Ozcan H, Zamfirescu C. Updates on promising thermochemical cycles for clean hydrogen production using nuclear energy. *Journal of Cleaner Production* 2020;262:121424.

- [14] Dincer I, Acar C. Review and evaluation of hydrogen production methods for better sustainability. *International Journal of Hydrogen Energy* 2015;40(34):11094-111.
- [15] Ewan BCR, Allen RWK. A figure of merit assessment of the routes to hydrogen. *International Journal of Hydrogen Energy* 2005;30(8):809-19.
- [16] Wang Q, Liu C, Luo R, et al. Thermodynamic analysis and optimization of the combined supercritical carbon dioxide Brayton cycle and organic Rankine cycle-based nuclear hydrogen production system. *International Journal of Energy Research* 2022;46(2):832-59.
- [17] Wang Q, Liu C, Luo R, et al. Thermo-economic analysis and optimization of the very high temperature gas-cooled reactor-based nuclear hydrogen production system using copper-chlorine cycle. *International Journal of Hydrogen Energy* 2021;46(62):31563-85.
- [18] Qu X, Zhao G, Wang J. Thermodynamic evaluation of hydrogen and electricity cogeneration coupled with very high temperature gas-cooled reactors. *International Journal of Hydrogen Energy* 2021;46(57):29065-75.
- [19] Naterer GF, Dincer I, Zamfirescu C. *Hydrogen production from nuclear energy*. Springer; 2013.
- [20] Al-Zareer M, Dincer I, Rosen MA. Development and assessment of a novel integrated nuclear plant for electricity and hydrogen production. *Energy Conversion and Management* 2017;134:221-34.
- [21] El-Emam RS, Khamis I. Advances in nuclear hydrogen production: Results from an IAEA international collaborative research project. *International Journal of Hydrogen Energy* 2019;44(35):19080-8.
- [22] Naterer GF, Suppiah S, Stolberg L, et al. Canada's program on nuclear hydrogen production and the thermochemical Cu-Cl cycle. *International Journal of Hydrogen Energy* 2010;35(20):10905-26.
- [23] Odukoya A, Naterer GF, Roeb M, et al. Progress of the IAHE Nuclear Hydrogen Division on international hydrogen production programs. *International Journal of Hydrogen Energy* 2016;41(19):7878-91.
- [24] Farsi A, Dincer I, Naterer GF. Review and evaluation of clean hydrogen production by the copper-chlorine thermochemical cycle. *Journal of Cleaner Production* 2020;276:123833.
- [25] Sun Y, Xu J, Zhang Z. R&D effort on nuclear hydrogen production technology in China. *International Journal of Nuclear Hydrogen Production and Applications* 2006;1(2):104-11.
- [26] Dong Z, Li B, Huang X, et al. Power-pressure coordinated control of modular high temperature gas-cooled reactors. *Energy* 2022;252:124042.
- [27] Zhang P, Wang L, Chen SG, et al. Progress of nuclear hydrogen production through the iodine-sulfur process in China. *Renewable and Sustainable Energy Reviews* 2018;81:1802-12.

- [28] Ling B, He Y, Wang L, et al. Introduction and preliminary testing of a 5 m³/h hydrogen production facility by Iodine–Sulfur thermochemical process. *International Journal of Hydrogen Energy* 2022;47(60):25117-29.
- [29] Bhattacharyya R, Singh KK, Grover RB, et al. Nuclear hydrogen production for industrial decarbonization: Creating the business case for the near term. *International Journal of Energy Research* 2022;46(5):6929-43.
- [30] Sandeep KC, Kamath S, Mistry K, et al. Experimental studies and modeling of advanced alkaline water electrolyser with porous nickel electrodes for hydrogen production. *International Journal of Hydrogen Energy* 2017;42(17):12094-103.
- [31] Dey S, Mukhopadhyay J, Lenka RK, et al. Synthesis and characterization of nanocrystalline Ba_{0.6}Sr_{0.4}Co_{0.8}Fe_{0.2}O₃ for application as an efficient anode in solid oxide electrolyser cell. *International Journal of Hydrogen Energy* 2020;45(7):3995-4007.
- [32] Thomas D, Baveja NA, Shenoy KT, et al. Mechanistic and kinetic study of thermolysis reaction with hydrolysis step products in Cu–Cl thermochemical cycle. *International Journal of Hydrogen Energy* 2021;46(24):12672-81.
- [33] Ahmed VN, Rao AS, Sujeesh S, et al. Role of operating conditions on cross contamination of products of the Bunsen reaction in iodine-sulfur process for production of hydrogen. *International Journal of Hydrogen Energy* 2017;42(49):29101-6.
- [34] Dulera IV, Sinha RK, Rama Rao A, et al. High temperature reactor technology development in India. *Progress in Nuclear Energy* 2017;101A:82-99.
- [35] Yan XL, Sato H, Sumita J, et al. Design of HTTR-GT/H₂ test plant. *Nuclear Engineering and Design* 2018;329:223-33.
- [36] Sato H, Nomoto Y, Horii S, et al. HTTR-GT/H₂ test plant – System performance evaluation for HTTR gas turbine cogeneration plant. *Nuclear Engineering and Design* 2018;329:247-54.
- [37] Zhiznin SZ, Timokhov VM, Gusev AL. Economic aspects of nuclear and hydrogen energy in the world and Russia. *International Journal of Hydrogen Energy* 2020;45(56):31353-66.
- [38] Kim J, Chang J, Park BH, et al. A study on the dynamic behavior of a sulfur trioxide decomposer for a nuclear hydrogen production. *International Journal of Hydrogen Energy* 2008;33(24):7361-70.
- [39] Chang JH, Kim YW, Lee KY, et al. A study of a nuclear hydrogen production demonstration plant. *Nuclear Engineering and Technology* 2007;39(2):111-22.
- [40] Shin Y, Chang J, Lee T, et al. Start-up behaviors of a H₂SO₄–H₂O distillation column for the 50 NL H₂/H sulfur–iodine cycle. *International Journal of Hydrogen Energy* 2014;39(26):14172-7.
- [41] Henderson AD, Taylor A. The US Department of Energy research and development programme on hydrogen production using nuclear energy. *International Journal of Nuclear Hydrogen Production and Applications* 2006;1(1):51-6.

- [42] Frick C, Talbot PW, Wendt DS, et al. Evaluation of hydrogen production feasibility for a light water reactor in the midwest. INL/EXT-19-55395, September 2019, Idaho National Laboratory, Idaho Falls, USA.
- [43] T-Raissi A. Water Splitting: Thermochemical. In: Encyclopedia of Inorganic and Bioinorganic Chemistry. John Wiley & Sons, Ltd; 2012.
- [44] Yildiz B, Kazimi MS. Efficiency of hydrogen production systems using alternative nuclear energy technologies. International Journal of Hydrogen Energy 2006;31(1):77-92.
- [45] Funk JE. Thermochemical hydrogen production: past and present. International Journal of Hydrogen Energy 2001;26(3):185-90.
- [46] Funk JE, Reinstrom RM. Energy Requirements in Production of Hydrogen from Water. Industrial & Engineering Chemistry Process Design and Development 1966;5(3):336-42.
- [47] El-Emam RS, Özcan H. Comprehensive review on the techno-economics of sustainable large-scale clean hydrogen production. Journal of Cleaner Production 2019;220:593-609.
- [48] Beghi GE. A decade of research on thermochemical hydrogen at the joint research centre – Ispra. Hydrogen systems. Presented at the International Symposium on Hydrogen Systems, 7–11 May 1985, Beijing, China; 1985:153–171.
- [49] Pinsky R, Sabharwall P, Hartvigsen J, et al. Comparative review of hydrogen production technologies for nuclear hybrid energy systems. Progress in Nuclear Energy 2020;123:103317.
- [50] Kasahara S, Iwatsuki J, Takegami H, et al. Current R&D status of thermochemical water splitting iodine-sulfur process in Japan Atomic Energy Agency. International Journal of Hydrogen Energy 2017;42(19):13477-85.
- [51] Zhang P, Zhou CL, Guo HF, et al. Design of integrated laboratory-scale iodine sulfur hydrogen production cycle at INET. International Journal of Energy Research 2016;40(11):1509-17.
- [52] Moore R, Parma E, Russ B, et al. An integrated laboratory-scale experiment on the sulfur – iodine thermochemical cycle for hydrogen production. Proceedings of the 4th International Topical Meeting on High Temperature Reactor Technology, 2008, Washington DC, USA.
- [53] Bertrand F, Germain T, Bentivoglio F, et al. Safety study of the coupling of a VHTR with a hydrogen production plant. Nuclear Engineering and Design 2011;241(7):2580-96.
- [54] Shin Y, Lee T, Lee K, et al. Start-up dynamic behaviors of a HI–I₂–H₂O distillation column for the sulfur-iodine hydrogen production cycle. International Journal of Hydrogen Energy 2015;40(39):13264–71.
- [55] Nakajima H, Sakurai M, Ikenoya K, et al. A study on a closed-cycle hydrogen production by thermochemical water-splitting IS process. Proceedings of the 7th International Conference on Nuclear Engineering, ICONE-7104, 1999, Tokyo, Japan.

- [56] Kubo S, Nakajima H, Kasahara S, et al. A demonstration study on a closed-cycle hydrogen production by the thermochemical water-splitting iodine–sulfur process. *Nuclear Engineering and Design* 2004;233(1-3):347–54.
- [57] Hiroki N, Yu K, Nobuyuki T, et al. Hydrogen production using thermochemical water-splitting Iodine–Sulfur process test facility made of industrial structural materials: Engineering solutions to prevent iodine precipitation. *International Journal of Hydrogen Energy* 2021;46(43):22328-43.
- [58] Zhang P, Chen SZ, Wang LJ, et al. Overview of nuclear hydrogen production research through iodine sulfur process at INET. *International Journal of Hydrogen Energy* 2010;35(7):2883-7.
- [59] Zhang P, Chen SZ, Wang LJ, et al. Study on a lab-scale hydrogen production by closed cycle thermo-chemical iodine–sulfur process. *International Journal of Hydrogen Energy* 2010;35(19):10166-72.
- [60] Brecher LE, Wu CK. Electrolytic decomposition of water. Westinghouse Electric Corp. US Patent No. 3888750; 1975.
- [61] Sattler C, Roeb M, Agrafiotis C, et al. Solar hydrogen production via sulphur based thermochemical water-splitting. *Solar Energy* 2017;156:30-47.
- [62] Carty R, Cox K, Funk J, et al. Process sensitivity studies of the Westinghouse Sulfur Cycle for hydrogen generation. *International Journal of Hydrogen Energy* 1977;2(1):17-22.
- [63] Lu PWT, Ammon RL. Sulfur dioxide depolarized electrolysis for hydrogen production: Development status. *International Journal of Hydrogen Energy* 1982;7(7):563-75.
- [64] Lu PWT. Technological aspects of sulfur dioxide depolarized electrolysis for hydrogen production. *International Journal of Hydrogen Energy* 1983;8(10):773-81.
- [65] Struck BD, Junginger R, Boltersdorf D, et al. The anodic oxidation of sulfur dioxide in the sulfuric acid hybrid cycle. *International Journal of Hydrogen Energy* 1980;5(5):487-97.
- [66] Junginger R, Struck BD. Separators for the electrolytic cell of the sulphuric acid hybrid cycle. *International Journal of Hydrogen Energy* 1982;7(4):331-40.
- [67] Goresek MB, Summers WA. Hybrid sulfur flowsheets using PEM electrolysis and a bayonet decomposition reactor. *International Journal of Hydrogen Energy* 2009;34(9):4097-114.
- [68] Goresek MB. Hybrid sulfur cycle flowsheets for hydrogen production using high-temperature gas-cooled reactors. *International Journal of Hydrogen Energy* 2011;36(20):12725-41.
- [69] Goresek MB, Corgnale C, Summers WA. Development of the hybrid sulfur cycle for use with concentrated solar heat. I. Conceptual design. *International Journal of Hydrogen Energy* 2017;42(33):20939-54.
- [70] Dokiya M, Kotera Y. Hybrid cycle with electrolysis using Cu-Cl system. *International Journal of Hydrogen Energy* 1976;1(2):117-21.

- [71] Carty RH, Mazumder MM, Schreiber JD, et al. Thermochemical Production of Hydrogen. Institute of Gas Technology, Chicago, USA. Final report 1981;30517:1-4.
- [72] Sim KS, Son YM, Kim JW. Some thermochemical cycles composed of copper compounds with three-step reactions. *International Journal of Hydrogen Energy* 1993;18(4):287-90.
- [73] Al-Zareer M, Dincer I, Rosen MA. Performance analysis of a supercritical water-cooled nuclear reactor integrated with a combined cycle, a Cu-Cl thermochemical cycle and a hydrogen compression system. *Applied Energy* 2017;195:646–58.
- [74] Al-Zareer M, Dincer I, Rosen MA. Assessment and analysis of hydrogen and electricity production from a Generation IV lead-cooled nuclear reactor integrated with a copper-chlorine thermochemical cycle. *International Journal of Energy Research* 2018;42(1):91–103.
- [75] Ratlamwala TAH, Dincer I. Energy and exergy analyses of a Cu–Cl cycle based integrated system for hydrogen production. *Chemical Engineering Science* 2012;84:564-73.
- [76] Razi F, Dincer I, Gabriel K. Energy and exergy analyses of a new integrated thermochemical copper-chlorine cycle for hydrogen production. *Energy* 2020;205:117985.
- [77] Ozbilen A, Dincer I, Rosen MA. Development of a four-step Cu–Cl cycle for hydrogen production – Part I: Exergoeconomic and exergoenvironmental analyses. *International Journal of Hydrogen Energy* 2016;41(19):7814–25.
- [78] Razi F, Dincer I, Gabriel K. A specific exergy costing assessment of the integrated copper-chlorine cycle for hydrogen production. *International Journal of Hydrogen Energy* 2020;45(56):31425-39.
- [79] Ozbilen A, Dincer I, Rosen MA. A comparative life cycle analysis of hydrogen production via thermochemical water splitting using a Cu–Cl cycle. *International Journal of Hydrogen Energy* 2011;36(17):11321-7.
- [80] Ozbilen A, Dincer I, Rosen MA. Life cycle assessment of hydrogen production via thermochemical water splitting using multi-step Cu–Cl cycles. *Journal of Cleaner Production* 2012;33:202-16.
- [81] Fütterer MA, Strydom G, Sato H, et al. The High Temperature Gas-Cooled Reactor. *Encyclopedia of Nuclear Energy* 2021;512-22, ISBN 9780128197325.
- [82] Elder R, Allen R. Nuclear heat for hydrogen production: Coupling a very high/high temperature reactor to a hydrogen production plant. *Progress in Nuclear Energy* 2009;51(3):500-25.
- [83] Qu X, Zhao G, Wang J, et al. Study on energy cascade utilization of hydrogen-electricity cogeneration system based on nuclear hydrogen production. *Atomic Energy Science and Technology* 2021;55(zengkan):37-44.
- [84] Ni H, Peng W, Qu X, et al. Thermodynamic analysis of a novel hydrogen-electricity-heat polygeneration system based on a very high-temperature gas-cooled reactor. *Energy* 2022;249:123695.

- [85] Kunitomi K, Yan X, Nishihara T, et al. JAEA's VHTR for hydrogen and electricity cogeneration: GTHTR300C. *Nuclear Engineering and Technology* 2007;39(1):9-20.
- [86] González Rodríguez D, Brayner de Oliveira Lira CA, García Parra LR, et al. Computational model of a sulfur-iodine thermochemical water splitting system coupled to a VHTR for nuclear hydrogen production. *Energy* 2018;147:1165-76.
- [87] Jaszczur M, Rosen MA, Śliwa T, et al. Hydrogen production using high temperature nuclear reactors: Efficiency analysis of a combined cycle. *International Journal of Hydrogen Energy* 2016;41(19):7861-71.
- [88] Jędrzejewski J, Hanuszkiewicz-Drapała M. Analyses of the Efficiency of a High-Temperature Gas-Cooled Nuclear Reactor Cogeneration System Generating Heat for the Sulfur–Iodine Cycle. *ASME Journal of Energy Resources Technology* 2018;140(11):112001.
- [89] Brown LC, Besenbruch GE, Lentsch RD, et al. High efficiency generation of hydrogen fuels using nuclear power. General Atomics (US), 2003.
- [90] Botterud A, Yildiz B, Conzelmann G, et al. The Market viability of nuclear hydrogen technologies. Argonne National Laboratory, 2007, ANL-07/13.
- [91] Cerri G, Salvini C, Corgnale C, et al. Sulfur–Iodine plant for large scale hydrogen production by nuclear power. *International Journal of Hydrogen Energy* 2010;35(9):4002-14.
- [92] Lee TH, Lee KY, Shin YJ. Preliminary economic evaluation comparison of hydrogen production using G4ECONS and HEEP code. Proceedings of the HTR, 2014, Weihai, China.
- [93] Oruc O, Dincer I. Assessing the potential of thermo-chemical water splitting cycles: A bridge towards clean and sustainable hydrogen generation. *Fuel* 2021;286(Part 2):119325.
- [94] Myagmarjav O, Tanaka N, Nomura M, et al. Development of a membrane reactor with a closed-end silica membrane for nuclear-heated hydrogen production. *Progress in Nuclear Energy* 2021;137:103772.
- [95] Ying Z, Wang YB, Zheng XY, et al. Experimental study and development of an improved sulfur-iodine cycle integrated with HI electrolysis for hydrogen production. *International Journal of Hydrogen Energy* 2020;45(24):13176-88.
- [96] Guo HF, Zhang P, Chen SZ, et al. Comparison of various circuit designs in the HI decomposition section of the iodine–sulfur process. *International Journal of Hydrogen Energy* 2012;37(17):12097-104.
- [97] Vitart X, Le Duigou A, Carles P. Hydrogen production using the sulfur–iodine cycle coupled to a VHTR: An overview. *Energy Conversion and Management* 2006;47(17):2740-7.
- [98] Guo HF, Kasahara S, Onuki K, et al. Simulation study on the distillation of hyper-pseudoazeotropic HI-I₂-H₂O mixture. *Industrial & Engineering Chemistry Research* 2011;50(20):11644-56.

- [99] Roth M, Knoche KF. Thermochemical water splitting through direct HI decomposition from H₂O–HI–I₂ solutions. *International Journal of Hydrogen Energy* 1989;14(8):545-9.
- [100] Tanaka N, Onuki K. Equilibrium potential across cation exchange membrane in HI–I₂–H₂O solution. *Journal of Membrane Science* 2010;357(1-2):73-9.
- [101] Guo H, Zhang P, Chen S, et al. Modeling and validation of the iodine-sulfur hydrogen production process. *AIChE Journal* 2014;60(2):546–58.
- [102] Kasahara S, Imai Y, Suzuki K, et al. Conceptual design of the iodine-sulfur process flowsheet with more than 50% thermal efficiency for hydrogen production. *Nuclear Engineering and Design* 2018;329:213-22.
- [103] Wang Z, Yang J, Zhang Y, et al. Simulation of hydrogen production by sulfur-iodine thermo-chemical cycle process. *Taiyangneng Xuebao/Acta Energetica Solaris Sinica* 2011;32(6):802-7.
- [104] Kasahara S, Hwang GJ, Nakajima H, et al. Effects of process parameters of the IS process on total thermal efficiency to produce hydrogen from water. *Journal of Chemical Engineering of Japan* 2003;36(7):887-99.
- [105] Wang Q, Liu C, Li D, et al. Optimization and comparison of two improved very high temperature gas-cooled reactor-based hydrogen and electricity cogeneration systems using iodine-sulfur cycle. *International Journal of Hydrogen Energy* 2022;47(33):14777-98.
- [106] Park J, Cho JH, Jung H, et al. Simulation and experimental study on the sulfuric acid decomposition process of SI cycle for hydrogen production. *International Journal of Hydrogen Energy* 2013;38(14):5507-16.
- [107] Aspen Technology, Inc., Aspen Physical Property System: Physical Property Methods. Version Number: V7.3, Aspen Technology, Inc., Burlington, MA, 2011.
- [108] Goldstein S, Borgard JM, Vitart X. Upper bound and best estimate of the efficiency of the iodine sulphur cycle. *International Journal of Hydrogen Energy* 2005;30(6):619-26.
- [109] Kasahara S, Kubo S, Hino R, et al. Flowsheet study of the thermochemical water-splitting iodine-sulfur process for effective hydrogen production. *International Journal of Hydrogen Energy* 2007;32(4):489-96.
- [110] Lee BJ, No HC, Yoon HJ, et al. Development of a flowsheet for iodine-sulfur thermo-chemical cycle based on optimized Bunsen reaction. *International Journal of Hydrogen Energy* 2009;34(5):2133-43.
- [111] Liberatore R, Lanchi M, Giaconia A, et al. Energy and economic assessment of an industrial plant for the hydrogen production by water-splitting through the sulfur-iodine thermochemical cycle powered by concentrated solar energy. *International Journal of Hydrogen Energy* 2012;37(12):9550-65.
- [112] González Rodríguez D, Brayner de Oliveira Lira CA, García Hernández CR, et al. Hydrogen production methods efficiency coupled to an advanced high-temperature accelerator driven system. *International Journal of Hydrogen Energy* 2019;44(3):1392-408.

- [113] Shin Y, Lee K, Kim Y, et al. A sulfur-iodine flowsheet using precipitation, electro dialysis, and membrane separation to produce hydrogen. *International Journal of Hydrogen Energy* 2012;37(21):16604-14.
- [114] Ying Z, Zheng XY, Zhang Y, et al. Development of a novel flowsheet for sulfur-iodine cycle based on the electrochemical Bunsen reaction for hydrogen production. *International Journal of Hydrogen Energy* 2017;42(43):26586-96.
- [115] Ying Z, Yang JY, Zheng XY, et al. Energy and exergy analyses of a novel sulfur-iodine cycle assembled with HI-I₂-H₂O electrolysis for hydrogen production. *International Journal of Hydrogen Energy* 2021;46(45):23139-48.
- [116] Ni H, Qu X, Peng W, et al. Analysis of internal heat exchange network and hydrogen production efficiency of iodine-sulfur cycle for nuclear hydrogen production. *International Journal of Energy Research* 2022;46(11):15665-82.
- [117] Juárez-Martínez LC, Espinosa-Paredes G, Vázquez-Rodríguez A, et al. Energy optimization of a Sulfur-Iodine thermochemical nuclear hydrogen production cycle. *Nuclear Engineering and Technology* 2021;53(6):2066-73.
- [118] Kowalczyk T, Badur J, Ziólkowski P. Comparative study of a bottoming SRC and ORC for Joule-Brayton cycle cooling modular HTR exergy losses, fluid-flow machinery main dimensions, and partial loads. *Energy* 2020;206:118072.
- [119] MATLAB. MATLAB&Simulink, MathWorks, USA. <https://www.mathworks.com/products/matlab.html>.
- [120] Lemmon EW, Huber ML, McLinden MO. NIST standard reference database 23: reference fluid thermodynamic and transport properties REFPROP, National Institute of Standards and Technology, Standard Reference Data Program, Gaithersburg.
- [121] McDonald CF. Power conversion system considerations for a high efficiency small modular nuclear gas turbine combined cycle power plant concept (NGTCC). *Applied Thermal Engineering* 2014;73(1):82-103.
- [122] Kowalczyk T, Badur J, Bryk M. Energy and exergy analysis of hydrogen production combined with electric energy generation in a nuclear cogeneration cycle. *Energy Conversion and Management* 2019;198:111805.
- [123] Sakaba N, Kasahara S, Onuki K, et al. Conceptual design of hydrogen production system with thermochemical water-splitting iodine-sulphur process utilizing heat from the high-temperature gas-cooled reactor HTTR. *International Journal of Hydrogen Energy* 2007;32(17):4160-9.
- [124] Wang Q, Macián-Juan R. Design and analysis of an iodine-sulfur thermochemical cycle-based hydrogen production system with an internal heat exchange network. *International Journal of Energy Research* 2022;46(9):11849-66.
- [125] Al-Zareer M, Dincer I, Rosen MA. Analysis and assessment of the integrated generation IV gas-cooled fast nuclear reactor and copper-chlorine cycle for hydrogen and electricity production. *Energy Conversion and Management* 2020;205:112387.

- [126] Yang X, Qu X, Wang J. Combined cycle-coupled high-temperature and very high-temperature gas-cooled reactors: Part I—Cycle optimization. *Annals of Nuclear Energy* 2019;134:193–204.
- [127] Wang Q, Macián-Juan R. Thermodynamic analysis of two novel very high temperature gas-cooled reactor-based hydrogen-electricity cogeneration systems using sulfur-iodine cycle and gas-steam combined cycle. *Energy* 2022;256:124671.
- [128] Liu Q, Shen A, Duan Y. Parametric optimization and performance analyses of geothermal organic Rankine cycles using R600a/R601a mixtures as working fluids. *Applied Energy* 2015;148:410-20.
- [129] Meng D, Liu Q, Ji Z. Performance analyses of regenerative organic flash cycles for geothermal power generation. *Energy Conversion and Management* 2020;224:113396.
- [130] Orhan MF, Dincer I, Naterer GF. Cost analysis of a thermochemical Cu–Cl pilot plant for nuclear-based hydrogen production. *International Journal of Hydrogen Energy* 2008;33(21):6006–20.
- [131] Peters MS, Timmerhaus KD. *Plant design and economics for chemical engineers*. New York, McGraw Hill, 1968.
- [132] Lee HJ, Sarfert F, Strathmann H, et al. Designing of an electro dialysis desalination plant. *Desalination* 2002;142(3):267-86.
- [133] Strathmann H. *Ion-Exchange Membrane Separation Processes*. Membrane Science and Technology Series, 9, Elsevier; 2004.
- [134] Nayar KG, Sundararaman P, O'Connor CL, et al. Feasibility study of an electro dialysis system for in-home water desalination in urban India. *Development Engineering* 2017;2:38-46.
- [135] Generous MM, Qasem NAA, Akbar UA, et al. Techno-economic assessment of electro dialysis and reverse osmosis desalination plants. *Separation and Purification Technology* 2021;272:118875.
- [136] Kim S, Yun SW, Lee B, et al. Steam reforming of methanol for ultra-pure H₂ production in a membrane reactor: Techno-economic analysis. *International Journal of Hydrogen Energy* 2019;44(4):2330-9.
- [137] Wu C, Wang S, Li J. Exergoeconomic analysis and optimization of a combined supercritical carbon dioxide recompression Brayton/organic flash cycle for nuclear power plants. *Energy Conversion and Management* 2018;171:936-52.
- [138] Kim J, Park JK, Yoon YS. Simplified sulfur-iodine cycle process to hydrogen blast furnace: Techno-economic and CO₂ mitigation analysis. *Journal of Cleaner Production* 2022;355:131855.
- [139] Sadeghi S, Ghandehariun S, Naterer GF. Exergoeconomic and multi-objective optimization of a solar thermochemical hydrogen production plant with heat recovery. *Energy Conversion and Management* 2020;225:113441.
- [140] Samanta S, Ghosh S. A thermo-economic analysis of repowering of a 250MW coal fired power plant through integration of Molten Carbonate Fuel Cell with carbon capture. *International Journal of Greenhouse Gas Control* 2016;51:48-55.

-
- [141] Wang X, Dai Y. Exergoeconomic analysis of utilizing the transcritical CO₂ cycle and the ORC for a recompression supercritical CO₂ cycle waste heat recovery: A comparative study. *Applied Energy* 2016;170:193-207.
- [142] Mohammadi K, Ellingwood K, Powell K. A novel triple power cycle featuring a gas turbine cycle with supercritical carbon dioxide and organic Rankine cycles: Thermo-economic analysis and optimization. *Energy Conversion and Management* 2020;220:113123.
- [143] Xiong J, Zhao H, Zheng C. Thermo-economic cost analysis of a 600 MWe oxy-combustion pulverized-coal-fired power plant. *International Journal of Greenhouse Gas Control* 2012;9:469-83.
- [144] Seyyedi SM, Hashemi-Tilehnoee M, Rosen MA. Exergy and exergoeconomic analyses of a novel integration of a 1000 MW pressurized water reactor power plant and a gas turbine cycle through a superheater. *Annals of Nuclear Energy* 2018;115:161-72.
- [145] https://www.globalpetrolprices.com/electricity_prices/
- [146] Wang C, Akkurt N, Zhang X, et al. Techno-economic analyses of multi-functional liquid air energy storage for power generation, oxygen production and heating. *Applied Energy* 2020;275:115392.
- [147] Wang Q, Wu W, Li D, et al. Thermodynamic analysis and optimization of four organic flash cycle systems for waste heat recovery. *Energy Conversion and Management* 2020;221:113171.
- [148] Bianchi G, McGinty R, Oliver D, et al. Development and analysis of a packaged Trilateral Flash Cycle system for low grade heat to power conversion applications. *Thermal Science and Engineering Progress* 2017;4:113-21.
- [149] Oh CH, Moore RL. Brayton cycle for high-temperature gas-cooled reactors. *Nuclear Technology* 2005;149(3):324-36.
- [150] Smitkova M, Janíček F, Riccardi J. Life cycle analysis of processes for hydrogen production. *International Journal of Hydrogen Energy* 2011;36(13):7844-51.

Publications

Peer-Reviewed Journal Papers

1. **Qi Wang**, Rafael Macián-Juan. Design and analysis of an iodine-sulfur thermochemical cycle-based hydrogen production system with an internal heat exchange network. *International Journal of Energy Research* 2022;46(9):11849-66.
2. **Qi Wang**, Rafael Macián-Juan. Thermodynamic analysis of two novel very high temperature gas-cooled reactor-based hydrogen-electricity cogeneration systems using sulfur-iodine cycle and gas-steam combined cycle. *Energy* 2022;256:124671.
3. **Qi Wang**, Chunyu Liu, Dantong Li, Rafael Macián-Juan. Optimization and comparison of two improved very high temperature gas-cooled reactor-based hydrogen and electricity cogeneration systems using iodine-sulfur cycle. *International Journal of Hydrogen Energy* 2022;47(33):14777-98.
4. **Qi Wang**, Rafael Macián-Juan, Dantong Li. Analysis and assessment of a novel organic flash Rankine cycle (OFRC) system for low-temperature heat recovery. *Energy Science and Engineering* 2022;10(8):3023–43.
5. **Qi Wang**, Chunyu Liu, Run Luo, Dantong Li, Rafael Macián-Juan. Thermodynamic analysis and optimization of the combined supercritical carbon dioxide Brayton cycle and organic Rankine cycle-based nuclear hydrogen production system. *International Journal of Energy Research* 2022;46(2):832-59.
6. **Qi Wang**, Chunyu Liu, Run Luo, Xiaodong Li, Dantong Li, Rafael Macián-Juan. Thermo-economic analysis and optimization of the very high temperature gas-cooled reactor-based nuclear hydrogen production system using copper-chlorine cycle. *International Journal of Hydrogen Energy* 2021;46(62):31563-85.

Scientific Presentation

1. **Qi Wang**. Research on Advanced Clean Hydrogen Production Technology Driven by Nuclear Energy. Doctoral Candidates' Day 2022, Technische Universität München, Germany, 2022.
2. **Qi Wang**. The role of carbon-free hydrogen production technology based on clean energy in promoting carbon peaking and carbon neutrality. The Seventh Youth Scholars Zhixing Forum, Northeastern University, China, 2022.
3. **Qi Wang**. Design and thermodynamic analysis of the integrated high temperature

gas-cooled reactor and sulfur-iodine thermochemical hydrogen production system. The Seventh Qilu Youth Forum, Shandong University, China, 2022.

Supervised Semester and Master Thesis

1. Shangbo Yuan. Thermodynamic Analysis of a High Temperature Gas-cooled Reactor-based Combined Heat and Power (CHP) System. Semester thesis, Technische Universität München, Germany, 2022.
2. Josef Riedl. Literature Review: Techno-economic analysis of nuclear assisted hydrogen production. Semester thesis, Technische Universität München, Germany, 2023.
3. Piotr Jacek Dawid. Thermodynamic and Economic Analysis of Supercritical CO₂ Brayton Cycle-Based Generation IV Nuclear Power Systems. Master thesis, Technische Universität München, Germany, 2023.
4. Shangbo Yuan. Thermodynamic Analysis of a High Temperature Gas-cooled Reactor-based Combined Cooling, Heating and Power System. Master thesis, Technische Universität München, Germany, 2023.